

# UC Davis

## UC Davis Electronic Theses and Dissertations

### Title

Dissection of cell plate dynamics during cytokinesis and the role of callose in cell plate maturation

### Permalink

<https://escholarship.org/uc/item/0c44m34d>

### Author

Sinclair, Rosalie Mason

### Publication Date

2024

Peer reviewed|Thesis/dissertation

Dissection Of Cell Plate Dynamics During Cytokinesis

And The Role Of Callose In Cell Plate Maturation

By

ROSALIE MASON SINCLAIR

DISSERTATION

Submitted in partial satisfaction of the requirements for the degree of

DOCTOR OF PHILOSOPHY

in

Plant Biology

in the

OFFICE OF GRADUATE STUDIES

of the

UNIVERSITY OF CALIFORNIA

DAVIS

Approved:

---

Georgia Drakakaki, Chair

---

Bo Liu,

---

Edwardo Blumwald,

Committee in Charge

2024

## Table of Contents

Abstract.....	ii
Acknowledgments.....	iv
Chapter 1. Introduction.....	1
Cytokinesis and the Formation of a New Cell	
Wall.....	2
Plant cytokinesis and the construction of new cell	
wall.....	24
Chapter 2. A biophysical model for plant cell plate maturation based on the contribution of a spreading force.....	37
A Biophysical Model For Plant Cell Plate Maturation Based On The Contribution Of A Spreading Force.....	38
Chapter 3. Quantitative cell plate development and identification of robust transition points between growth phases.....	50
Four-dimensional quantitative analysis of Arabidopsis cell plate development identifies robust transition points between growth phases.....	51
Conclusion and Future perspectives.....	107
Appendix.....	108

## Abstract

The cell wall is an integral and dynamic structure surrounding plant cells, involved in plant growth and development. During cytokinesis, cell plate formation takes place, via fusion of cytokinetic vesicles, that after membrane transformation and deposition of polysaccharides transitions to a new cross wall. Callose, a  $\beta(1,3)$  glucan polysaccharide, is transiently deposited at the cell plate during this fundamental process. Callose deposition is thought to play a vital role in stabilizing the cell plate and contributing to a spreading force during cell plate expansion.

Cytokinesis-specific callose synthases are recalcitrant to study by genetic means, because null mutations in the corresponding genes cause lethality. Additionally, limitations in live cell imaging of polysaccharides add to the difficulties in elucidating the biological role and regulation of callose biosynthesis at the cell plate.

To overcome these challenges, I have taken a multidisciplinary approach. To better understand the transition from a vesicular network to a fenestrated sheet and finally a mature cell plate, we implemented a modeling approach, adopting the Helfrich energy that examines the elastic properties of lipid bilayers. Our model predicts the requirement of a spreading/stabilizing force for cell plate expansion and maturation. The transient accumulation of callose, coinciding with the predicted cell plate stages requiring this spreading force, are consistent with the proposed model. Furthermore, we used a specific cytokinetic callose inhibitor, Endosidin7 (ES7), to dissect the role of callose. ES7 does not inhibit wound or stress-induced callose deposition; however, it specifically causes failure in cell plate expansion and maturation, indicating that callose is a contributor to the stabilizing or spreading force as predicted by our model.

We further used advanced light microscopic techniques to explore cell plate dynamics. I studied cell plate development across four dimensions using a cytokinesis-specific GTPase YFP-RABA2a as a vesicle marker. With the aid of a robust cell plate volume analysis pipeline, I identified three easily trackable cell plate developmental phases that can be interrogated to study cell plate development. Inhibition of callose through ES7 suppressed phase transitions, establishing a critical role and timing of polysaccharide deposition in cell plate expansion and maturation.

Using this suite of interdisciplinary techniques, we contributed to breaking apart the molecular black box surrounding callose deposition during cytokinesis.

## **Acknowledgments**

I would like to express sincerest gratitude to my advisor Georga Drakakaki for their support, guidance, and enthusiasm throughout my journey. Your excitement for the unicorn images late at night coming back from the SP8, meant the world to me. Your genuine appreciation for the effort behind obtaining those images made all the hard work worthwhile. I am grateful for the honest conversations we shared. Your insights not only helped me grow as a researcher but also as a human being. Your mentorship extended beyond the boundaries of academia. From navigating complex methodologies while orchestrating collaborative efforts, your guidance has been the cornerstone of my academic journey. Your patience, wisdom, and belief in my potential have propelled me forward, especially during the challenges of my PhD.

I am thankful for the trust you placed in me when I doubted myself in the early years of my research journey. Your mentorship has not only shaped my academic endeavors but has also inspired me to strive for excellence in all aspects of my life.

Thank you for being more than just an advisor; thank you for being a mentor, a guide, and a friend. I am honored to have had the opportunity to learn from you and to have been a part of your academic family.

I extend my gratitude to my thesis committee members, Bo Liu and Edwardo Blumwald. While our group meetings were infrequent, their individual interactions throughout my tenure at UC Davis proved invaluable. Bo's graciousness from the outset of my rotation, inclusive of celebrating Chinese New Year together, fostered a sense of belonging and community beyond the lab. Whether serendipitously meeting Bo in the hallways at the microscope and having small meetings or a formal sit down his insights were always enlightening and gave me something new to consider. Similarly, Edwardo provided invaluable guidance during my formative research stages, even before formally

joining my committee. Our discussions during my initial year, while I was still refining my research acumen, were instrumental in shaping my academic. Particularly during pivotal moments such as my Qualifying Examination, the encouragement and guidance offered all the way to these last steps of my Ph.D. You both have my gratitude for helping shape my time here and my studies in many ways have left indelible marks on my doctoral experience.

The collective camaraderie and support within the Drakakaki lab, encompassing training sessions, shared boba teas, and unwavering guidance, enriched my doctoral journey immeasurably. Every member since 2017 has contributed significantly to my growth, for which I am profoundly grateful.

Furthermore, I am indebted to the PBGG community and Craft Center for providing a nurturing environment and fostering a sense of belonging, crucial for grounding me amidst the rigors of academia. To all past and present members, your unwavering support beyond scholarly pursuits has been indispensable, aiding me in overcoming every obstacle encountered along this arduous path.

Thank you all for this opportunity, and amazing journey both professionally and personally.

Rosalie Mason Sinclair

A handwritten signature in black ink, appearing to read "Rosalie Mason Sinclair". The signature is fluid and cursive, with a prominent initial "R" and a long, sweeping underline.

## Chapter 1. Introduction

In this chapter an overview of plant cytokinesis, membrane transitions and polysaccharide delivery during cell plate development is discussed, along with key molecular mechanisms involved in stage transitions. This summary is accompanied by an animation of plant cytokinesis for educational use. Additionally, the chapter delves into the contribution of various emerging technologies to our understanding of cell plate formation, while also addressing remaining questions and offering future perspectives on this fundamental process. The chapter is published in the form of one manuscript and a book chapter as cited below.

Cytokinesis and the formation of a new cell wall.

Sinclair, R., Chang, M., & Drakakaki, G. (2023). *Plant Cell Walls*, 482–503.

<https://doi.org/10.1201/9781003178309-25>

Plant cytokinesis and the construction of new cell wall

Sinclair, R., Hsu, G., Davis, D., Chang, M., Rosquete, M., Iwasa, J.H. and Drakakaki, G. (2022),

Plant cytokinesis and the construction of new cell wall. *FEBS Lett*, 596: 2243- DOI:

10.1002/1873-3468.14426

---

# 25 Cytokinesis and the Formation of a New Cell Wall

*Rosalie Sinclair, Mingqin Chang, and Georgia Drakakaki*  
University of California Davis

## PLANT CYTOKINESIS, A UNIQUE AND FUNDAMENTAL PROCESS

Eduard Strasburger, one of the founders of modern plant cell biology and director of the Botany Institute and the Botanical Garden at the University of Bonn from 1881 to 1912, first elucidated the principles of plant cytokinesis. Early in his career, Strasburger characterised and named the distinct stages of mitosis. Using the green algae *Cladophora glomerata*, due to its large cell size, Strasburger illuminated the differences between plant and animal cytokinesis in his book *Über Zellbildung und Zelltheilung* (1876; “On Cell Formation and Cell Division”). While cytokinesis in vacuolated cells has been described since the 1940s with the description of a phragmosome (Sinnott and Bloch 1940), the formation of the cell plate was first illustrated at the ultrastructural level in the 1960s (Hepler and Newcomb 1967). For several decades, major discoveries were based on microscopy techniques followed by in-depth molecular analyses towards the end of the 20th century.

Cytokinesis is the final step in cell division, in which the cytoplasm of two newly formed daughter cells separates. Regulated cell division along with coordination of cell expansion is essential for plant development and cell shape determination (Rasmussen and Bellinger 2018; Sablowski and Gutierrez 2022; Yi and Goshima 2022). Plant cytokinesis is a fundamental process of plant life that is distinct from animal cytokinesis, which occurs through the formation of a cleavage furrow. Plant cells separate through the centrifugal formation of a cell plate that grows outwards and develops into the new cell wall, partitioning the cytoplasm of the dividing cell starting from the centre of the cell.

Cell plate formation is a tightly regulated process of choreographed vesicle delivery via the phragmoplast, followed by vesicle fusion and membrane transformation, which occurs concurrently with the time-specific deposition of polysaccharides (Drakakaki 2015; Smertenko et al. 2017; Sinclair et al. 2022). In plant cytokinesis, a phragmoplast structure serves as a scaffold for the assembly of the cell plate. In contrast, during animal cytokinesis, an actomyosin contractile ring is formed to separate the two daughter cells. Furthermore, while animal cytokinesis is characterised by the formation of a cleavage furrow inwards from the cell periphery, in plants, the construction of a cell plate begins from the centre of the dividing cell at the division

plane, expanding centrifugally outwards until fused with the parental cell wall.

Despite their stark differences, during late cytokinesis the midzone/midbody in animal cells (Glotzer 2005) shares some features with the plant phragmoplast/cell plate (Otegui et al. 2005). Membrane delivery is required for both the growth of the midbody in animal cytokinesis and cell plate formation in plants. While the midbody fills a remaining gap in the ingrowing furrow (Glotzer 2005; Steigemann and Gerlich 2009) and the plant cell plate expands radially, both structures ultimately enable the separation of the two daughter cells (Jürgens 2005; Otegui et al. 2005). How these structures have evolved to fulfil their specific functions (Farmer and Prekeris 2022) in different types of eukaryotic cells remains unknown.

This chapter provides an overview of plant cytokinesis, focusing on cell plate development, by first describing the different stages and the overall progression from the point of view of both the prevailing membrane and cytoskeletal arrays, as informed by different microscopy techniques. Cytoskeletal arrangement, followed by molecular components of the endomembrane system and polysaccharide deposition that together contribute to the formation of the cell plate and the new cell wall are discussed. The contribution of technological advances to our current knowledge in cell plate development is emphasised along with current limitations and emerging technologies that can be used to further decipher the mysteries of this fundamental aspect of plant life.

## CELL PLATE FORMATION: A MULTISTAGE DYNAMIC PROCESS

Electron microscopy was a major tool that contributed to advancing our understanding of the details of plant cytokinesis (Pickett-Heaps and Northcote 1966; Hepler and Newcomb 1967; Palevitz and Hepler 1974; Gunning et al. 1978). It allowed for the discovery of several aspects of phragmoplast development and cell plate orientation. During the mid-1990s, the Staehelin group used high pressure freezing (HPF) freeze substitution (Samuels et al. 1995) along with electron tomography to capture details on both cytoskeletal and membrane conformations in three dimensions thus informing models of cell plate

formation (Otegui et al. 2001; Segui-Simarro et al. 2004). Fluorescence microscopy using labelled tubulin provided early insights into microtubule polymerisation and translocation of the expanding phragmoplast (Asada et al. 1991). The development of fluorescence and confocal laser scanning microscopy, along with the generation of distinct markers for membrane and cytoskeleton components, allowed for a dynamic illustration of the process (reviewed in Lee and Liu 2013; McMichael et al. 2013; Boruc and Van Damme 2015; Jurgens et al. 2015; Smertenko et al. 2017, 2018; Buschmann and Müller 2019; Sinclair et al. 2022). The *Nicotiana tabacum* Bright-Yellow-2 (BY-2) cell culture system has been an excellent tool to observe larger cells and synchronisation of the cell cycle (Kakimoto and Shibaoka 1989; Samuels et al. 1995; Kumagai-Sano et al. 2006). In summary, cell plate development has been described in the literature through two perspectives: first, cytokinesis can be staged based on cytoskeletal development, which mainly focuses on the microtubule array; and the second is based on the membrane conformations of the cell plate structure during cell plate development, characterised by

four developmental stages that can exist simultaneously in different areas of a given cell plate.

Here, we will discuss centrifugal growth of the cell plate primarily through morphological changes of the membrane with reference to the corresponding cytoskeletal conformations (Figures 25.1 and 25.2). We should note that morphological changes of the membrane have been primarily defined using electron microscopy, while the cytoskeletal and overall phragmoplast conformations illustrated in the figures have been described using fluorescence imaging; hence, there are differences in the spatial resolution of the experimental data underlying these concepts.

### CENTRIFUGAL GROWTH OF THE CELL PLATE

During plant cytokinesis, a specialised structure known as the phragmoplast delivers cytokinetic vesicles to the ribosome-excluding cell plate assembly matrix (CPAM). The phragmoplast originates from microtubules of the central spindle that separates the chromosomes (Euteneuer and McIntosh 1980; Lee et al. 2001). The microtubules orient with plus ends

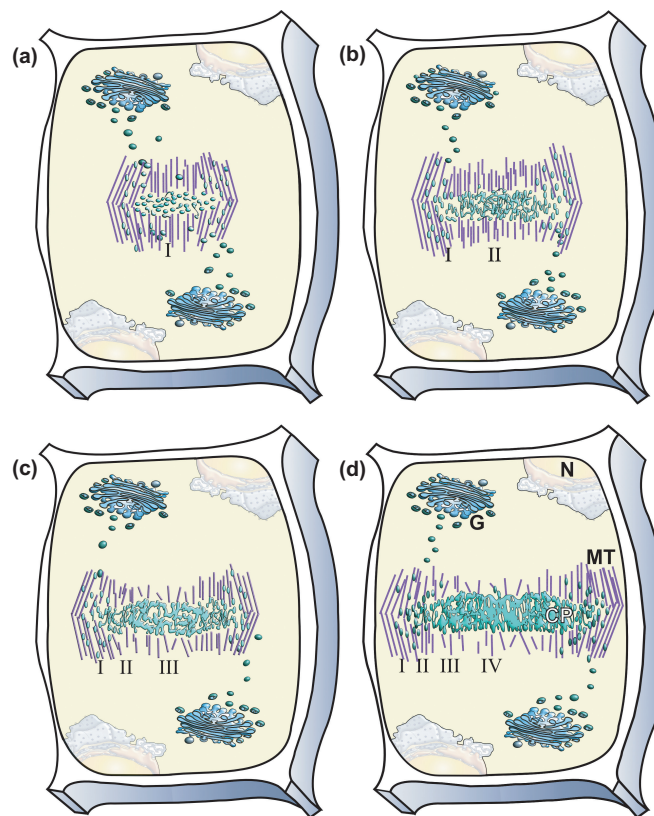


**FIGURE 25.1** Cell plate assembly occurs centrifugally in multiple stages. (A) During the fusion of the Golgi-derived vesicle stage (FVS) (I), cytokinetic vesicles guided by the phragmoplast accumulate at the centre of the dividing cell, at the cell plate assembly matrix (CPAM), where fusion starts to occur. (B) Vesicles undergo fusion and fission and conformational changes, resulting in the tubular-vesicular network (TVN) (Stage II). (C) Interconnected membrane structures transition to a tubular network (TN) (Stage III). The membrane network further expands to a continuous planar fenestrated sheet (PFS) (Stage IV). (D) Deposition of additional polysaccharides facilitates transition to a new cell wall, separating the two daughter cells. Note that different stages can occur simultaneously; structures are not to scale. This simplified representation emphasises cell plate membranes. Note that many subcellular compartments are omitted for simplicity and that the location of the nucleus is not exact. For a more accurate representation, see Videos S1, S2 in Sinclair et al. (2022). CP, Cell Plate; MT, Microtubules; G, Golgi; N, Nucleus.

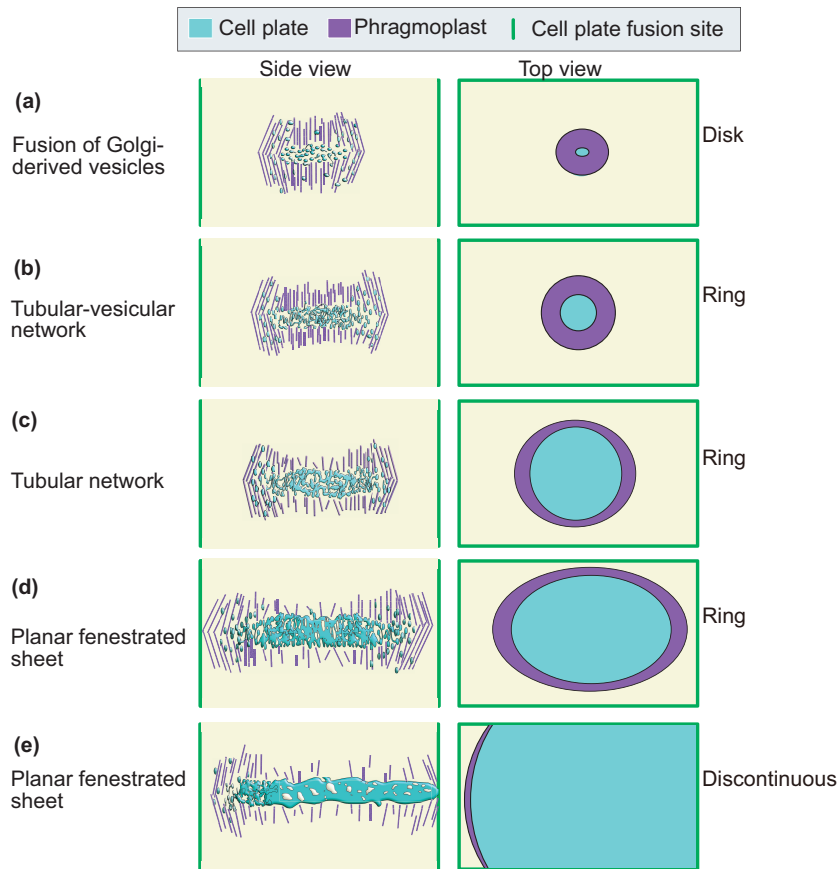


**FIGURE 25.2** Schematic representation of the cell plate development through two perspectives. Cell plate assembly occurs centrifugally in simultaneously occurring stages termed by the mature state of the centre-most material. On the left, a view of membrane fusion staging nomenclature; on the right, a two-dimensional phragmoplast at the stages shown as the top view of the corresponding cell plate. (A) During the FVS stage, cytokinetic vesicles guided by the phragmoplast accumulate at the centre of the dividing cell, at the CPAM, where fusion starts to occur. This represents a disk-like tight bundling of the phragmoplast microtubules. (B) Vesicles undergo fusion and fission and conformational changes resulting in tubular-vesicular network (TVN). The phragmoplast continues to expand with the membrane material and shows a ring conformation. (C) Interconnected membrane structures transition to a tubular network (TN). The ring phragmoplast persists. The membrane network further expands to a continuous PFS (D). The microtubules begin to depolymerise in the centre but do not disperse until a connection to the parental cell wall is formed in (E), where they change to a discontinuous conformation. Occasionally, the cell plate connects unevenly to the parental cell wall, causing a discontinuous phragmoplast, while the remaining end continues to mature until it fuses to the parental cell wall completing cytokinesis (E).

towards the division plane maintaining the same orientation as the spindle; the two arrays are on either side of the division plane that was previously established by the preprophase band (PPB) (Lloyd and Buschmann 2007; Schaefer et al. 2017). These microtubules run in a similar orientation to actin microfilaments (Kakimoto and Shibaoka 1987; Palevitz 1987; Traas et al. 1987; Schmit and Lambert 1990).

During the early stages, polymerisation and alignment of microtubules shape the phragmoplast into a disk, facilitating the delivery of vesicles at the cell division plane. When vesicles reach the division plane, they immediately start to fuse together, forming dumbbell and hourglass-shaped conformations with tubular connections (Figures 25.1 and 25.3). The tubulated vesicles continue to morph into a network and transition to a smooth yet wavy membrane disk. Cell plate expansion is radial with a small diameter disk eventually expanding across the entire plane of division (Samuels et al. 1995). The microtubules depolymerise at regions where vesicles have already formed a

smooth network at the centre, while they continue to polymerise at the edge of the cell plate (Murata et al. 2013) to form a microtubular ring. This ring continues to expand and grow along the direction of cell plate expansion. This is known as a ring stage phragmoplast (Figures 25.2B, C and D). Thus, the cell plate itself contains a gradient of stages ranging from mature at the cell plate centre to newly accumulated membranes at the leading edge. As portions of the cell plate reach the parental cell wall, they disturb the ring conformation, resulting in a discontinuous ring. This stage is known as a discontinuous ring phragmoplast (Figure 25.2E). In vacuolate shoot cells, instead of symmetrical cell plate expansion, polarised cytokinesis has been observed, in which the cell plate initially anchors on one side of the cell, followed by growth of the cell plate that ultimately joins the opposite site (Cutler and Ehrhardt 2002). This type of cell plate growth is proposed to provide mechanical support during the building of the cell wall in large cells (Cutler and Ehrhardt 2002).

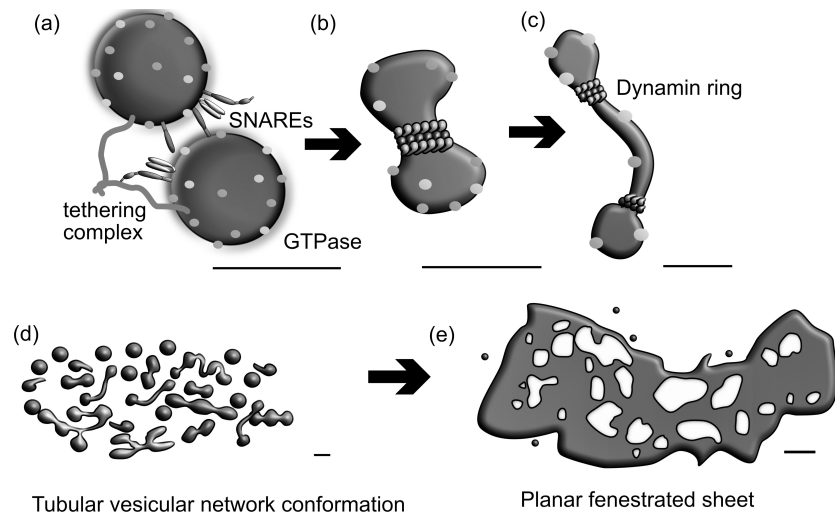


**FIGURE 25.3** Cell plate membrane transitions from vesicles to planar fenestrated sheet (PFS). During the early stages of cell plate assembly, delivery of cytokinetic vesicles, regulated by molecular switches, such as RAB GTPases, undergo initial fusion and fission. Vesicle fusion is assisted by tethering complexes and SNAREs (A). The Dynamin DRPC1 wraps around the necks of fused vesicles and causes fission and tubulation (B). Tubular vesicular stretching is accomplished by dynamin rings assembled around the vesicles creating dumbbell-like structures (C) that increase in complexity as more membrane is added and transitions to the tubular-vesicular network (TVN) stage (D). With the presence of a spreading force, TVN transitions to the PFS (E). Schematic description of vesicle fusion is adapted from data collected using electron microscopy (Samuels et al., 1995; Segui-Simarro et al. 2004). Scale bars 50 nm (A) to (D) 0.25  $\mu\text{m}$  (E).

#### DESCRIPTION OF CELL PLATE DEVELOPMENTAL STAGES BASED ON MEMBRANE CONFORMATIONS

Despite the dynamic nature of cell plate development, electron microscopy of high pressure cryofixed cells has been the preferred method for the characterisation of vesicle fusion and membrane transition due to the excellent sample preservation and spatial resolution that the method can provide. Electron micrographs allowed for 2D resolution of the cell plate and established foundational models using synchronised BY-2 cells (Samuels et al. 1995). The models were refined with the advancement of this technique into high resolution electron tomography, with 3D renderings of 2D tilt series images of serial sections that covered a large area of the cell plate. Montaged frame images could cover approximately a  $4.5 \times 4.5\text{-}\mu\text{m}$  cell plate area, at a nanometre resolution (Otegui et al. 2001; Segui-Simarro et al. 2004). This enabled a deeper understanding of the structure of vesicle fusion and transitions of membrane conformations during cell plate development, while overcoming the limitation posed by artefacts caused by conventional chemical fixation. Based on these excellent studies, we know that distinct membrane transition stages can exist simultaneously.

During the initial *fusion of Golgi-derived vesicles stage* (FVS), vesicular fusion and fission events start with the delivery of cytokinetic vesicles via phragmoplast microtubules. Upon vesicle fusion and fission, dumbbell structures are formed. The morphology of the cell plate membrane changes as more vesicle materials are added (Samuels et al. 1995; Segui-Simarro et al. 2004). Cytokinetic vesicles regulated by GTPases, such as RABA2a (Chow et al. 2008), are fused via the activity of SNARE complexes. A key cytokinetic-specific SNARE is KNOLLE, which was first

discovered in 1997 (Lauber et al. 1997). Tethering complexes also assist in this process (Rybak et al. 2014). For details, see below and Figures 25.1A and 25.2.

The morphology of the cell plate membrane changes as more membrane materials are added to the initial cell plate, which transitions to a *tubular-vesicular network* (TVN) stage. As the vesicles fuse, they tubulate largely due to the activity of dynamin-related proteins (Otegui et al. 2001; Segui-Simarro et al. 2004; Konopka and Bednarek 2008). The dynamin springs wrap around the necks of fused vesicles, leading to both fission and tubulation, by stretching the vesicle membranes into long tubes, hourglass, and dumbbell conformations to create a membrane network (Otegui et al. 2001; Segui-Simarro et al. 2004) Figure 25.3. The membrane conformation at this stage is uneven with rough tubulations. The deposition of the polysaccharide callose is reported to begin at this stage (Samuels et al. 1995). Other cell wall polysaccharides, delivered via Golgi-derived vesicles, including hemicellulose and pectin, are suggested to be deposited in small amounts at this stage (Samuels et al. 1995; Drakakaki 2015) (Figure 25.1B).

Further morphological membrane changes occur that transition the TVN into a smoother membrane while still maintaining the tubular connectivity known as the *tubular network* (TN) stage (Samuels et al. 1995). The membrane network now encloses a large lumen where polysaccharides can be deposited. Callose is prominently deposited at this stage, while cellulose deposits at a later stage (Samuels et al. 1995). Clathrin-coated vesicles (CCVs) recycle excess cell plate materials from the maturing cell plate and allow the cell plate to begin to thin into a smoother structure (Segui-Simarro et al. 2004) (Figure 25.1C).

As the cell plate nears full maturation at the *planar fenestrated sheet* (PFS) stage, a plasma membrane (PM) sheet with small pits can now be seen. These pits originated from the large cavities of the TN and will shrink with membrane expansion (Samuels et al. 1995; Segui-Simarro et al. 2004). It is thought that most pits are closed, but some remain open for plasmodesmata development and contain strands of endoplasmic reticulum (ER) (Hepler 1982; Segui-Simarro et al. 2004) (Figure 25.1D).

Though it is not considered a stage of cell plate maturation, cell plate fusion with the parental cell wall and PM is followed by flattening of the cell plate and is an important process to finalise cytokinesis (Mineyuki and Gunning 1990). Membrane “finger-like fusion tubes” extend from the cell plate to meet the parental cell wall (Samuels et al. 1995). Notably, callose has been observed at the junction of the cell plate and the parental cell wall (Samuels et al. 1995). A recently developed animation provides an overview of plant cytokinesis (Videos S1, S2 in Sinclair et al. 2022).

## MOLECULAR COMPONENTS INVOLVED IN CYTOKINESIS AND CELL PLATE DEVELOPMENT

As outlined above, cytokinesis and the formation of the cell plate is a dynamic process requiring the coordination of the cytoskeleton, endomembrane trafficking, polysaccharide deposition, and assembly into a new cell wall (Sinclair et al. 2022). At the turn of the century, technology allowed for the sequencing of different genomes, starting with the model plant *Arabidopsis* (Meinke et al. 1998; Tabata et al. 2000). Further, confocal microscopy became a routine tool for analysis in plants, allowing for live imaging of events using both fluorescent markers and dyes (Livanos et al. 2017; Komis et al. 2018). The development of molecular and genetic tools enabled the study of gene function in mutants using either loss or gain of function phenotypes and contextualised the subcellular behaviour of cytokinetic markers (Cheung et al. 2022), providing a better handle on the functional analysis of the studied molecular components and their role in cytokinesis (McMichael and Bednarek 2013; Boruc and Van Damme 2015; Smertenko et al. 2017; Gu and Rasmussen 2022). The sections below briefly explore selected, well-studied critical components of this process and emphasise plant endomembranes and polysaccharide deposition during cytokinesis (Figure 25.4).

### CYTOSKELETON AND DIVISION-PLANE ORIENTATION

Division-plane determination controls the cellular patterns created in meristems that will ultimately shape plant development. During cytokinesis, the cytoskeleton is the backbone of the phragmoplast, a multicomponent machinery that facilitates the construction of the cell plate from membranes and oligosaccharides (Lee and Liu 2013; Smertenko 2018). For details on cytoskeletal and division-plane orientation, we refer readers to these excellent reviews (Rasmussen and Bellinger 2018; Smertenko 2018;

Smertenko et al. 2018; Buschmann and Müller 2019; Lee and Liu 2019; Müller 2019; Gu and Rasmussen 2022). The cytoskeleton is the primary system on which the vesicles are delivered to the CPAM. This requires the coordination of microtubules, microfilaments, microtubule-associated proteins (MAPs), and actin binding proteins (ABPs) including kinesin and myosin motor proteins.

The involvement of the cytoskeleton in cytokinesis begins much earlier than the establishment of the phragmoplast. The cell division-plane and phragmoplast orientation are determined by the PPB early in the G2 stage of mitosis (Wick and Duniec 1983; Wick and Duniec 1984; Mineyuki et al. 1988). The PPB consists of a cortical ring of microtubules, actin filaments, cytoskeleton-interacting proteins, and other components that underlie the cortical division zone (CDZ), which is disassembled during prometaphase (Wick and Duniec 1983, 1984). The PPB deposits landmark proteins, aiding in the determination of the CDZ, which supports the alignment of the phragmoplast. The phragmoplast builds upon the remaining mitotic spindle in the centre of the division plane and expands towards the cell cortex during cytokinesis (Lee and Liu 2013; Smertenko 2018). Early ancestors of land plants did not divide through the PPB/phragmoplast system, suggesting that during the course of evolution the PPB and phragmoplast were gradually modified (Buschmann and Zachgo 2016). One hypothesis is that instead of a fully developed PPB, a few cortical microtubules are sufficient to establish a CDZ (Buschmann and Müller 2019). The enigmatic role of PPB is an active area of research awaiting future discoveries. Several critical proteins for phragmoplast positioning accumulate at the division site prior to phragmoplast cell cortex interaction (Rasmussen and Bellinger 2018). One of the earliest discovered proteins associated with the cortical division plane is TANGLED1 (TAN1), a microtubule-cross-linking protein regulating phragmoplast positioning (Smith et al. 1996; Cleary and Smith 1998; Smith et al. 2001; Martinez et al. 2020). Confocal fluorescence microscopy allowed for the understanding that AtTAN1 remains behind at the division site after the PPB is disassembled, providing cortical guidance cues for the phragmoplast (Walker et al. 2007). During telophase, TAN1 along with other division site associated proteins, may organise the cortical microtubule array, which is then incorporated into the phragmoplast and guides it to the division site (Bellinger et al. 2021). In *Arabidopsis*, mutations in TAN1 display aberrant phenotypes caused by division-plane defects and short roots but only when combined with mutants of AUXIN INDUCED IN ROOT CULTURES9 (AIR9), a microtubule binding protein accumulating at the division site and capable of associating with the PPB memory (Buschmann et al. 2006; Mir et al. 2018).

Additionally, the kinesin12-related proteins Phragmoplast Orienting Kinesins (POKs), POK1 and POK2, core members of division-plane orientation, localise to both the phragmoplast midline and the division site and are involved in phragmoplast positioning. Their function can be dependent on the other core member TAN1 (Lipka et al. 2014; Martinez et al.

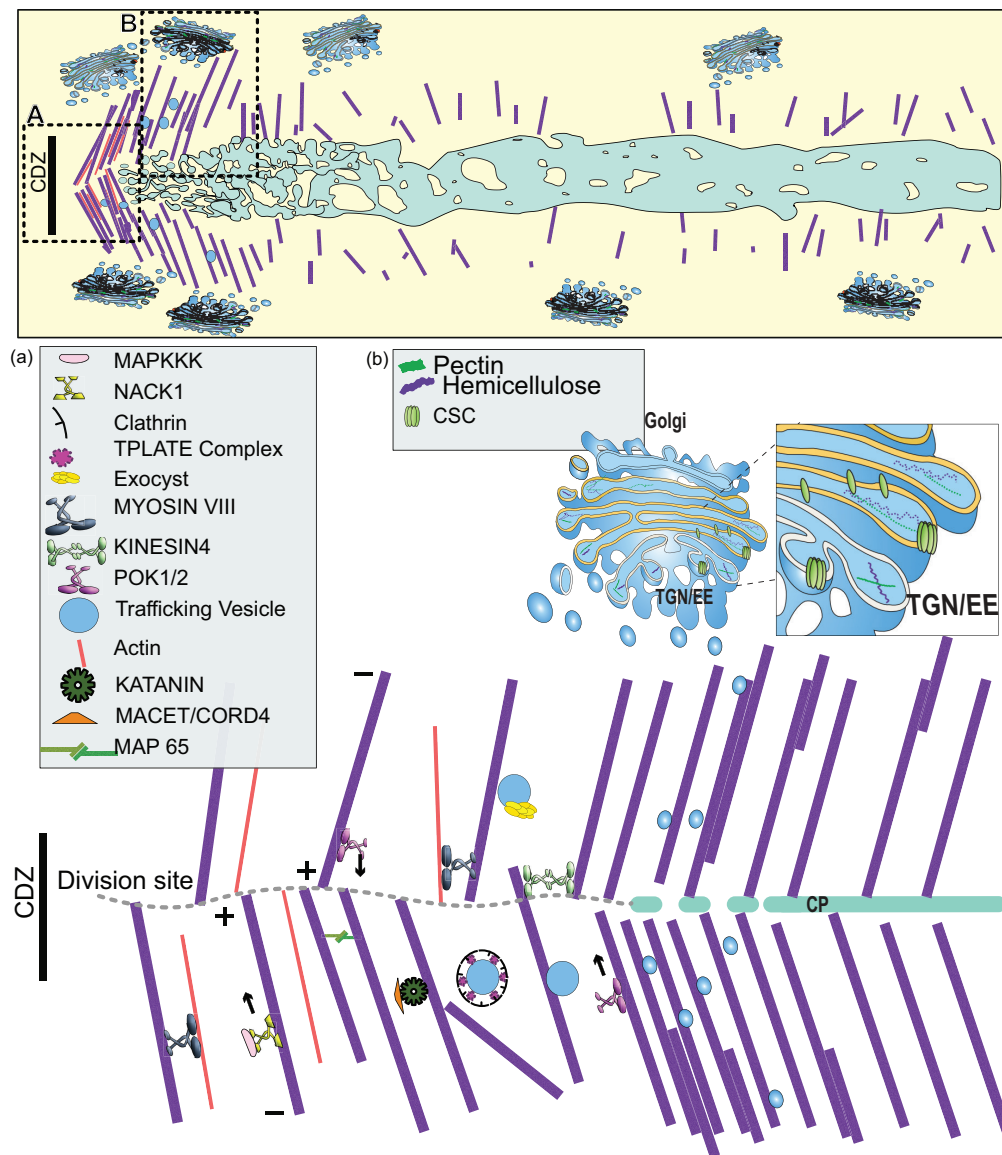


**FIGURE 25.4** Conceptual model of plant cytokinesis with a focus on cytoskeletal elements. (A) Key components of the cell cortex underlying the phragmoplast, membrane, and cell wall structures that form the cell plate (teal) from left to right maturation. (B) Pectin and hemicellulose are synthesised in the Golgi and are transported via cytokinetic vesicles along microtubules in a spatiotemporally regulated manner to the plasma membrane, supporting the construction and assembly of the cell plate.

2017; Herrmann et al. 2018; Buschmann and Müller 2019; Gu and Rasmussen 2022; Mills et al. 2022). Absence of POKs leads to phragmoplast guidance defects and abnormal cell plate insertion that deviates from the positions marked by PBB (Müller et al. 2006; Lipka et al. 2014; Martinez et al. 2017). The affinity of POKs with MAP65-3/PLE that cross-links interdigitating microtubules and other members of the Microtubule-associated protein 65 (MAP65) family suggests that such potential interactions regulate phragmoplast guidance and balance phragmoplast organisation (Ho et al. 2011; Herrmann et al. 2018; Buschmann and Müller 2019; Müller 2019). Three IQ67 DOMAIN (IQD) proteins physically interact with POKs and PHGAPs, likely providing a scaffold for division-plane maintenance (Kumari et al. 2021) (Figure 25.4).

During cytokinesis, microtubules in the phragmoplast transition through the disk, ring, and discontinuous ring conformation by the addition of new microtubules nucleating on the leading edge of the phragmoplast. The plant gamma-tubulin ring complex nucleates microtubules on the sides of extant microtubules and is a necessary component for microtubule recruitment and phragmoplast organisation during cell plate formation (Nakamura et al. 2010; Ho et al. 2011; Hotta et al. 2012). When cells enter mitosis, the nuclear envelope serves as a microtubule nucleation site on the surface (Wick and Duniec 1983), with the gamma-tubulin ring complex marking sites where microtubules emanate. Notably, the nuclear envelope also generates new microtubules towards the end of the cell division cycle (Hasezawa et al. 1991).

MAP65 isoforms cross-link anti-parallel microtubules in the phragmoplast midzone, thereby stabilising the phragmoplast structure. Their loss of function displays wider midzones and cytokinetic defects (Smertenko et al. 2000; Hussey et al. 2002; Müller et al. 2004, 2019; Ho et al. 2011; Kosetsu et al. 2013; Smertenko et al. 2018).

Phragmoplast function is regulated via signalling pathways that involve different kinases and their interactions with downstream targets. Among those, the MAPK cascade is the best characterised (Smertenko et al. 2018). The turnover of the phragmoplast microtubules can be controlled by the kinesin-like protein NACK1 (Sasabe et al. 2015). This motor protein functions in a MAP kinase signalling pathway, regulating phragmoplast expansion by controlling the depolymerisation of microtubules (Nishihama et al. 2001, 2002). Further, the microtubule-severing complex KATANIN and its interactors function in phragmoplast organisation and expansion (Sasaki et al. 2019; Panteris et al. 2021) (Figure 25.4A).

Kinesins are motor proteins that primarily bind to microtubules but have also been shown to associate with actin (Klotz and Nick 2012; Tian et al. 2015). They are critical factors in spindle assembly (Liu and Lee 2022) and are responsible for vesicle and organelle transport (Nebenführ and Dixit 2018). During cytokinesis, kinesins direct Golgi-derived vesicles towards the developing cell plate; however, which kinesins are responsible remains elusive. Both plus and minus end-directed kinesins have been implemented in cytokinesis (Nebenführ and Dixit 2018). It is proposed that a number of kinesins play a fundamental and non-redundant role in cytokinesis and phragmoplast positioning, demonstrating the complexity of cell plate formation (Gu and Rasmussen 2022). This remains a rich area of research requiring attention and unique adaptation of tools to elucidate cargo delivery, phragmoplast signalling, organisation, and dynamics.

Regulated cell division contributes to the formation of the entire plant body. While the majority of divisions are symmetrical, asymmetrical cell divisions contribute to the development of new cell types (Rasmussen and Bellinger 2018). The orientation of the cell plate has been studied from a cell geometrical perspective since the 1800s (Hofmeister 1863; Sachs 1878; Errera 1886) and has been recently revisited (Besson and Dumais 2014; Martinez et al. 2018; Rasmussen and Bellinger 2018). Geometric properties can be used to generate predictions of cell plate orientation (Martinez et al. 2018) from a set of minimal area configurations (Errera 1886). However, simple geometry is likely not the only contributing factor, as local triggers or environmental stresses, such as wounding, can alter division-plane orientation (Rasmussen and Bellinger 2018). Continuing studies in mutants with cell division orientation defects, such as *tan1* (Martinez et al., 2017), can put the current models to test and uncover the interaction between molecular factors and stochasticity in cell plate orientation.

## ENDOMEMBRANE COMPONENTS

The plant endomembrane system coordinates the production and delivery of membrane and secretory cargo required for cell plate formation; it also coordinates the recycling of excess materials. The conventional secretory pathway—ER—Golgi—*trans*-Golgi Network (TGN)—PM—is the dominant cytokinetic vesicle pathway; however, endocytic pathways also contribute to cell plate formation (Richter et al. 2014). Delivery of cytokinetic vesicles is highly regulated and involves RAB GTPases and tethering complexes, bringing the cytokinetic vesicles in close proximity to the target membrane at the cell plate, while vesicle fusion is facilitated by other complexes (Figure 25.3A-C). Of RAB GTPases, the RABA clade is well-studied in plant cytokinesis, although a complete roadmap of GTPases is yet to be elucidated. RABA2 and RABA3 are implicated in the delivery and incorporation of new membrane material to the cell plate based on their localisation at the leading edge (Chow et al. 2008), which is persistent through cell plate development (Park et al. 2014). During cytokinesis, RABA2a and RABA1e are likely associated with different vesicle populations, as demonstrated by their behaviour under treatment with the inhibitor of cytokinesis-specific callose Endosidin7 (ES7; Davis et al. 2016). In addition to RABAs, RABEs also show cell plate localisation and interact with the Stomatal Cytokinesis-Defective (SCD) complex that regulates trafficking at the cell plate (Speth et al. 2009; Ahn et al. 2013; Mayers et al. 2017).

The late-secretory ADP-ribosylation factor guanine-nucleotide exchange factors ARF GEFs (BIG1–4) regulate trafficking of newly synthesised proteins and endocytosed cargo from the TGN/EE to the forming cell plate (Richter et al. 2014). Transport Protein Particle (TRAPP) tethering complexes act as GEFs (Jones et al. 2000; Wang et al. 2000; Pinar et al. 2015). TRAPP II acts upstream of RABA1c to facilitate the membrane trafficking from TGN to the cell plate (Qi et al. 2011). Recent extensive protein interaction assays showed that TRAPP II functions upstream of RABA2a, postulating that TRAPP II is a GEF for RABA2a (Kalde et al. 2019). In addition to TRAPPs, the exocyst tethering complex also functions in cytokinesis. The localisation of the two complexes is complementary with the exocyst being present at the onset and towards the end of cytokinesis (Rybak et al., 2014). However, when overlapping, subunits of the exocyst complex interact with TRAPP subunits acting synergistically in regulation of cell plate development (Rybak et al. 2014; Vukasinovic and Zarsky 2016).

The fusion of cytokinetic vesicles is mediated by soluble N-ethylmaleimide-sensitive factor protein attachment protein receptor (SNARE) complexes (El Kasmi et al. 2013). The timeline of their discovery also brings perspective on the development of approaches that have been used to

unravel the molecular components in cytokinesis. Early studies on these genes started with the genetic analysis of embryo pattern formation (Mayer et al. 1991), which uncovered two members of the SNARE complex: the syntaxin KNOLLE (Lukowitz et al. 1996) and the accessory protein SEC1/Munc18 protein KEULE (Assaad et al. 2001). The phenotype of unfused vesicles at the cell plate in the corresponding mutants as well as the mitotic expression of KNOLLE supported the importance of these proteins in cytokinesis (Lauber et al. 1997; Waizenegger et al. 2000).

The initial discovery in genetics was followed by protein interaction screens and mutant phenotypes that eventually allowed for the identification of two functional complexes in *Arabidopsis* (El Kasmi et al. 2013; Cheung et al. 2022). These complexes consist of (i) the Q-SNARE KNOLLE and its partners Qbc-SNARE SNAP33 and either R-SNAREs VAMP721/VAMP722 or (ii) KNOLLE and its partners Qb-SNARE NPSN11, Qc-SNARE SYP71, and also R-SNAREs VAMP721/VAMP722 (Lauber et al. 1997; Heese et al. 2001; Zheng et al. 2002; Zhang et al. 2011; El Kasmi et al. 2013; Jurgens et al. 2015). Sec1/Munc18 (SM) proteins, such as KEULE, assist in SNARE complex formation, which is essential for vesicle fusion during cytokinesis (Assaad et al. 2001). The significance of having two functional complexes involving KNOLLE still remains to be determined. Interestingly, among the SNARE proteins involved in cytokinesis, only KNOLLE is cell cycle-specific and thus is widely accepted as a cytokinesis marker

(Figures 25.3A–C, 25.5, and 25.6A). The formation of cis-SNARE complexes takes place in the ER and are disassembled when they reach the cell plate (Karnahl et al. 2017). From an evolutionary point of view, Qa-SNARE SYP132, a non-specialised ancient Qa-SNARE, has counterparts in lower plants and functionally overlaps with the flowering plant-specific KNOLLE, showing a transition from ancient to flowering plant cytokinesis complexes (Park et al. 2018).

Ultrastructural studies support the estimate that 70% of the overall membrane materials accumulated at the CPAM are recycled and removed as the membranes mature and flatten during the transition from the TVN to PFS stages (Samuels et al. 1995; Otegui et al. 2001). Membrane recycling is therefore as important as vesicle delivery. Different components of CCVs, such as the clathrin chain, adaptor protein complexes, and dynamin-related proteins that help the scission of CCVs, are present at the cell plate (Fujimoto et al. 2008; Konopka et al. 2008; Konopka and Bednarek 2008; Fujimoto et al. 2010; Song et al. 2012; McMichael and Bednarek 2013). The role of clathrin-mediated recycling in cell plate maturation is further supported by the presence of TPLATE, a peripherally associated complex on CCVs that helps generate membrane curvature (Van Damme et al. 2011; Johnson et al. 2021) (Figure 25.5 and 25.6A). Cell wall biosynthetic complexes, such as cellulose synthases or SNAREs, can be recycled from the cell plate once their function is complete (Boutté et al. 2010; Gadeyne et al. 2014; Sanchez-Rodriguez et al. 2018; Dahhan and Bednarek 2022).

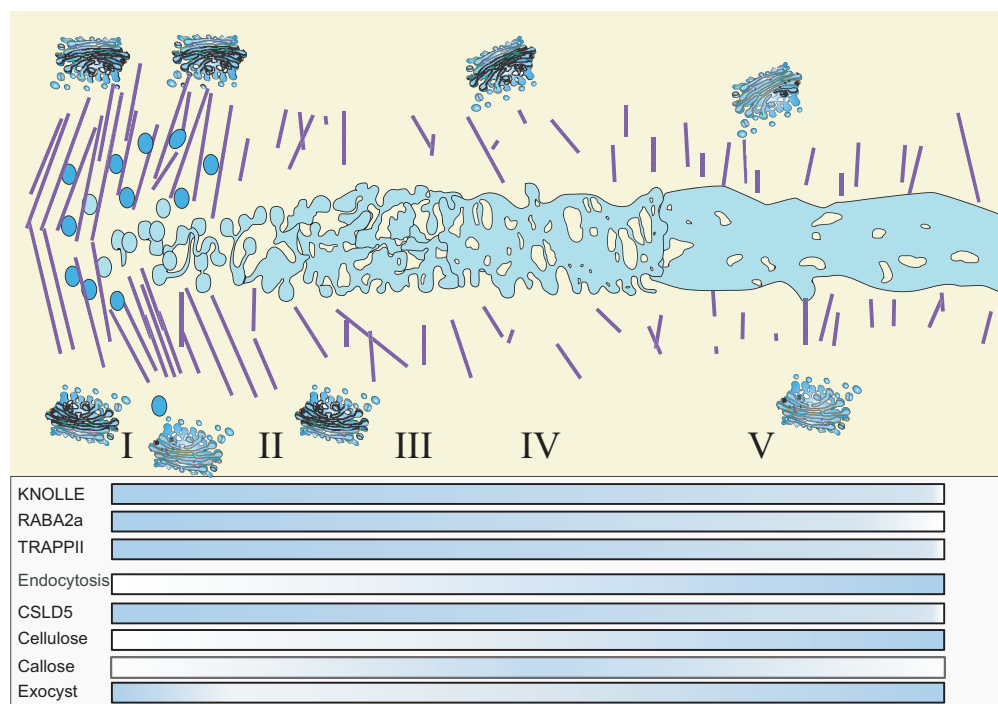


**FIGURE 25.5** Visual representation of the temporal activity of selected components involved in cell plate formation. Temporal distribution of tethering complexes Exocyst and TRAPP II, SNARE-KNOLLE, RABA2a, membrane recycling and endocytosis, and polysaccharide deposition (cellulose and callose, blue) throughout the stages of cell plate formation. (I) Fusion of Golgi-derived vesicles stage FVS, (II) tubular-vesicular network (TVN) stage, (III) tubular network (TN) stage, (IV) planar fenestrated sheet (PFS), and (V) cross wall. Structures are not to scale.

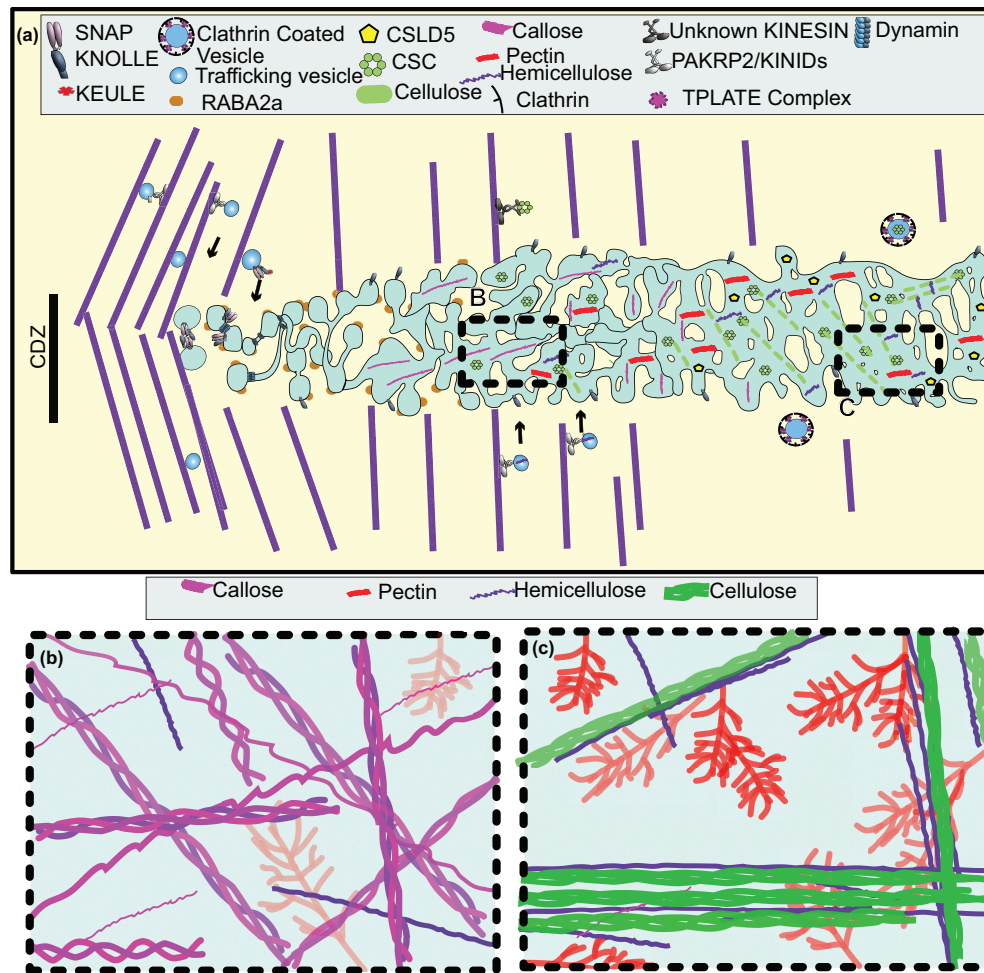


**FIGURE 25.6** Proposed model of cell plate maturation and key contributing elements. (A) Cell plate initiation stage comprising tubular-vesicular network (TVN)-derived secretory vesicles that migrate along the phragmoplast towards the cell equator. Vesicle docking and fusion facilitated by SNAREs and the tethering complex such as Exocyst and TRAPP. In the early stage of cell plate formation, RABA2a (orange) and KNOLLE (blue) labelled vesicles with guidance from the phragmoplast vigorously accumulate at the centre of the dividing cell. Vesicles at the CPAM change their structure by fusion and fission (blue tubular membrane structures in TVN) facilitated by SNARE-mediated fusion and dynamin-based restriction. Callose (hot pink lines) starts depositing at the tubular network (TN) stage to support membrane structures and facilitate the transition to the PFS stage. At the more mature stages, additional polysaccharides, such as cellulose (green dashed lines), are deposited along with higher levels of cross-linking polysaccharides such as hemicellulose (purple) and pectin (red). Membrane remodelling is assisted by the removal of excess material at the centre via clathrin-mediated recycling. Microtubule depolymerisation takes place at the centre. Note that different stages can occur simultaneously. Structures are not to scale. (B) Cartoon representation of cell plate composition starting at the TN stage. Callose (pink) deposition starts at the TN stage. Callose is thought to stabilise the membrane network structure and provide a spreading force for cell plate expansion and transition to a fenestrated sheet. Hemicellulose (purple) and pectin (red) are thought to be present but in low abundance. (C) Cartoon representation of cell plate composition as the cell plate continues to mature in later stages as cellulose (green) begin to replace callose (pink). When the cell plate transitions to a cross wall, it contains cell wall polysaccharides such as cellulose, hemicellulose (purple), pectin (red), and glycoproteins (not shown). Cell plate assembly is complete when the cell wall polysaccharides are organised into the typical cell wall meshwork of polysaccharides, with cellulose completely replacing callose.

#### POLYSACCHARIDE DEPOSITION AND ASSEMBLY OF THE NEW CELL WALL: CELLULOSE AND CALLOSE

Unlike the cytoskeleton and endomembrane trafficking components during cytokinesis, little is known about polysaccharide deposition and assembly during cell plate maturation. Most of the knowledge in the field is derived from

the detection of cell wall components using polysaccharide-specific epitopes and immunocytochemistry. Variations in the immunocytochemistry approaches and/or tissue types/preparations contribute to the challenge of distinguishing the various stages of the developing cell plate, thus understating the time-dependent transition of the process. A detailed study has been impeded by the technical limitations

to perform live imaging of polysaccharides. Though useful inhibitors are increasingly available to bypass the common lethality phenotypes of cytokinesis mutants, many challenges remain in understanding cell plate-specific polysaccharide deposition events.

Callose, a  $\beta$ -(1,3)-linked glucan, and cellulose, a  $\beta$ -(1,4)-linked glucan, are the two glucan polymers that are synthesised directly at the cell plate membrane. Our early understanding of callose deposition at the cell plate is based on a study by Samuels et al. (1995) using immuno electron microscopy on cryofixed samples. The deposition of callose in the cell plate is transient; it first appears at the TVN stage and is the dominant polysaccharide until the PFS stage (Samuels et al. 1995). It is also found at the junction of the parental cell wall connected with the cell plate, though its function at the cell junction remains unknown. Callose is the prominent component of the cell plate but, unlike cellulose, is rarely present in the fully mature cell wall except in plasmodesmata (Wu et al. 2018) and during transient responses such as response to external stressors (Chen and Kim 2009; Zaveska Drabkova and Honys 2017).

Although callose deposition at the cell plate has been well documented, the molecular understanding of its biosynthesis and removal remains elusive. The callose synthase (CalS) family, also known as the glucan synthase-like (GSL) family, comprises 12 members in Arabidopsis (Chen and Kim 2009). Among the 12 members, CalS10/GSL8 is likely responsible for callose deposition at the cell plate as *gsl8* mutants display typical cytokinetic effects that are seedling-lethal (Chen et al. 2009; Thiele et al. 2009; Guseman et al. 2010). Ectopically expressed CalS1/GSL6 has been localised to the cell plate of BY-2 cells (Hong et al. 2001); however, no cytokinesis defects in mutants have been reported thus far, suggesting that it is unlikely a major isoform contributing to the specificity of callose to cytokinesis. The major hurdles in studying the regulation of callose biosynthesis at the cell plate is the difficulty in generating functional fluorescently tagged CalS lines and conditional mutants that can be monitored in a temporal manner to determine the impact of loss of function in the development of the cell plate.

It has been suggested that CalSs work in a complex at the cell plate (Schneider et al. 2016; Zaveska Drabkova and Honys 2017). *gsl8* mutants show canonical cytokinesis defects and continue to be the only one in the family to show significant cytokinesis failures (Chen et al. 2009; Thiele et al. 2009; Guseman et al. 2010). Genetic and biochemical interactions between GSL8 and GSL10 make the latter a potential interactor of GSL8 at the cell plate. One plausible hypothesis is that callose synthases form complexes similar to cellulose synthases (Saatian et al. 2018). However, if a specific complex of GSL8 exists at the cell plate, its composition remains to be determined. The *in situ* biosynthesis of callose at the plasma membrane is supported by the direct appearance at the cell plate and its absence in secretory vesicles. Callose synthases are likely trafficked through TGN/early endosome (EE) pathways and have been identified

in TGN/EE proteomes such as that of SYP61 (Drakakaki et al. 2012), RABF2b/ARA7, and RABD2a/ARA5 (Heard et al. 2015). GSLs are also trafficked via unconventional trafficking pathways, with the involvement of either multivesicular bodies (Bohlenius et al. 2010) or exosomes (Ellinger et al. 2013). Such trafficking has been shown for the GSL isoform GSL5/PMR4 to sites of callose accumulation in response to the plant pathogen *Blumeria graminis* f. sp. *Hordei* (Ellinger et al. 2013), but information about the trafficking of GSL8 is lacking.

The biosynthesis of callose requires high concentrations of calcium (Him et al. 2001), suggesting that a calcium gradient proximal to the cell plate is required for its regulation (Wolniak et al. 1980; Aidemark et al. 2009). This has been a long-standing hypothesis based on observations made in the early 1970s describing the inhibition of cytokinesis resulting from reduced calcium levels after caffeine treatments (Paul and Goff 1973). In support of this hypothesis, a study found that cell plate formation in tobacco BY-2 cells is inhibited under treatment with BAPTA, a calcium chelating buffer (Jurgens M 1994). Similarly, the *Physcomitrella patens sabre* mutant has cytokinesis defects that are caused by abnormal ER-cell plate connections, and delayed/aberrant callose accumulation (Cheng and Bezanilla 2021). A tempting hypothesis is that the irregular callose pattern in the *sabre* mutant is due to abnormal calcium levels at the vicinity of the cell plate. In addition to synthesis and dynamic structure, the transient accumulation of callose requires regulated hydrolysis once the cell plate transforms into a new cell wall. Callose is synthesised at the plasma membrane and is thought to remain near the surface instead of embedding deeply into the cell plate lumen. This facilitates easy access to hydrolytic enzymes to remove the polymers once the cell plate is stabilised by additional polysaccharide deposition deep inside the structure as it matures (Albersheim et al. 2011). The (1,3)- $\beta$ -glucanase family contains 50 members in Arabidopsis; at present, no specific member has been assigned to callose degradation at the cell plate (Doxey et al. 2007; Levy et al. 2007).

Callose is rapidly deposited in the cell plate lumen (Samuels et al. 1995). Callose polymers are known to self-assemble into different structures (Falch and Stokke 2001). Further, single, double, and triple stranded loops can be formed, giving the polymer a dynamic rigidity and possibly contributing to its modularity in response to different triggers (Falch and Stokke 2001) (Figure 25.6B). With the advancement of imaging modules and the development of recombinantly expressed CalSs, different callose-formed structures, their conformation, and physicochemical properties can be better resolved.

The dominant and transient deposition of callose during the early delicate membrane network stage was postulated to mechanically stabilise the young cell plate until a more permanent cell wall is assembled (Samuels et al. 1995). In addition, the specific cytokinetic callose chemical inhibitor ES7 has been used to characterise the necessity for

callose at the cell plate and its dynamics (Park et al. 2014). Interestingly, ES7 does not inhibit wound or stress-induced callose accumulation. The inhibition of cytokinesis-specific callose accumulation with ES7 demonstrates a temporal dependency on callose in expansion and maturation of the cell plate in both land plants and algae, uncovering the evolutionarily conserved role of the polymer in the completion of cytokinesis (Park et al. 2014; Davis et al. 2020).

A recent study by Jawaid et al. (2022) used biophysical modelling to dissect the transition between the TVN stage to PFS and a mature cell plate. Cell plate sub-structures were approximated with testable shapes, and the Helfrich free energy model for membranes was adopted to understand the transition from a vesicular network to a fenestrated sheet and mature cell plate (Figure 25.3 D,E). To reach a mature cell plate (Figure 25.3 D,E), the proposed model requires an additional element: the onset of a two-dimensional spreading/stabilising force coupled with a concurrent loss of spontaneous curvature. The absence of a spreading/stabilising force predicts failure of maturation (Jawaid et al. 2022). The transient accumulation of callose, coinciding with the predicted stages requiring this spreading force, is consistent with the proposed model's concept, lending support for the role of callose in cell plate maturation (Jawaid et al. 2022).

Cellulose is the second polysaccharide directly synthesised at the cell plate (Chen et al. 2018). A distinguishing feature of cellulose deposition in higher-plant cell walls, in contrast to other cellulosic organisms, is its organisation into paracrystalline microfibrils, the deposition of which is associated with the orientation of the cortical microtubules (Ledbetter and Porter 1963). Cellulose microfibrils consist of  $\beta$ -(1,4)-linked glucans synthesised at the plasma membrane by cellulose synthase (CESA) complexes (CSCs) and are produced at the plasma membrane during late to completed cytokinesis stage. For detailed information about cellulose, please refer to Chapter 1 by Doblin et al. Though cellulose is the main load-bearing polymer in parental plant cell walls, cellulose appears to be only a minor component of the early stage cell plate (Samuels et al. 1995). For their biosynthetic function, each cellulose synthase complex requires a minimum of three catalytic cellulose synthase proteins (Desprez et al. 2007; Persson et al. 2007; Wilson et al. 2021). Although not present until the late stages of cytokinesis, specific cellulose-deficient mutants exhibit cytokinesis-deficient phenotypes, suggesting an essential role for cellulose in cell plate maturation (Zuo et al. 2000).

The temporal dynamics of cellulose at the cell plate was first observed by electron microscopy in tobacco BY-2 and *Arabidopsis* root tip cells (Samuels et al. 1995). During the late TN stage, cellulose deposition begins. The deposition of cellulose coincides with the flattening and stiffening of the cell plate as its content increases steadily through the remaining stages, mainly the PSF, seemingly replacing callose (Samuels et al. 1995). In 2014, *in vivo* imaging of cellulose synthase reported its accumulation at the TVN stage, concurrent with the presence of cellulose (Miart et al. 2014). This study also suggested that CSC delivery occurs through

phragmoplast-associated vesicles during the TVN stage or directly by the Golgi apparatus to the CPAM (Miart et al. 2014) (Figure 25.6C). Variations in immunocytochemistry approaches and/or tissues paired with the challenge to distinguish the different maturation stages that simultaneously occur at the developing cell plate could account for the contrasting information on the timing of cellulose biosynthesis at the cell plate.

Recently, it has been shown that one member of the Cellulose Synthase-Like D family, CSLD5, is targeted to newly forming cell plates of dividing cells (Park et al. 2011; Gu et al. 2016). The direct product of CSLD5 has not yet been identified, but similar to the product of CSLD3, it is likely a  $\beta$ -(1,4)-glucan polysaccharide (Yang et al. 2020), providing a framework for crystalline cellulose (Figure 25.6A).

### GOLGI-SYNTHESISED POLYSACCHARIDES AND STRUCTURAL PROTEINS

The matrix polysaccharides hemicellulose and pectin are synthesised in the Golgi apparatus and transported to the cell plate via Golgi-derived vesicles. *Hemicellulose* in dicotyledonous plants is most abundant as xyloglucan (XyG), a  $\beta$ -1,4 glucan, featuring a regular pattern of xylosylations (Keegstra 2010; Scheller and Ulvskov 2010; Pauly and Keegstra 2016; Julian and Zobotina 2022). The molecular machinery for its biosynthesis in the Golgi is well understood (Julian and Zobotina 2022) and described in detail in Chapter 2. Notably, no studies have been conducted focusing on the localisation and behaviour of biosynthetic proteins specifically during cytokinesis, except the presence of endoxyloglucan transferase (EXGT), a cellulose/xyloglucan network modifying enzyme (Yokoyama and Nishitani 2001). Most of our current knowledge of matrix cell wall polysaccharide transport is derived from a very limited number of immunohistochemical electron microscopy analyses using antibodies raised against polysaccharide epitopes (Moore et al. 1986; Moore and Staehelin 1988; Moore et al. 1991; Lynch and Staehelin 1992; McFarlane et al. 2008; Young et al. 2008; Kang et al. 2011). An early study in sycamore maple (*Acer pseudoplatanus*) cells suggests an “assembly line” model consisting of the initial biosynthesis of the XyG backbone followed by the addition of side chains in Golgi sub-compartments, with the TGN largely containing fully substituted XyG glycans (Zhang and Staehelin 1992). However, recent vesicle glycomic studies using a large-scale antibody ELISA of TGN/EE-isolated vesicles marked by the syntaxin SYP61 suggest that diverse glycans are generated in Golgi/TGN and are transported to the apoplast in their final assembly (Wilkop et al. 2019). Studies using red clover roots have shown that during cell division, XyG is transported through TGN-derived secretory vesicles to the forming cell plate. The polysaccharide is detected at the TVN stage, most likely delivered by secretory vesicles, with its presence most abundant upon completion of the new cell wall (Moore and Staehelin 1988).

The presence of a cellulose/xyloglucan network modifying enzyme at the cross wall of dividing BY-2 cells suggests polysaccharide modification during cell wall assembly at the cell plate (Yokoyama and Nishitani 2001).

While the type of secretory vesicles that carry polysaccharides to the cell plate and their cargo is still largely unknown, glycomic analysis of SYP61 TGN/EE vesicles has shown that this pathway is involved in the traffic of both XyG and pectin oligosaccharides. The ECHIDNA (ECH) and the YIP family of RAB GTPase interacting proteins associated with SYP61 are implicated in TGN polysaccharide trafficking (Gendre et al. 2011; Kang et al. 2011; Gendre et al. 2013; McFarlane et al. 2013). Therefore, it is plausible that TGN/EE subdomains, including the aforementioned components and the SNARE proteins SYP42/SYP43 (Uemura et al. 2012), are involved in polysaccharide secretion. During cytokinesis, the whole secretory machinery is recruited towards the development of the cell plate; thus, it is likely that similar to the SYP61 pathway, cytokinetic vesicles carry xyloglucan oligosaccharides in different forms of substitution for their assembly into the nascent cell wall. A daunting task remains in the glycomic analysis of cytokinetic vesicles. Specifically, when isolated with the help of cytokinetic markers, it will be necessary to dissect the forms of hemicellulose oligosaccharides that are transported to the cell plate.

*Pectin*, first isolated in 1825 by the French chemist and pharmacist Henri Braconnot, is another Golgi-synthesised polysaccharide. The pectin structure comprises a backbone with galacturonic acid residues, with subgroups determining its diversification and classification into the following main types: homogalacturonan (HG), rhamnogalacturonan I (RG-I), and rhamnogalacturonan II (RG-II), and substituted galacturonans. Pectin accounts for up to 35% of the primary cell wall in dicotyledonous plants, and the other polysaccharides are considered to be embedded in it (Mohnen 2008; Caffall and Mohnen 2009; Atmodjo et al. 2013; Du et al. 2022). For a more in-depth discussion on pectin structure and biosynthesis, refer to Chapter 5. The backbones of all pectins are synthesised in the Golgi with side group modifications thought to be added in different Golgi cisternae, which are presumably transported to the cell plate through secretory vesicles. Non-esterified RG-I and HG are present in the *cis* and medial Golgi, while arabinose-containing side chains of RG-I are detected only in the TGN, demonstrating specificity of Golgi cisternae in pectin biosynthesis (Zhang and Staehelin 1992). While pectins are synthesised and secreted in a methyl esterified form at the cell wall, they are de-esterified by pectin methyl-esterases (PMEs), which leads to their acidification and allows for further cross-linking (Caffall and Mohnen 2009; Albersheim et al. 2011). The presence of methyl esterified pectin at the cell plate has been detected with the aid of the JIM7 monoclonal antibody at the cell plate of Arabidopsis and BY-2 dividing cells (Toyooka et al. 2009; Rybak et al. 2014). The absence of RG-I in the cell plate using RG-I-specific polyclonal antibodies, but presence in the middle

lamella of red clover (*Trifolium pretense* L.), suggests that acidification of the polysaccharide occurs at later stages (Moore and Staehelin 1988).

PMEs have also been shown to be transported to the cell plate through a Golgi-derived, but TGN-independent pathway in tobacco BY-2 cells, as demonstrated by Brefeldin A (BFA) insensitivity (Wang et al. 2016). RG-II, a more complex form of pectin, serves as the site of borate cross-linking within pectin to facilitate gel formation. Notably, RG-II has also been detected at the cell plate, which was illustrated using immunoelectron microscopy in tobacco BY-2 cells (Zhou et al. 2017).

The association of specific molecular components of endomembrane trafficking and the corresponding pathways that are specialised in polysaccharide delivery to the cell plate are currently limited to a small number of proteins involved in vesicle trafficking. These include the Secretory Carrier Membrane Protein 2 (SCAMP2), which is associated with the transport of methyl esterified pectin to the cell plate (Toyooka et al. 2009) or tethering complexes, such as the Exocyst and TRAPP II, associated with pectin delivery at the cell plate (Rybak et al. 2014).

The few studies in this field combined with variation within cell types and species dependencies account for our limited understanding of vesicle-mediated polysaccharide transport at the cell plate (Drakakaki 2015; Sinclair et al. 2022). The recent glycomic analysis of SYP61 TGN/EE vesicles showed that both matrix oligosaccharide glycans can be present in the same vesicle population (Wilkop et al. 2019). Interestingly, both methyl esterified pectin and the partially esterified pectin HG backbone were included in the SYP61 glycome, suggesting that both forms of pectin may exist throughout the endomembrane system (Wilkop et al. 2019). It is likely that a combination of pectin glycans are also transported to the cell plate via cytokinetic vesicles, which should be further investigated via glycomic analysis. Given that secretory traffic is heavily recruited towards cell plate formation (Richter et al. 2014) and that the abundance of structural polysaccharides increases in later stages of cell plate formation, a question remains on the regulation of polysaccharide deposition during cytokinesis. One plausible hypothesis is that the regulation is directly conducted on the biosynthesis level at the Golgi apparatus before transport and sorting takes place.

During the fusion of the cross wall with the mother cell wall, the cell plate membrane fuses with the plasma membrane of the mother cell. Initially, the cross wall is generally homogeneous and is continuously developed via the deposition of cellulose and other matrix polysaccharides on each side. This generates a central layer rich in pectin known as the *middle lamella*. Dissolution of the region within the mother cell wall at the junction with the cross wall allows for the rearrangement of the cell wall, its development, and the generation of a three-way junction (Albersheim et al. 2011). The pectin-rich middle lamella differentiates as the adjacent cell wall develops in

sequence via a mechanism that it is not well understood. De-esterification of HG along with abundance of RG-I in the middle lamella (Moore and Staehelin 1988) suggest a maturation step and stiffening process of the negatively charged pectin molecules. The middle lamella cements the two daughter cells together and provides a source of adhesion and cell separation as well as helps to transfer load distribution. Further, it accommodates cell to cell communication, changes in cell geometry, and is involved in modification of cell wall chemistry in response to abiotic stress (reviewed in Zamil and Geitmann 2017). Interestingly, in the onion epidermis, cell fracture does not occur directly at the middle lamella but instead at the cell wall (Zamil et al. 2014, 2015), emphasising its mechanical properties and supporting the load-bearing role of pectin in the cell wall (Dick-Pérez et al. 2011; Peaucelle et al. 2012; Cosgrove 2022). Further, the spatial distribution of pectin modifications in the middle lamella reflects their mechanical role against load-bearing forces (Zamil and Geitmann 2017). With the combination of modelling and tools to study the spatiotemporal biochemical transition and the physicochemical properties of this layer, we will gain a better understanding of how the middle lamella differentiates and responds to the diverse stresses that it can face. For further information regarding aspects of the middle lamella and its applications, please see Chapters 23 and 24.

*Structural proteins* of the cell wall contribute to its physical properties but have no described catalytic activity. Structural proteins constitute roughly 5–10% of the cell wall dry matter (Jamet et al. 2008). These include glycine-rich proteins (GRPs), proline-rich proteins (PRPs), and hydroxyproline-rich glycoproteins (HRGPs), which are so named after the amino acids they enrich. A fourth class, arabinogalactan proteins (AGPs), has been implicated in diverse roles such as cell–cell recognition, cell fate, embryogenesis, and xylem development within a number of species (Albersheim et al. 2011; Showalter and Basu 2016; Silva et al. 2020). An in-depth review of AGPs is provided in Chapter 16.

A member of HRP, EXTENSIN3 (EXT3), is specifically associated with cell plate development. EXTENSINs self-assemble into dendritic networks (Cannon et al. 2008). This form of self-assembly structure has the potential to react with negatively charged pectin, affecting the organisation of the new cell wall material and the overall cell wall assembly during late cytokinesis (Cannon et al. 2008). AtEXT3 was enriched in the junctions of the mother cell wall and the leading edge of the cell plate, and was shown to be critical in the completion of cell wall formation in *Arabidopsis* (Hall and Cannon 2002; Cannon et al. 2008). Interestingly, recent studies showed that AtEXT3 is not essential for embryogenesis and plant development in *Arabidopsis*, suggesting that its function is likely redundant with other related proteins (Doll et al. 2022). In addition to AtEXT3, AGPs labelled by the monoclonal antibody LM14 have been detected at the cell plate, emphasising the overall importance of AGPs at the cell plate (Yu and Zhao 2012).

The expansion and maturation of the cell plate associates with microtubule depolymerisation. The communication of the expanding cell plate with the phragmoplast is likely carried by complex networks that include the aforementioned kinase pathways as well as other proteins (Smertenko et al. 2018). Many discoveries are awaiting with regard to the identification of these signalling components.

## CHALLENGES, EMERGING TECHNOLOGIES, AND FUTURE PERSPECTIVES

Cell plate development is a process that requires both spatial and temporal resolution. Compared to the large number of publications on vesicle trafficking during plant cytokinesis that describe several molecular components, such as SNARE complexes, GTPases, and tethering factors (McMichael and Bednarek 2013; Jurgens et al. 2015; Smertenko et al. 2017; Gu and Rasmussen 2022), the literature related to polysaccharide deposition during cell plate formation is limited. Formative studies based on electron microscopy and tomography coupled with antibody labelling of polysaccharides provide excellent resolution and have shaped our current conceptual models (Moore and Staehelin 1988; Samuels et al. 1995; Segui-Simarro et al. 2004). However, electron microscopy is a laborious and destructive process, limiting the number of studies that can be undertaken. To capture the different cytokinetic stages that occur simultaneously in an expanding cell plate (see Video S1 in Sinclair et al. 2022), a four-dimensional (4D) approach is required to depict long-term imaging in a biologically relevant (i.e., multicellular) system. This poses several challenges and opportunities for development.

Historically, ultrastructural and immunofluorescence studies were followed by genetic screenings, which allowed for the identification of several key proteins and interesting mutants in cytokinesis. However, in-depth investigations are hampered by lethal phenotypes (Sollner et al. 2002; Strompen et al. 2002; McMichael and Bednarek 2013). Live imaging using fluorescent proteins and other probes has informed dynamics of endomembrane components that are amenable to tagging. However, several proteins, some of which have enzymatic activity and are multi-spanning membrane proteins, are recalcitrant to fluorescent tagging or recombinant expression. CRISPR-Cas9 editing, inducible systems that can be cell cycle-induced, conditional mutants, such as the temperature-sensitive *tplate* mutant (Wang et al. 2021), and recombineering toolsets for direct chromosomal tagging (Brumos et al. 2020) can allow for functional analyses that overcome many of the challenges faced with canonical cytokinesis mutants. The advancement of single cell omics technologies may prove instrumental in combination with cell cycle markers to establish expression and biochemical profiles. In addition, it may lead to gene discovery in regulatory components. Further, *in silico* protein structure analysis, such as AlphaFold (Callaway 2022), can expedite the functional characterisation of identified proteins.

Because it overcomes lethality challenges, chemical biology has played an important role in dissecting cell plate development. For example, by specifically inhibiting cytokinetic callose deposition, the small molecule ES7 informed the role of this polymer in cytokinesis, which was tested using a biophysical model that dissected the behaviour of endomembrane components during cell plate development (Park et al. 2014; Davis et al. 2016; Jawaid et al. 2022). Similarly, SMIFH2 informed the role of formins in cytokinesis (Zhang et al. 2021). Furthermore, the use of nanotechnology in plants as sensors, probes, and delivery vehicles holds promise in both imaging, chemical, and genetic manipulation of cell plate development (Kwak et al. 2017; Lew et al. 2018; Dong et al. 2019; Sanzari et al. 2019).

Extensive biochemical analysis on the polysaccharide content of a cell plate is challenging due to the diverse stages of cytokinesis in plants. Further, comparisons of reported studies on diverse sets of plant systems is an added complexity. The ever-increasing number of antibodies to visualise specific polysaccharide epitopes are useful in understanding the *de novo* formation of the new cell wall (Pattathil et al. 2010; Hervé et al. 2011; Lee et al. 2011; Avci et al. 2012; Duffieux et al. 2020). These antibodies can be coupled with electron tomography analysis of dividing cells (Otegui 2020). In addition, they can facilitate large-scale analysis of subcellular compartments, as shown for Golgi or specialised TGN populations, to better understand transport routes of polysaccharide cargo of cytokinetic vesicles (Okekeogbu et al. 2019; Parsons et al. 2019; Wilkop et al. 2019). While these antibodies can be informative enough to provide a biochemical profile of isolated cell walls, subcellular compartments, and hopefully cytokinetic vesicles, their incorporation in a live imaging system still awaits development. It is potentially worth exploring the isolation of specific antibody fragments that can be genetically encoded and targeted at the cell plate.

Recent light microscopy advances allow for a better understanding of plant cell dynamics (Komis et al. 2018; DeVree et al. 2021). Super resolution techniques can provide more insight into the specificity of cytokinetic vesicles and the different cell plate stages, while light sheet microscopy provides information about cell plate development dynamics under longer temporal imaging of events. Structured illumination microscopy has been instrumental to better understand CESA dynamics at the PM (Duncombe et al. 2022) and can potentially be applied to dissect protein dynamics at different cell plate stages. Lattice light sheet microscopy (LLSM) affords imaging at much faster rates, with less light exposure of the sample, minimising photobleaching and phototoxic effects (Chen et al. 2014); this can extend the observation time necessary to capture cytokinesis events. LLSM has been used to dissect mitosis and endomembrane dynamics in a variety of systems (Chen et al. 2014; Aguet et al. 2016; Sen et al. 2021). Plant research is slowly embracing the benefits that light sheet microscopy and vertical imaging have to offer (Vypelová

et al. 2017; Glanc et al. 2018; Ovečka et al. 2021). However, the potential of LLSM has not been explored to understand mechanisms that regulate cytokinesis in plants.

Additionally, there has been a recent increase in both qualitatively and quantitatively analysing microscopy results, which in turn can be used to build cell plate development models and interrogate specific components. Quantitative analysis can help dissect characteristic patterns of vesicle motion during developmental stages by using spatiotemporal image correlation spectroscopy (STICS), an imaging domain extension of fluorescence correlation spectroscopy, overcoming the diffraction limits of light microscopy (van Oostende-Triplet et al. 2017). Further, the development of custom image analysis software, such as Fluorescence Morphological Operators Software (FluMOS), allows for the automated measurement of the dimensions of the expanding cell plate and the distinction of different phases during cell plate expansion (van Oostende-Triplet et al. 2017). Artificial intelligence can be used to analyse large datasets by image segmentation, classification, and restoration, overcoming many of the challenges of microscopy (von Chamier et al. 2019). The development of biophysical and mathematical models for cell plate development (Jawaid et al. 2022) can provide insights into the contribution of individual components in cytokinesis and can be used to interrogate the biomechanical contribution of polysaccharides in cell plate maturation. Similarly, 3D cell shape segmentation coupled with modelling can facilitate the prediction of division-plane orientations and aid in the characterisation of contributing proteins (Martinez et al. 2018). Such synergy of information can help inform how cell plate development is regulated.

The generation of probes that allow live imaging of the cell wall, such as Pontamine Fast Scarlet 4B for cellulose, aniline blue fluorochrome for callose, fluorophore-functionalised chitosan oligosaccharides (COS), and metabolic click-mediated labelling for pectin (Anderson et al. 2012; DeVree et al. 2021; Ropitiaux et al. 2022), are necessary to understand the spatiotemporal transition of cell plate development and maturation (DeVree et al. 2021). To date, the combination of imaging both cell wall biosynthetic enzymes together with their products remains a challenge but promises to uncover how cell wall assembly is regulated during cytokinesis.

Biomechanical readouts of the cell plate are necessary to interrogate biophysical models. Once adapted to study cytokinesis, biomechanical methods using Brillouin microscopy, which assess stiffness through the thickness of the cell wall (Prevedel et al. 2019, Altartouri et al. 2019), or atomic force microscopy, which can assess external topography and elasticity of plant cells (Braybrook 2015), will be able to better describe the changes in the transition of the cell plate to a new cell wall and how this is regulated in different genetic backgrounds. Focused ion beam scanning electron microscopy (Czymmek et al. 2020; Weiner et al. 2021; Zechmann et al. 2022) has become more accessible

through the development of commercial instrumentation that can complement studies using serial sectioning transmission electron microscopy, and thus contributes to an increased pool of 3D cell plate reconstructions that can be used to inform developing models. Biochemical analysis of isolated compartments (Wilkop et al. 2019; Dahhan et al. 2022) has been instrumental in identifying both protein and biochemical cargo, and its adaptation for isolating cytokinetic vesicles can reveal the nature of diverse cargo transported at the cell plate.

Over the last 50 years, the characterisation of cell plate development and identification of several molecular components has been achieved; however, many questions remain unanswered. Some of these related to cell plate expansion are as follows: (i) How many types of cytokinetic vesicles exist and what is their cargo? (ii) Which motor proteins specifically regulate cytokinetic vesicles and cargo delivery to the CPAM? (iii) What are the signalling mechanisms regulating cell plate orientation, cell plate expansion, and phragmoplast organisation? (iv) How is phragmoplast guidance achieved mechanistically? (v) What are the physicochemical properties of the assembled polysaccharide deposits during cell plate formation? (vi) How do specific polysaccharides, such as callose, contribute to the two-dimensional spreading force necessary for cell plate expansion and maturation? (vii) What regulates the fusion of the cell plate with the parental cell wall? (viii) What polysaccharides are deposited in each stage of cell plate development and how is this regulated? (ix) What is the function of the PPB? With all these tools in place, exciting discoveries in plant cytokinesis are awaiting, which together will form a complete picture of the formation of such an essential and dynamic structure for plant development—the new cell wall.

## ACKNOWLEDGEMENTS

We apologise to colleagues whose work could not be included in this review due to space limitations. This work was supported by NSF, Grant MCB 1818219 and by a Hatch grant from the United States Department of Agriculture (CA-D-PLS-2132-H). We would like to thank Dr. Buschmann for the thorough and constructive comments on this chapter. This chapter is dedicated in the memory of Prof. Andrew Staehelin for his ground breaking discoveries in plant cytokinesis and cell walls as well as his dedication to training of plant cell biologists.

## REFERENCES

Aguet F, Upadhyayula S, Gaudin R, Chou YY, Cocucci E, He K, Chen BC, Mosaliganti K, Pasham M, Skillern W, Legant WR, Liu TL, Findlay G, Marino E, Danuser G, Megason S, Betzig E, Kirchhausen T (2016) Membrane dynamics of dividing cells imaged by lattice light-sheet microscopy. *Mol Biol Cell* 27:3418–3435.

Ahn CS, Han JA, Pai HS (2013) Characterization of in vivo functions of *Nicotiana benthamiana* RabE1. *Planta* 237:161–172.

Aidemark M, Andersson CJ, Rasmusson AG, Widell S (2009) Regulation of callose synthase activity in situ in alamethicin-permeabilized *Arabidopsis* and tobacco suspension cells. *BMC Plant Biol* 9:27.

Albersheim P, Darvill A, Roberts K, Sederoff R, Staehelin LA (2011) Plant Cell Walls. Garland Science, New York.

Altartouri B, Bidhendi AJ, Tani T, Conrad C, Chebli Y, Liu N, Karunakaran C, Scarcelli G, Geitmann A (2019) Pectin chemistry and cellulose crystallinity govern pavement cell morphogenesis in a multi-step mechanism. *Plant Physiology* 181:127–141.

Anderson CT, Wallace IS, Somerville CR (2012) Metabolic click-labeling with a fucose analog reveals pectin delivery, architecture, and dynamics in *Arabidopsis* cell walls. *Proc Natl Acad Sci U S A* 109:1329–1334.

Asada T, Sonobe S, Shibaoka H (1991) Microtubule translocation in the cytokinetic apparatus of cultured tobacco cells. *Nature* 350:238–241.

Assaad FF, Huet Y, Mayer U, Jurgens G (2001) The cytokinesis gene KEULE encodes a Sec1 protein that binds the syntaxin KNOLLE. *J Cell Biol* 152:531–543.

Atmodjo MA, Hao ZY, Mohnen D (2013) Evolving views of pectin biosynthesis. *Annual Review of Plant Biology* 64:747–+.

Avci U, Pattathil S, Hahn MG (2012) Immunological approaches to plant cell wall and biomass characterization: immunolocalization of glycan epitopes. *Methods Mol Biol* 908:73–82.

Bellinger MA, Uyehara AN, Martinez P, McCarthy MC, Rasmussen CG (2021) Cell cortex microtubules contribute to division plane positioning during telophase in maize. *BioRxiv preprint server for biology*.

Besson S, Dumais J (2014) Stochasticity in the symmetric division of plant cells: when the exceptions are the rule. *Front Plant Sci* 5:538.

Bohlenius H, Morch SM, Godfrey D, Nielsen ME, Thordal-Christensen H (2010) The multivesicular body-localized GTPase ARFA1b/1c is important for callose deposition and ROR2 syntaxin-dependent preinvasive basal defense in barley. *Plant Cell* 22:3831–3844.

Boruc J, Van Damme D (2015) Endomembrane trafficking over-arching cell plate formation. *Curr Opin Plant Biol* 28:92–98.

Boutté Y, Frescatada-Rosa M, Men S, Chow CM, Ebine K, Gustavsson A, Johansson L, Ueda T, Moore I, Jürgens G, Grebe M (2010) Endocytosis restricts *Arabidopsis* KNOLLE syntaxin to the cell division plane during late cytokinesis. *Embo j* 29:546–558.

Braybrook SA (2015) Measuring the elasticity of plant cells with atomic force microscopy. *Methods Cell Biol* 125:237–254.

Brumos J, Zhao C, Gong Y, Soriano D, Patel AP, Perez-Amador MA, Stepanova AN, Alonso JM (2020) An improved recombinering toolset for plants. *Plant Cell* 32:100–122.

Buschmann H, Chan J, Sanchez-Pulido L, Andrade-Navarro MA, Doonan JH, Lloyd CW (2006) Microtubule-associated AIR9 recognizes the cortical division site at preprophase and cell-plate insertion. *Curr Biol* 16:1938–1943.

Buschmann H, Zachgo S (2016) The evolution of cell division: from streptophyte algae to land plants. *Trends Plant Sci* 21:872–883.

Buschmann H, Müller S (2019) Update on plant cytokinesis: rule and divide. *Curr Opin Plant Biol* 52:97–105.

Caffall KH, Mohnen D (2009) The structure, function, and biosynthesis of plant cell wall pectic polysaccharides. *Carbohydr Res* 344:1879–1900.

Callaway E (2022) What's next for AlphaFold and the AI protein-folding revolution. *Nature* 604:234–238.

- Cannon MC, Terneus K, Hall Q, Tan L, Wang Y, Wegenhart BL, Chen L, Lamport DT, Chen Y, Kieliszewski MJ (2008) Self-assembly of the plant cell wall requires an extensin scaffold. *Proc Natl Acad Sci U S A* 105:2226–2231.
- Chen XY, Kim JY (2009) Callose synthesis in higher plants. *Plant Signal Behav* 4:489–492.
- Chen XY, Liu L, Lee E, Han X, Rim Y, Chu H, Kim SW, Sack F, Kim JY (2009) The arabidopsis callose synthase gene *GSL8* is required for cytokinesis and cell patterning. *Plant Physiology* 150:105–113.
- Chen BC, Legant WR, Wang K, Shao L, Milkie DE, Davidson MW, Janetopoulos C, Wu XS, Hammer JA, 3rd, Liu Z, English BP, Mimori-Kiyosue Y, Romero DP, Ritter AT, Lippincott-Schwartz J, Fritz-Laylin L, Mullins RD, Mitchell DM, Bembenek JN, Reymann AC, Böhme R, Grill SW, Wang JT, Seydoux G, Tulu US, Kiehart DP, Betzig E (2014) Lattice light-sheet microscopy: imaging molecules to embryos at high spatiotemporal resolution. *Science* 346:1257998.
- Chen HW, Persson S, Grebe M, McFarlane HE (2018) Cellulose synthesis during cell plate assembly. *Physiol Plant* 164:17–26.
- Cheng X, Bezanilla M (2021) SABRE populates ER domains essential for cell plate maturation and cell expansion influencing cell and tissue patterning. *Elife* 10:e65166.
- Cheung AY, Cosgrove DJ, Hara-Nishimura I, Jürgens G, Lloyd C, Robinson DG, Staehelin LA, Weijers D (2022) A rich and bountiful harvest: Key discoveries in plant cell biology. *Plant Cell* 34:53–71.
- Chow CM, Neto H, Foucart C, Moore I (2008) Rab-A2 and Rab-A3 GTPases define a trans-golgi endosomal membrane domain in Arabidopsis that contributes substantially to the cell plate. *Plant Cell* 20:101–123.
- Cleary AL, Smith LG (1998) The Tangled1 gene is required for spatial control of cytoskeletal arrays associated with cell division during maize leaf development. *Plant Cell* 10:1875–1888.
- Cosgrove DJ (2022) Building an extensible cell wall. *Plant Physiology* 189(3):1246–1277.
- Cutler SR, Ehrhardt DW (2002) Polarized cytokinesis in vacuolate cells of Arabidopsis. *Proc Natl Acad Sci U S A* 99:2812–2817.
- Czymmek K, Sawant A, Goodman K, Pennington J, Pedersen P, Hoon M, Otegui MS (2020) Imaging Plant Cells by High-Pressure Freezing and Serial block-face scanning electron microscopy. *Methods Mol Biol* 2177:69–81.
- Dahhan DA, Bednarek SY (2022) Advances in structural, spatial, and temporal mechanics of plant endocytosis. *FEBS Lett* 596(17):2269–2287.
- Dahhan DA, Reynolds GD, Cárdenas JJ, Eeckhout D, Johnson A, Yperman K, Kaufmann WA, Vang N, Yan X, Hwang I, Heese A, De Jaeger G, Friml J, Van Damme D, Pan J, Bednarek SY (2022) Proteomic characterization of isolated Arabidopsis clathrin-coated vesicles reveals evolutionarily conserved and plant-specific components. *Plant Cell* 34(6):2150–2173.
- Davis DJ, McDowell SC, Park E, Hicks G, Wilkop TE, Drakakaki G (2016) The RAB GTPase RABA1e localizes to the cell plate and shows distinct subcellular behavior from RABA2a under Endosidin 7 treatment. *Plant Signal Behav* 11:e984520.
- Davis DJ, Wang M, Sørensen I, Rose JKC, Domozych DS, Drakakaki G (2020) Callose deposition is essential for the completion of cytokinesis in the unicellular alga *Penium margaritaceum*. *J Cell Sci* 133.
- Desprez T, Juraniec M, Crowell EF, Jouy H, Pochylova Z, Parcy F, Hofte H, Gonneau M, Vernhettes S (2007) Organization of cellulose synthase complexes involved in primary cell wall synthesis in Arabidopsis thaliana. *Proc Natl Acad Sci U S A* 104:15572–15577.
- DeVree BT, Steiner LM, Głazowska S, Ruhnnow F, Herburger K, Persson S, Mravec J (2021) Current and future advances in fluorescence-based visualization of plant cell wall components and cell wall biosynthetic machineries. *Biotechnol Biofuels* 14:78.
- Dick-Pérez M, Zhang Y, Hayes J, Salazar A, Zabolina OA, Hong M (2011) Structure and interactions of plant cell-wall polysaccharides by two- and three-dimensional magic-angle-spinning solid-state NMR. *Biochemistry-Columbus* 50:989.
- Doll NM, Berenguer E, Truskina J, Ingram G (2022) AtEXT3 is not essential for early embryogenesis or plant viability in Arabidopsis. *New Phytol* 236:1629–1633.
- Dong R, Li Y, Li W, Zhang H, Liu Y, Ma L, Wang X, Lei B (2019) Recent developments in luminescent nanoparticles for plant imaging and photosynthesis. *Journal of Rare Earths* 37:903–915.
- Doxey AC, Yaish MW, Moffatt BA, Griffith M, McConkey BJ (2007) Functional divergence in the Arabidopsis beta-1,3-glucanase gene family inferred by phylogenetic reconstruction of expression states. *Mol Biol Evol* 24:1045–1055.
- Drakakaki G (2015) Polysaccharide deposition during cytokinesis: Challenges and future perspectives. *Plant Sci* 236:177–184.
- Drakakaki G, van de Ven W, Pan S, Miao Y, Wang J, Keinath NF, Weatherly B, Jiang L, Schumacher K, Hicks G, Raikhel N (2012) Isolation and proteomic analysis of the SYP61 compartment reveal its role in exocytic trafficking in Arabidopsis. *Cell Res* 22:413–424.
- Du J, Anderson CT, Xiao C (2022) Dynamics of pectic homogalacturonan in cellular morphogenesis and adhesion, wall integrity sensing and plant development. *Nat Plants* 8:332–340.
- Duffieux D, Marcus SE, Knox JP, Hervé C (2020) Monoclonal Antibodies, Carbohydrate-Binding Modules, and Detection of Polysaccharides in Cell Walls from Plants and Marine Algae. *Methods Mol Biol* 2149:351–364.
- Duncombe SG, Chethan SG, Anderson CT (2022) Super-resolution imaging illuminates new dynamic behaviors of cellulose synthase. *Plant Cell* 34:273–286.
- El Kasmi F, Krause C, Hiller U, Stierhof YD, Mayer U, Conner L, Kong L, Reichardt I, Sanderfoot AA, Jurgens G (2013) SNARE complexes of different composition jointly mediate membrane fusion in Arabidopsis cytokinesis. *Mol Biol Cell* 24:1593–1601.
- Ellinger D, Naumann M, Falter C, Zwikowics C, Jamrow T, Manisseri C, Somerville SC, Voigt CA (2013) Elevated early callose deposition results in complete penetration resistance to powdery mildew in Arabidopsis. *Plant Physiol* 161:1433–1444.
- Errera L (1886) Sur une condition fondamentale d'équilibre des cellules vivantes. *Annales de la Société belge de microscopie* 13:12–16.
- Euteneuer U, McIntosh JR (1980) Polarity of midbody and phragmoplast microtubules. *J Cell Biol* 87:509–515.
- Falch BH, Stokke BT (2001) Structural stability of (1→3)-β-D-glucan macrocycles. *Carbohydr Polym* 44:113–121.
- Farmer T, Prekeris R (2022) New signaling kid on the block: the role of the postmitotic midbody in polarity, stemness, and proliferation. *Mol Biol Cell* 33:pe2.

- Fujimoto M, Arimura S, Nakazono M, Tsutsumi N (2008) Arabidopsis dynamin-related protein DRP2B is co-localized with DRP1A on the leading edge of the forming cell plate. *Plant Cell Rep* 27:1581–1586.
- Fujimoto M, Arimura S, Ueda T, Takanashi H, Hayashi Y, Nakano A, Tsutsumi N (2010) Arabidopsis dynamin-related proteins DRP2B and DRP1A participate together in clathrin-coated vesicle formation during endocytosis. *Proc Natl Acad Sci U S A* 107:6094–6099.
- Gadeyne A, Sanchez-Rodriguez C, Vanneste S, Di Rubbo S, Zaubner H, Vanneste K, Van Leene J, De Winne N, Eeckhout D, Persiau G, Van De Slijke E, Cannoot B, Vercruyse L, Mayers JR, Adamowski M, Kania U, Ehrlich M, Schweighofer A, Ketelaar T, Maere S, Bednarek SY, Friml J, Gevaert K, Witters E, Russinova E, Persson S, De Jaeger G, Van Damme D (2014) The TPLATE adaptor complex drives clathrin-mediated endocytosis in plants. *Cell* 156:691–704.
- Gendre D, McFarlane HE, Johnson E, Mouille G, Sjodin A, Oh J, Levesque-Tremblay G, Watanabe Y, Samuels L, Bhalerao RP (2013) Trans-Golgi network localized ECHIDNA/Ypt interacting protein complex is required for the secretion of cell wall polysaccharides in Arabidopsis. *Plant Cell* 25:2633–2646.
- Gendre D, Oh J, Boutte Y, Best JG, Samuels L, Nilsson R, Uemura T, Marchant A, Bennett MJ, Grebe M, Bhalerao RP (2011) Conserved Arabidopsis ECHIDNA protein mediates trans-Golgi-network trafficking and cell elongation. *Proc Natl Acad Sci U S A* 108:8048–8053.
- Glanc M, Fendrych M, Friml J (2018) Mechanistic framework for cell-intrinsic re-establishment of PIN2 polarity after cell division. *Nature Plants* 4:1082–1088.
- Glotzer M (2005) The molecular requirements for cytokinesis. *Science* 307:1735–1739.
- Gu F, Bringmann M, Combs JR, Yang J, Bergmann DC, Nielsen E (2016) Arabidopsis CSLD5 functions in cell plate formation in a cell cycle-dependent manner. *Plant Cell* 28:1722–1737.
- Gu Y, Rasmussen CG (2022) Cell biology of primary cell wall synthesis in plants. *Plant Cell* 34:103–128.
- Gunning BE, Hardham AR, Hughes JE (1978) Evidence for initiation of microtubules in discrete regions of the cell cortex in Azolla root-tip cells, and an hypothesis on the development of cortical arrays of microtubules. *Planta* 143:161–179.
- Guseman JM, Lee JS, Bogenschutz NL, Peterson KM, Virata RE, Xie B, Kanaoka MM, Hong Z, Torii KU (2010) Dysregulation of cell-to-cell connectivity and stomatal patterning by loss-of-function mutation in Arabidopsis chorus (glucan synthase-like 8). *Development* 137:1731–1741.
- Hall Q, Cannon MC (2002) The cell wall hydroxyproline-rich glycoprotein RSH is essential for normal embryo development in Arabidopsis. *Plant Cell* 14:1161–1172.
- Hasezawa S, Marc J, Palevitz BA (1991) Microtubule reorganization during the cell cycle in synchronized BY-2 tobacco suspensions. *Cell motility and the cytoskeleton* 18:94–106.
- Heard W, Sklenar J, Tome DF, Robatzek S, Jones AM (2015) Identification of regulatory and cargo proteins of endosomal and secretory pathways in Arabidopsis thaliana by proteomic dissection. *Mol Cell Proteomics* 14:1796–1813.
- Heese M, Gansel X, Sticher L, Wick P, Grebe M, Granier F, Jurgens G (2001) Functional characterization of the KNOLLE-interacting t-SNARE AtSNAP33 and its role in plant cytokinesis. *J Cell Biol* 155:239–249.
- Hepler PK (1982) Endoplasmic reticulum in the formation of the cell plate and plasmodesmata. *Protoplasma* 111:121–133.
- Hepler PK, Newcomb EH (1967) Fine structure of cell plate formation in the apical meristem of Phaseolus roots. *J Ultrastruct Res* 19:498–513.
- Herrmann A, Livanos P, Lipka E, Gadeyne A, Hauser MT, Van Damme D, Müller S (2018) Dual localized kinesin-12 POK2 plays multiple roles during cell division and interacts with MAP65-3. *EMBO Rep* 19:e46085.
- Hervé C, Marcus SE, Knox JP (2011) Monoclonal antibodies, carbohydrate-binding modules, and the detection of polysaccharides in plant cell walls. *Methods Mol Biol* 715:103–113.
- Him JLK, Pelosi L, Chanzy H, Putaux JL, Bulone V (2001) Biosynthesis of (1,3)-beta-D-glucan (callose) by detergent extracts of a microsomal fraction from Arabidopsis thaliana. *European Journal of Biochemistry* 268:4628–4638.
- Ho C-MK, Hotta T, Guo F, Roberson RW, Lee Y-RJ, Liu B (2011) Interaction of antiparallel microtubules in the phragmoplast is mediated by the microtubule-associated protein MAP65-3 in Arabidopsis. *The Plant Cell* 23:2909–2923.
- Ho CM, Hotta T, Guo F, Roberson RW, Lee YR, Liu B (2011) Interaction of antiparallel microtubules in the phragmoplast is mediated by the microtubule-associated protein MAP65-3 in Arabidopsis. *Plant Cell* 23:2909–2923.
- Hofmeister W (1863) Zusätze und Berichtigungen zu den 1851 veröffentlichten Untersuchungen der Entwicklung höherer Kryptogamen. *Jahrb Wiss Bot* 3:259–293.
- Hong Z, Delauney AJ, Verma DP (2001) A cell plate-specific callose synthase and its interaction with phragmoplastin. *Plant Cell* 13:755–768.
- Hotta T, Kong Z, Ho CM, Zeng CJ, Horio T, Fong S, Vuong T, Lee YR, Liu B (2012) Characterization of the Arabidopsis augmin complex uncovers its critical function in the assembly of the acentrosomal spindle and phragmoplast microtubule arrays. *Plant Cell* 24:1494–1509.
- Hussey PJ, Hawkins TJ, Igarashi H, Kaloriti D, Smertenko A (2002) The plant cytoskeleton: recent advances in the study of the plant microtubule-associated proteins MAP-65, MAP-190 and the Xenopus MAP215-like protein, MOR1. *Plant Mol Biol* 50:915–924.
- Jamet E, Albenne C, Boudart G, Irshad M, Canut H, Pont-Lezica R (2008) Recent advances in plant cell wall proteomics. *Proteomics* 8:893–908.
- Jawaid MZ, Sinclair R, Bulone V, Cox DL, Drakakaki G (2022) A biophysical model for plant cell plate maturation based on the contribution of a spreading force. *Plant Physiol* 188:795–806.
- Johnson A, Dahhan DA, Gnyliukh N, Kaufmann WA, Zheden V, Costanzo T, Mahou P, Hrtyan M, Wang J, Aguilera-Servin J, van Damme D, Beaurepaire E, Loose M, Bednarek SY, Friml J (2021) The TPLATE complex mediates membrane bending during plant clathrin-mediated endocytosis. *Proc Natl Acad Sci U S A* 118:e2113046118.
- Jones S, Newman C, Liu F, Segev N (2000) The TRAPP complex is a nucleotide exchanger for Ypt1 and Ypt31/32. *Mol Biol Cell* 11:4403–4411.
- Julian JD, Zabotina OA (2022) Xyloglucan biosynthesis: from genes to proteins and their functions. *Front Plant Sci* 13:920494.
- Jürgens G (2005) Cytokinesis in higher plants. *Annual Review of Plant Biology* 56:281–299.
- Jurgens G, Park M, Richter S, Touihri S, Krause C, El Kasmí F, Mayer U (2015) Plant cytokinesis: a tale of membrane traffic and fusion. *Biochem Soc Trans* 43:73–78.

- Jurgens M HL, Rivers BA, Hepler PK (1994) BAPTA-calcium buffers modulate cell plate formation in stamen hairs of *Tradescantia*-evidence for calcium gradients. *Protoplasma* 183:86–99.
- Kakimoto T, Shibaoka H (1987) Actin filaments and microtubules in the preprophase band and phragmoplast of tobacco cells. *Protoplasma* 140:151–156.
- Kakimoto T, Shibaoka H (1989) Cytoskeletal ultrastructure of phragmoplast-nuclei complexes isolated from cultured tobacco cells. In M Tazawa, ed, *Cell Dynamics: Molecular Aspects of Cell Motility Cytoskeleton in Cellular Structure and Activity*. Springer Vienna, Vienna, pp 95–103.
- Kalde M, Elliott L, Ravikumar R, Rybak K, Altmann M, Klaeger S, Wiese C, Abele M, Al B, Kalbfuß N, Qi X, Steiner A, Meng C, Zheng H, Kuster B, Falter-Braun P, Ludwig C, Moore I, Assaad FF (2019) Interactions between Transport Protein Particle (TRAPP) complexes and Rab GTPases in *Arabidopsis*. *Plant J* 100:279–297.
- Kang BH, Nielsen E, Preuss ML, Mastronarde D, Staehelin LA (2011) Electron tomography of RabA4b- and PI-4Kbeta1-labeled trans Golgi network compartments in *Arabidopsis*. *Traffic* 12:313–329.
- Karnahl M, Park M, Mayer U, Hiller U, Jürgens G (2017) ER assembly of SNARE complexes mediating formation of partitioning membrane in *Arabidopsis* cytokinesis. *Elife* 6:e25327.
- Keegstra K (2010) Plant cell walls. *Plant Physiol* 154:483–486.
- Klotz J, Nick P (2012) A novel actin-microtubule cross-linking kinesin, NtKCH, functions in cell expansion and division. *New Phytol* 193:576–589.
- Komis G, Novák D, Ovečka M, Šamajová O, Šamaj J (2018) Advances in imaging plant cell dynamics. *Plant Physiol* 176:80–93.
- Konopka CA, Backues SK, Bednarek SY (2008) Dynamics of *Arabidopsis* dynamin-related protein 1C and a clathrin light chain at the plasma membrane. *Plant Cell* 20:1363–1380.
- Konopka CA, Bednarek SY (2008) Comparison of the dynamics and functional redundancy of the *Arabidopsis* dynamin-related isoforms DRP1A and DRP1C during plant development. *Plant Physiol* 147:1590–1602.
- Kosetsu K, de Keijzer J, Janson ME, Goshima G (2013) Microtubule-associated Protein65 is essential for maintenance of phragmoplast bipolarity and formation of the cell plate in *Physcomitrella patens*. *Plant Cell* 25:4479–4492.
- Kumagai-Sano F, Hayashi T, Sano T, Hasezawa S (2006) Cell cycle synchronization of tobacco BY-2 cells. *Nature Protocols* 1:2621–2627.
- Kumari P, Dahiya P, Livanos P, Zergiebel L, Kölling M, Poeschl Y, Stamm G, Hermann A, Abel S, Müller S, Bürstenbinder K (2021) IQ67 DOMAIN proteins facilitate preprophase band formation and division-plane orientation. *Nat Plants* 7:739–747.
- Kwak SY, Wong MH, Lew TTS, Bisker G, Lee MA, Kaplan A, Dong J, Liu AT, Koman VB, Sinclair R, Hamann C, Strano MS (2017) Nanosensor Technology Applied to Living Plant Systems. *Annu Rev Anal Chem (Palo Alto Calif)* 10:113–140.
- Laubner MH, Waizenegger I, Steinmann T, Schwarz H, Mayer U, Hwang I, Lukowitz W, Jurgens G (1997) The *Arabidopsis* KNOLLE protein is a cytokinesis-specific syntaxin. *J Cell Biol* 139:1485–1493.
- Ledbetter MC, Porter KR (1963) A “Microtubule” in Plant Cell Fine Structure. *J Cell Biol* 19:239–250.
- Lee KJ, Marcus SE, Knox JP (2011) Cell wall biology: perspectives from cell wall imaging. *Mol Plant* 4:212–219.
- Lee YJ, Liu B (2019) Microtubule nucleation for the assembly of acentrosomal microtubule arrays in plant cells. *New Phytol* 222:1705–1718.
- Lee YR, Giang HM, Liu B (2001) A novel plant kinesin-related protein specifically associates with the phragmoplast organelles. *Plant Cell* 13:2427–2439.
- Lee YR, Liu B (2013) The rise and fall of the phragmoplast microtubule array. *Curr Opin Plant Biol* 16:757–763.
- Levy A, Guenoune-Gelbart D, Epel BL (2007) beta-1,3-Glucanases: plasmodesmal gate keepers for intercellular communication. *Plant Signal Behav* 2:404–407.
- Lew TTS, Wong MH, Kwak SY, Sinclair R, Koman VB, Strano MS (2018) Rational design principles for the transport and subcellular distribution of nanomaterials into plant protoplasts. *Small* 14:e1802086.
- Lipka E, Gadeyne A, Stöckle D, Zimmermann S, De Jaeger G, Ehrhardt DW, Kirik V, Van Damme D, Müller S (2014) The phragmoplast-orienting kinesin-12 class proteins translate the positional information of the preprophase band to establish the cortical division zone in *Arabidopsis thaliana*. *Plant Cell* 26:2617–2632.
- Liu B, Lee YJ (2022) Spindle assembly and mitosis in plants. *Annu Rev Plant Biol* 73:227–254.
- Livanos P, Chugh M, Müller S (2017) Analysis of phragmoplast kinetics during plant cytokinesis. *Methods Mol Biol* 1662:137–150.
- Lloyd C, Buschmann H (2007) Plant division: remembering where to build the wall. *Curr Biol* 17:R1053–1055.
- Lukowitz W, Mayer U, Jurgens G (1996) Cytokinesis in the *Arabidopsis* embryo involves the syntaxin-related KNOLLE gene product. *Cell* 84:61–71.
- Lynch MA, Staehelin LA (1992) Domain-specific and cell type-specific localization of two types of cell wall matrix polysaccharides in the clover root tip. *J Cell Biol* 118:467–479.
- Martinez P, Allsman LA, Brakke KA, Hoyt C, Hayes J, Liang H, Neher W, Rui Y, Roberts AM, Moradifam A, Goldstein B, Anderson CT, Rasmussen CG (2018) Predicting division planes of three-dimensional cells by soap-film minimization. *Plant Cell* 30:2255–2266.
- Martinez P, Dixit R, Balkunde RS, Zhang A, O’Leary SE, Brakke KA, Rasmussen CG (2020) TANGLED1 mediates microtubule interactions that may promote division plane positioning in maize. *Journal of Cell Biology* 219.
- Martinez P, Luo A, Sylvester A, Rasmussen CG (2017) Proper division plane orientation and mitotic progression together allow normal growth of maize. *Proc Natl Acad Sci U S A* 114:2759–2764.
- Mayer U, Ruiz RAT, Berleth T, Miséra S, Jürgens G (1991) Mutations affecting body organization in the *Arabidopsis* embryo. *Nature* 353:402–407.
- Mayers JR, Hu T, Wang C, Cardenas JJ, Tan Y, Pan J, Bednarek S (2017) SCD1 and SCD2 Form a Complex that Functions with the Exocyst and RabE1 in Exocytosis and Cytokinesis. *Plant Cell*.
- McFarlane HE, Watanabe Y, Gendre D, Carruthers K, Levesque-Tremblay G, Haughn GW, Bhalerao RP, Samuels L (2013) Cell wall polysaccharides are mislocalized to the vacuole in *echidna* mutants. *Plant Cell Physiol* 54:1867–1880.
- McFarlane HE, Young RE, Wasteneys GO, Samuels AL (2008) Cortical microtubules mark the mucilage secretion domain of the plasma membrane in *Arabidopsis* seed coat cells. *Planta* 227:1363–1375.
- McMichael CM, Bednarek SY (2013) Cytoskeletal and membrane dynamics during higher plant cytokinesis. *New Phytol* 197:1039–1057.

- McMichael CM, Reynolds GD, Koch LM, Wang C, Jiang N, Nadeau J, Sack FD, Gelderman MB, Pan J, Bednarek SY (2013) Mediation of clathrin-dependent trafficking during cytokinesis and cell expansion by Arabidopsis stomatal cytokinesis defective proteins. *Plant Cell* 25:3910–3925.
- Meinke DW, Cherry JM, Dean C, Rounsley SD, Koornneef M (1998) Arabidopsis thaliana: a model plant for genome analysis. *Science* 282:662, 679–682.
- Miart F, Desprez T, Biot E, Morin H, Belcram K, Hofte H, Gonneau M, Vernhettes S (2014) Spatio-temporal analysis of cellulose synthesis during cell plate formation in Arabidopsis. *Plant J* 77:71–84.
- Mills AM, Morris VH, Rasmussen CG (2022) Localization of PHRAGMOPLAST ORIENTING KINESIN1 at the division site depends on the microtubule binding proteins TANGLED1 and AUXIN-INDUCED IN ROOT CULTURES9 in Arabidopsis. *Plant Cell* 34(11):4583–4599.
- Mineyuki Y, S. Gunning BE (1990) A role for preprophase bands of microtubules in maturation of new cell walls, and a general proposal on the function of preprophase band sites in cell division in higher plants. *Journal of Cell Science* 97:527–537.
- Mineyuki Y, Wick SM, Gunning BE (1988) Preprophase bands of microtubules and the cell cycle: Kinetics and experimental uncoupling of their formation from the nuclear cycle in onion root-tip cells. *Planta* 174:518–526.
- Mir R, Morris VH, Buschmann H, Rasmussen CG (2018) Division plane orientation defects revealed by a synthetic double mutant phenotype. *Plant Physiol* 176:418–431.
- Mohnen D (2008) Pectin structure and biosynthesis. *Curr Opin Plant Biol* 11:266–277.
- Moore PJ, Darvill AG, Albersheim P, Staehelin LA (1986) Immunogold localization of xyloglucan and rhamnogalacturonan I in the cell walls of suspension-cultured sycamore cells. *Plant Physiol* 82:787–794.
- Moore PJ, Staehelin LA (1988) Immunogold localization of the cell-wall-matrix polysaccharides rhamnogalacturonan I and xyloglucan during cell expansion and cytokinesis in *Trifolium pratense* L.; implication for secretory pathways. *Planta* 174:433–445.
- Moore PJ, Swords KM, Lynch MA, Staehelin LA (1991) Spatial organization of the assembly pathways of glycoproteins and complex polysaccharides in the Golgi apparatus of plants. *J Cell Biol* 112:589–602.
- Müller S (2019) Plant cell division - defining and finding the sweet spot for cell plate insertion. *Current Opinion in Cell Biology* 60:9–18.
- Müller S, Han S, Smith LG (2006) Two kinesins are involved in the spatial control of cytokinesis in Arabidopsis thaliana. *Current Biology* 16:888–894.
- Müller S, Smertenko A, Wagner V, Heinrich M, Hussey PJ, Hauser MT (2004) The plant microtubule-associated protein AtMAP65-3/PLE is essential for cytokinetic phragmoplast function. *Curr Biol* 14:412–417.
- Murata T, Sano T, Sasabe M, Nonaka S, Higashiyama T, Hasezawa S, Machida Y, Hasebe M (2013) Mechanism of microtubule array expansion in the cytokinetic phragmoplast. *Nat Commun* 4:1967.
- Nakamura M, Ehrhardt DW, Hashimoto T (2010) Microtubule and katanin-dependent dynamics of microtubule nucleation complexes in the acentrosomal Arabidopsis cortical array. *Nat Cell Biol* 12:1064–1070.
- Nebenführ A, Dixit R (2018) Kinesins and myosins: Molecular motors that coordinate cellular functions in plants. *Annu Rev Plant Biol* 69:329–361.
- Nishihama R, Ishikawa M, Araki S, Soyano T, Asada T, Machida Y (2001) The NPK1 mitogen-activated protein kinase kinase is a regulator of cell-plate formation in plant cytokinesis. *Genes Dev* 15:352–363.
- Nishihama R, Soyano T, Ishikawa M, Araki S, Tanaka H, Asada T, Irie K, Ito M, Terada M, Banno H, Yamazaki Y, Machida Y (2002) Expansion of the cell plate in plant cytokinesis requires a kinesin-like protein/MAPKKK complex. *Cell* 109:87–99.
- Okekeogbu IO, Pattathil S, Gonzalez Fernandez-Nino SM, Aryal UK, Penning BW, Lao J, Heazlewood JL, Hahn MG, McCann MC, Carpita NC (2019) Glycome and proteome components of golgi membranes are common between two Angiosperms with distinct cell-wall structures. *Plant Cell* 31:1094–1112.
- Otegui MS (2020) Electron Tomography and Immunogold Labeling as Tools to Analyze De Novo Assembly of Plant Cell Walls. In ZA Popper, ed, *The Plant Cell Wall: Methods and Protocols*. Springer New York, New York, NY, pp 365–382.
- Otegui MS, Mastrorade DN, Kang BH, Bednarek SY, Staehelin LA (2001) Three-dimensional analysis of syncytial-type cell plates during endosperm cellularization visualized by high resolution electron tomography. *Plant Cell* 13:2033–2051.
- Otegui MS, Verbrugghe KJ, Skop AR (2005) Midbodies and phragmoplasts: analogous structures involved in cytokinesis. *Trends Cell Biol* 15:404–413.
- Ovečka M, Sojka J, Tichá M, Komis G, Basheer J, Marchetti C, Šamajová O, Kuběnová L, Šamaj J (2021) Imaging plant cells and organs with light-sheet and super-resolution microscopy. *Plant Physiology* 188:683–702.
- Palevitz B (1987) Accumulation of F-actin during cytokinesis in *Allium*. Correlation with microtubule distribution and the effects of drugs. *Protoplasma* 141:24–32.
- Palevitz BA, Hepler PK (1974) The control of the plane of division during stomatal differentiation in *Allium*. *Chromosoma* 46:297–326.
- Panteris E, Kouskouveli A, Pappas D, Adamakis IS (2021) Cytokinesis in fra2 Arabidopsis thaliana p60-katanin mutant: defects in cell plate/daughter wall formation. *Int J Mol Sci* 22.
- Park E, Diaz-Moreno SM, Davis DJ, Wilkop TE, Bulone V, Drakakaki G (2014) Endosidin 7 specifically arrests late cytokinesis and inhibits callose biosynthesis, revealing distinct trafficking events during cell plate maturation. *Plant Physiol* 165:1019–1034.
- Park M, Krause C, Karnahl M, Reichardt I, El Kasmi F, Mayer U, Stierhof YD, Hiller U, Strompen G, Bayer M, Kientz M, Sato MH, Nishimura MT, Dangel JL, Sanderfoot AA, Jürgens G (2018) Concerted action of evolutionarily ancient and novel SNARE complexes in flowering-plant Cytokinesis. *Dev Cell* 44:500–511.e504.
- Park S, Szumlanski AL, Gu F, Guo F, Nielsen E (2011) A role for CSLD3 during cell-wall synthesis in apical plasma membranes of tip-growing root-hair cells. *Nat Cell Biol* 13:973–980.
- Parsons HT, Stevens TJ, McFarlane HE, Vidal-Melgosa S, Griss J, Lawrence N, Butler R, Sousa MML, Salemi M, Willats WGT, Petzold CJ, Heazlewood JL, Lilley KS (2019) Separating golgi proteins from cis to trans reveals underlying properties of cisternal localization. *Plant Cell* 31:2010–2034.
- Pattathil S, Avci U, Baldwin D, Swennes AG, McGill JA, Popper Z, Bootten T, Albert A, Davis RH, Chennareddy C, Dong R, O’Shea B, Rossi R, Leoff C, Freshour G, Narra R, O’Neil M, York WS, Hahn MG (2010) A comprehensive toolkit of plant cell wall glycan-directed monoclonal antibodies. *Plant Physiol* 153:514–525.

- Paul DC, Goff CW (1973) Comparative effects of caffeine, its analogues and calcium deficiency on cytokinesis. *Exp Cell Res* 78:399–413.
- Pauly M, Keegstra K (2016) Biosynthesis of the plant cell wall matrix polysaccharide Xyloglucan. *Annu Rev Plant Biol* 67:235–259.
- Peaucelle A, Braybrook S, Höfte H (2012) Cell wall mechanics and growth control in plants: the role of pectins revisited. *Front Plant Sci* 3:121.
- Persson S, Paredes A, Carroll A, Palsdottir H, Doblin M, Poindexter P, Khitrov N, Auer M, Somerville CR (2007) Genetic evidence for three unique components in primary cell-wall cellulose synthase complexes in Arabidopsis. *Proc Natl Acad Sci U S A* 104:15566–15571.
- Pickett-Heaps JD, Northcote DH (1966) Organization of microtubules and endoplasmic reticulum during mitosis and cytokinesis in wheat meristems. *J Cell Sci* 1:109–120.
- Pinar M, Arst HN, Jr., Pantazopoulou A, Tagua VG, de los Rios V, Rodriguez-Salarichs J, Diaz JF, Penalva MA (2015) TRAPP II regulates exocytic Golgi exit by mediating nucleotide exchange on the Ypt31 ortholog RabERAB11. *Proc Natl Acad Sci U S A* 112:4346–4351.
- Prevedel R, Diz-Munoz A, Ruocco G, Antonacci G (2019) Brillouin microscopy: an emerging tool for mechanobiology. *Nat Methods* 16:969–977.
- Qi X, Kaneda M, Chen J, Geitmann A, Zheng H (2011) A specific role for Arabidopsis TRAPP II in post-Golgi trafficking that is crucial for cytokinesis and cell polarity. *Plant J* 68:234–248.
- Rasmussen CG, Bellinger M (2018) An overview of plant division-plane orientation. *New Phytol* 219:505–512.
- Richter S, Kientz M, Brumm S, Nielsen ME, Park M, Gavidia R, Krause C, Voss U, Beckmann H, Mayer U, Stierhof YD, Jurgens G (2014) Delivery of endocytosed proteins to the cell-division plane requires change of pathway from recycling to secretion. *Elife* 3:e02131.
- Ropitiaux M, Hays Q, Baron A, Fourmois L, Boulogne I, Vauzeilles B, Lerouge P, Mollet JC, Lehner A (2022) Dynamic imaging of cell wall polysaccharides by metabolic click-mediated labeling of pectins in living elongating cells. *Plant J* 110(3):916–924.
- Rybak K, Steiner A, Synek L, Klaefer S, Kulich I, Facher E, Wanner G, Kuster B, Zarsky V, Persson S, Assaad FF (2014) Plant cytokinesis is orchestrated by the sequential action of the TRAPP II and exocyst tethering complexes. *Dev Cell* 29:607–620.
- Saatian B, Austin RS, Tian G, Chen C, Nguyen V, Kohalmi SE, Geelen D, Cui Y (2018) Analysis of a novel mutant allele of GSL8 reveals its key roles in cytokinesis and symplastic trafficking in Arabidopsis. *BMC Plant Biol* 18:295.
- Sablowski R, Gutierrez C (2022) Cycling in a crowd: Coordination of plant cell division, growth, and cell fate. *Plant Cell* 34:193–208.
- Sachs J (1878) Über die Anordnung der Zellen in jüngsten Pflanzentheilen. *Arb Bot Inst Wurzburg* 2:46–104.
- Samuels AL, Giddings TH, Jr., Staehelin LA (1995) Cytokinesis in tobacco BY-2 and root tip cells: a new model of cell plate formation in higher plants. *J Cell Biol* 130:1345–1357.
- Sanchez-Rodriguez C, Shi Y, Kesten C, Zhang D, Sancho-Andres G, Ivakov A, Lampugnani ER, Sklodowski K, Fujimoto M, Nakano A, Bacic A, Wallace IS, Ueda T, Van Damme D, Zhou Y, Persson S (2018) The cellulose synthases are cargo of the TPLATE adaptor complex. *Mol Plant* 11:346–349.
- Sanzari I, Leone A, Ambrosone A (2019) Nanotechnology in plant science: to make a long story short. *Frontiers in Bioengineering and Biotechnology* 7:120.
- Sasabe M, Ishibashi N, Haruta T, Minami A, Kurihara D, Higashiyama T, Nishihama R, Ito M, Machida Y (2015) The carboxyl-terminal tail of the stalk of Arabidopsis NACK1/HINKEL kinesin is required for its localization to the cell plate formation site. *J Plant Res* 128:327–336.
- Sasaki T, Tsutsumi M, Otomo K, Murata T, Yagi N, Nakamura M, Nemoto T, Hasebe M, Oda Y (2019) A novel katanin-tethering machinery accelerates cytokinesis. *Curr Biol* 29:4060–4070.e4063.
- Schaefer E, Belcram K, Uyttewaal M, Duroc Y, Goussot M, Legland D, Laruelle E, de Tauzia-Moreau ML, Pastuglia M, Bouchez D (2017) The preprophase band of microtubules controls the robustness of division orientation in plants. *Science* 356:186–189.
- Scheller HV, Ulvskov P (2010) Hemicelluloses. *Annu Rev Plant Biol* 61:263–289.
- Schmit AC, Lambert AM (1990) Microinjected fluorescent phalloidin in vivo reveals the F-actin dynamics and assembly in higher plant mitotic cells. *Plant Cell* 2:129–138.
- Schneider R, Hanak T, Persson S, Voigt CA (2016) Cellulose and callose synthesis and organization in focus, what's new? *Curr Opin Plant Biol* 34:9–16.
- Segui-Simarro JM, Austin JR, White EA, Staehelin LA (2004) Electron tomographic analysis of somatic cell plate formation in meristematic cells of Arabidopsis preserved by high-pressure freezing. *Plant Cell* 16:836–856.
- Sen O, Harrison JU, Burroughs NJ, McAtosh AD (2021) Kinetochore life histories reveal an Aurora-B-dependent error correction mechanism in anaphase. *Dev Cell* 56:3082–3099.e3085.
- Showalter AM, Basu D (2016) Extensin and arabinogalactan-protein biosynthesis: glycosyltransferases, research challenges, and biosensors. *Front Plant Sci* 7:814.
- Silva J, Ferraz R, Dupree P, Showalter AM, Coimbra S (2020) Three decades of advances in arabinogalactan-protein biosynthesis. *Front Plant Sci* 11:610377.
- Sinclair R, Hsu G, Davis D, Chang M, Rosquete M, Iwasa JH, Drakakaki G (2022) Plant cytokinesis and the construction of new cell wall. *FEBS Lett* 596(17):2243–2255.
- Sinnott EW, Bloch R (1940) Cytoplasmic behavior during division of vacuolate plant cells. *Proc Natl Acad Sci U S A* 26:223–227.
- Smertenko A (2018) Phragmoplast expansion: the four-stroke engine that powers plant cytokinesis. *Curr Opin Plant Biol* 46:130–137.
- Smertenko A, Assaad F, Baluska F, Bezani M, Buschmann H, Drakakaki G, Hauser MT, Janson M, Mineyuki Y, Moore I, Muller S, Murata T, Otegui MS, Panteris E, Rasmussen C, Schmit AC, Samaj J, Samuels L, Staehelin LA, Van Damme D, Wasteneys G, Zarsky V (2017) Plant cytokinesis: terminology for structures and processes. *Trends Cell Biol* 27:885–894.
- Smertenko A, Hewitt SL, Jacques CN, Kacprzyk R, Liu Y, Marcec MJ, Moyo L, Ogden A, Oung HM, Schmidt S, Serrano-Romero EA (2018) Phragmoplast microtubule dynamics - a game of zones. *J Cell Sci* 131.
- Smertenko A, Saleh N, Igarashi H, Mori H, Hauser-Hahn I, Jiang CJ, Sonobe S, Lloyd CW, Hussey PJ (2000) A new class of microtubule-associated proteins in plants. *Nat Cell Biol* 2:750–753.
- Smith LG, Gerttula SM, Han S, Levy J (2001) Tangled1: a microtubule binding protein required for the spatial control of cytokinesis in maize. *J Cell Biol* 152:231–236.
- Smith LG, Hake S, Sylvester AW (1996) The tangled-1 mutation alters cell division orientations throughout maize leaf development without altering leaf shape. *Development* 122:481–489.

- Sollner R, Glasser G, Wanner G, Somerville CR, Jurgens G, Assaad FF (2002) Cytokinesis-defective mutants of Arabidopsis. *Plant Physiol* 129:678–690.
- Song K, Jang M, Kim SY, Lee G, Lee GJ, Kim DH, Lee Y, Cho W, Hwang I (2012) An A/ENTH domain-containing protein functions as an adaptor for clathrin-coated vesicles on the growing cell plate in Arabidopsis root cells. *Plant Physiol* 159:1013–1025.
- Speth EB, Imboden L, Hauck P, He SY (2009) Subcellular localization and functional analysis of the Arabidopsis GTPase RabE. *Plant Physiol* 149:1824–1837.
- Steigemann P, Gerlich DW (2009) Cytokinetic abscission: cellular dynamics at the midbody. *Trends in Cell Biology* 19:606–616.
- Strompen G, El Kasmi F, Richter S, Lukowitz W, Assaad FF, Jurgens G, Mayer U (2002) The Arabidopsis HINKEL gene encodes a kinesin-related protein involved in cytokinesis and is expressed in a cell cycle-dependent manner. *Curr Biol* 12:153–158.
- Tabata S, Kaneko T, Nakamura Y, Kotani H, Kato T, Asamizu E, Miyajima N, Sasamoto S, Kimura T, Hosouchi T, Kawashima K, Kohara M, Matsumoto M, Matsuno A, Muraki A, Nakayama S, Nakazaki N, Naruo K, Okumura S, Shinpo S, Takeuchi C, Wada T, Watanabe A, Yamada M, Yasuda M, Sato S, de la Bastide M, Huang E, Spiegel L, Gnoj L, O'Shaughnessy A, Preston R, Habermann K, Murray J, Johnson D, Rohlfing T, Nelson J, Stoneking T, Pepin K, Spieth J, Sekhon M, Armstrong J, Becker M, Belter E, Cordum H, Cordes M, Courtney L, Courtney W, Dante M, Du H, Edwards J, Fryman J, Haakensen B, Lamar E, Latreille P, Leonard S, Meyer R, Mulvaney E, Ozersky P, Riley A, Strowmatt C, Wagner-McPherson C, Wollam A, Yoakum M, Bell M, Dedhia N, Parnell L, Shah R, Rodriguez M, See LH, Vil D, Baker J, Kirchoff K, Toth K, King L, Bahret A, Miller B, Marra M, Martienssen R, McCombie WR, Wilson RK, Murphy G, Bancroft I, Volckaert G, Wambutt R, Düsterhöft A, Stiekema W, Pohl T, Entian KD, Terryn N, Hartley N, Bent E, Johnson S, Langham SA, McCullagh B, Robben J, Grymonprez B, Zimmermann W, Ramsperger U, Wedler H, Balke K, Wedler E, Peters S, van Staveren M, Dirkse W, Mooijman P, Lankhorst RK, Weitzenegger T, Bothe G, Rose M, Hauf J, Berneiser S, Hempel S, Feldpausch M, Lamberth S, Villarreal R, Gielen J, Ardiles W, Bents O, Lemcke K, Kolesov G, Mayer K, Rudd S, Schoof H, Schueller C, Zaccaria P, Mewes HW, Bevan M, Franz P (2000) Sequence and analysis of chromosome 5 of the plant Arabidopsis thaliana. *Nature* 408:823–826.
- Thiele K, Wanner G, Kindziarski V, Jurgens G, Mayer U, Pacht F, Assaad FF (2009) The timely deposition of callose is essential for cytokinesis in Arabidopsis. *Plant Journal* 58:13–26.
- Tian J, Han L, Feng Z, Wang G, Liu W, Ma Y, Yu Y, Kong Z (2015) Orchestration of microtubules and the actin cytoskeleton in trichome cell shape determination by a plant-unique kinesin. *Elife* 4:e09351.
- Toyooka K, Goto Y, Asatsuma S, Koizumi M, Mitsui T, Matsuoka K (2009) A mobile secretory vesicle cluster involved in mass transport from the Golgi to the plant cell exterior. *Plant Cell* 21:1212–1229.
- Traas JA, Doonan JH, Rawlins DJ, Shaw PJ, Watts J, Lloyd CW (1987) An actin network is present in the cytoplasm throughout the cell cycle of carrot cells and associates with the dividing nucleus. *The Journal of cell biology* 105:387–395.
- Uemura T, Kim H, Saito C, Ebine K, Ueda T, Schulze-Lefert P, Nakano A (2012) Qa-SNAREs localized to the trans-Golgi network regulate multiple transport pathways and extracellular disease resistance in plants. *Proc Natl Acad Sci U S A* 109:1784–1789.
- Van Damme D, Gadeyne A, Vanstraelen M, Inze D, Van Montagu MC, De Jaeger G, Russinova E, Geelen D (2011) Adaptin-like protein TPLATE and clathrin recruitment during plant somatic cytokinesis occurs via two distinct pathways. *Proc Natl Acad Sci U S A* 108:615–620.
- van Oostende-Triplet C, Guillet D, Triplet T, Pandzic E, Wiseman PW, Geitmann A (2017) Vesicle dynamics during plant cell cytokinesis reveals distinct developmental phases. *Plant Physiol* 174:1544–1558.
- von Chamier L, Laine RF, Henriques R (2019) Artificial intelligence for microscopy: what you should know. *Biochem Soc Trans* 47:1029–1040.
- Vukasinovic N, Zarsky V (2016) Tethering complexes in the Arabidopsis endomembrane system. *Front Cell Dev Biol* 4:46.
- Vyplelová P, Ovečka M, Šamaj J (2017) Alfalfa root growth rate correlates with progression of microtubules during mitosis and cytokinesis as revealed by environmental light-sheet microscopy. *Front Plant Sci* 8:1870.
- Waizenegger I, Lukowitz W, Assaad F, Schwarz H, Jürgens G, Mayer U (2000) The Arabidopsis KNOLLE and KEULE genes interact to promote vesicle fusion during cytokinesis. *Curr Biol* 10:1371–1374.
- Walker KL, Muller S, Moss D, Ehrhardt DW, Smith LG (2007) Arabidopsis TANGLED identifies the division plane throughout mitosis and cytokinesis. *Curr Biol* 17:1827–1836.
- Wang H, Zhuang X, Wang X, Law AH, Zhao T, Du S, Loy MM, Jiang L (2016) A distinct pathway for polar exocytosis in plant cell wall formation. *Plant Physiol* 172:1003–1018.
- Wang J, Yperman K, Grones P, Jiang Q, Dragwidge J, Mylle E, Mor E, Nolf J, Eeckhout D, De Jaeger G, De Rybel B, Pleskot R, Van Damme D (2021) Conditional destabilization of the TPLATE complex impairs endocytic internalization. *Proc Natl Acad Sci U S A* 118:e2023456118.
- Wang W, Sacher M, Ferro-Novick S (2000) TRAPP stimulates guanine nucleotide exchange on Ypt1p. *J Cell Biol* 151:289–296.
- Weiner E, Pinsky JM, Nicastro D, Otegui MS (2021) Electron microscopy for imaging organelles in plants and algae. *Plant Physiology* 188:713–725.
- Wick SM, Duniec J (1983) Immunofluorescence microscopy of tubulin and microtubule arrays in plant cells. I. Preprophase band development and concomitant appearance of nuclear envelope-associated tubulin. *J Cell Biol* 97:235–243.
- Wick SM, Duniec J (1984) Immunofluorescence microscopy of tubulin and microtubule arrays in plant cells. II. Transition between the pre-prophase band and the mitotic spindle. *Protoplasma* 122:45–55.
- Wilkop T, Pattathil S, Ren G, Davis DJ, Bao W, Duan D, Peralta AG, Domozych DS, Hahn MG, Drakakaki G (2019) A hybrid approach enabling large-scale glycomic analysis of post-golgi vesicles reveals a transport route for polysaccharides. *Plant Cell* 31:627–644.
- Wilson TH, Kumar M, Turner SR (2021) The molecular basis of plant cellulose synthase complex organisation and assembly. *Biochem Soc Trans* 49:379–391.
- Wolniak SM, Hepler PK, Jackson WT (1980) Detection of the membrane-calcium distribution during mitosis in Haemanthus endosperm with chlorotetracycline. *J Cell Biol* 87:23–32.
- Wu SW, Kumar R, Iswanto ABB, Kim JY (2018) Callose balancing at plasmodesmata. *J Exp Bot* 69:5325–5339.
- Yang J, Bak G, Burgin T, Barnes WJ, Mayes HB, Peña MJ, Urbanowicz BR, Nielsen E (2020) Biochemical and genetic analysis identify CSLD3 as a beta-1,4-glucan synthase that functions during plant cell wall synthesis. *Plant Cell* 32:1749–1767.

- Yi P, Goshima G (2022) Division site determination during asymmetric cell division in plants. *Plant Cell*. 34:2120–2139
- Yokoyama R, Nishitani K (2001) Endoxyloglucan transferase is localized both in the cell plate and in the secretory pathway destined for the apoplast in tobacco cells. *Plant and Cell Physiology* 42:292–300.
- Young RE, McFarlane HE, Hahn MG, Western TL, Haughn GW, Samuels AL (2008) Analysis of the Golgi apparatus in Arabidopsis seed coat cells during polarized secretion of pectin-rich mucilage. *Plant Cell* 20:1623–1638.
- Yu M, Zhao J (2012) The cytological changes of tobacco zygote and proembryo cells induced by beta-glucosyl Yariv reagent suggest the involvement of arabinogalactan proteins in cell division and cell plate formation. *BMC Plant Biol* 12:126.
- Zamil MS, Geitmann A (2017) The middle lamella—more than a glue. *Phys Biol* 14:015004.
- Zamil MS, Yi H, Puri VM (2014) Mechanical characterization of outer epidermal middle lamella of onion under tensile loading. *Am J Bot* 101:778–787.
- Zamil MS, Yi H, Puri VM (2015) The mechanical properties of plant cell walls soft material at the subcellular scale: the implications of water and of the intercellular boundaries. *Journal of Materials Science* 50:6608–6623.
- Zaveska Drabkova L, Honys D (2017) Evolutionary history of callose synthases in terrestrial plants with emphasis on proteins involved in male gametophyte development. *PLoS One* 12:e0187331.
- Zechmann B, Möstl S, Zellnig G (2022) Volumetric 3D reconstruction of plant leaf cells using SEM, ion milling, TEM, and serial sectioning. *Planta* 255:118.
- Zhang GF, Staehelin LA (1992) Functional compartmentation of the golgi apparatus of plant cells: immunocytochemical analysis of high-pressure frozen- and freeze-substituted sycamore maple suspension culture cells. *Plant Physiol* 99:1070–1083.
- Zhang L, Smertenko T, Fahy D, Koteyeva N, Moroz N, Kuchařová A, Novák D, Manoilov E, Smertenko P, Galva C, Šamaj J, Kostyukova AS, Sedbrook JC, Smertenko A (2021) Analysis of formin functions during cytokinesis using specific inhibitor SMIFH2. *Plant Physiol* 186:945–963.
- Zhang L, Zhang H, Liu P, Hao H, Jin JB, Lin J (2011) Arabidopsis R-SNARE proteins VAMP721 and VAMP722 are required for cell plate formation. *PLoS One* 6:e26129.
- Zheng H, Bednarek SY, Sanderfoot AA, Alonso J, Ecker JR, Raikhel NV (2002) NPSN11 is a cell plate-associated SNARE protein that interacts with the syntaxin KNOLLE. *Plant Physiol* 129:530–539.
- Zhou Y, Awano T, Kobayashi M, Matoh T, Takabe K (2017) Immunocytochemical detection of rhamnogalacturonan II on forming cell plates in cultured tobacco cells. *Biosci Biotechnol Biochem* 81:899–905.
- Zuo J, Niu QW, Nishizawa N, Wu Y, Kost B, Chua NH (2000) KORRIGAN, an Arabidopsis endo-1,4-beta-glucanase, localizes to the cell plate by polarized targeting and is essential for cytokinesis. *Plant Cell* 12:1137–1152.

## Plant cytokinesis and the construction of new cell wall

Rosalie Sinclair<sup>1</sup>, Grace Hsu<sup>2</sup>, Destiny Davis<sup>1,\*</sup>, Mingqin Chang<sup>1</sup>, Michel Rosquete<sup>1,†</sup>, Janet H. Iwasa<sup>2</sup> and Georgia Drakakaki<sup>1</sup> 

<sup>1</sup> Department of Plant Sciences, University of California Davis, Davis, CA, USA

<sup>2</sup> Department of Biochemistry, School of Medicine, University of Utah, Salt Lake City, UT, USA

### Correspondence

G. Drakakaki, Department of Plant Sciences  
University of California Davis, Davis, CA,  
95616, USA  
Tel: 5307521664  
E-mail: gdrakakaki@ucdavis.edu

### Present address

\*Lawrence Berkeley National Lab,  
Emeryville, CA, USA

†Plant Biology Laboratory, Salk Institute for  
Biological Studies, La Jolla, CA, USA

(Received 14 April 2022, revised 19 May  
2022, accepted 20 May 2022, available  
online 15 July 2022)

doi:10.1002/1873-3468.14426

Edited by Diane Bassham

**Cytokinesis in plants is fundamentally different from that in animals and fungi. In plant cells, a cell plate forms through the fusion of cytokinetic vesicles and then develops into the new cell wall, partitioning the cytoplasm of the dividing cell. The formation of the cell plate entails multiple stages that involve highly orchestrated vesicle accumulation, fusion and membrane maturation, which occur concurrently with the timely deposition of polysaccharides such as callose, cellulose and cross-linking glycans. This review summarizes the major stages in cytokinesis, endomembrane components involved in cell plate assembly and its transition to a new cell wall. An animation that can be widely used for educational purposes further summarizes the process.**

**Keywords:** animation; callose; cell plate; cell wall; cytokinesis; model; phragmoplast; SNARE; *trans*-Golgi network; vesicle trafficking

Cytokinesis is a fundamental process characterized by highly coordinated events in space and time. Regulated cell division along with coordination of cell expansion is essential for plant development and cell shape determination [1–3]. In plant cytokinesis, a process fundamentally different from cytokinesis in animals and fungi, *de novo* formation of a cell plate partitions the cytoplasm of the dividing cell [4–8]. During somatic cell cytokinesis, the orchestrated delivery of cytokinetic

vesicles guided by the phragmoplast leads to the development of the cell plate. Recent reviews describe phragmoplast dynamics, cell plate orientation, membrane dynamics and cell wall polysaccharide delivery [2,4,8–14]. In this article, an overview of the membrane transitions is discussed; we also describe the polysaccharide delivery required for the construction of the new cell wall. This brief summary is accompanied by an animation of plant cytokinesis for educational use.

### Abbreviations

ABP, actin binding protein; ARF, ADP-ribosylation factor; BIG, brefeldin A-inhibited guanine nucleotide-exchange protein; BY-2, bright yellow 2; CalS, callose synthase; CESA, cellulose synthase; COS, chitosan oligosaccharides; CPAM, cell plate assembly matrix; CSC, cellulose synthase complex; CSLD, cellulose synthase like-D; CCVs, clathrin-coated vesicles; ER, endoplasmic reticulum; ES7, endosidin 7; FVS, fusion of vesicles stage; GEF, guanine exchange factor; GSL, glucan synthase like; HG, homogalacturonan; MAP, microtubule-associated protein; PFS, planar fenestrated sheet; PM, plasma membrane; POK, phragmoplast orienting kinesin; PPB, preprophase band; RG-I, rhamnogalacturonan I; RG-II, rhamnogalacturonan II; SCD, stomatal cytokinesis-defective; SM, Sec1/Munc18; SNARE, soluble N-ethylmaleimide-sensitive factor protein attachment protein receptor; SYP61, syntaxin of Plant 61; TAN1, TANGLED1; TN, tubular network; TGN, *trans*-Golgi network; TRAPP, transport protein particle; TVN, tubular-vesicular network; VAMP, vesicle-associated membrane protein; XyG, xyloglucan.

## Cytokinesis – a multistage process animated for educational use

During cytokinesis, the orchestrated delivery of cytokinetic vesicles guided by the phragmoplast (a structure composed of cytoskeletal polymers, associated proteins and membranes) [8] leads to the development of the cell plate, which transitions via four membrane morphological stages [6,15]. The overview of cytokinesis is animated in Video S1, S2, and Fig. 1, with emphasis on cell plate development. First, at the fusion of vesicles stage (FVS), cytokinetic vesicles guided by the phragmoplast arrive at the division plane where fusion occurs (Fig. 2). Upon vesicle fusion and fission, dumb-bell structures are formed. The morphology of the cell plate membrane changes as more vesicle materials are added. As the vesicles fuse, they tubulate largely due to the activity of dynamin-related proteins [12,15,16]. The dynamin-like springs wrap around the neck of fused vesicles, leading to fission and tubulation. This aids in the creation of a membrane network [15] and marks the transition to stage II, known as Tubular-Vesicular Network (TVN) [6,15]. The SH3 Domain-Containing Protein 2 (SH3P2) has also been implicated in this process [17]. The membrane morphology then evolves largely through the expansion of the network to a smoother structure known as the tubular network (TN) stage. At this stage (III), the polysaccharide callose is predominantly deposited in a transient manner [6]. Clathrin-coated vesicles recycle excess materials from the maturing cell plate and

allow the cell plate to form a thinner and smoother structure. As the cell plate continues to smoothen and expand, it forms a fenestrated sheet. At this planar fenestrated sheet (PFS) stage (IV), the distinct plasma membrane sheet is apparent. The fenestrae that are left open often contain endoplasmic reticulum (ER) strands and are sites of plasmodesmata formation [6]. Deposition of polysaccharides, such as cellulose, help stiffen the cell plate. Membrane structures described as ‘finger like fusion tubes’ extend from the cell plate to meet the parental cell wall [6,15]. Finally, the cell plate fuses with the parental cell wall and plasma membrane, concluding cytokinesis. Notably, callose is also present at the junction of the cell plate and the parental cell wall [6].

Polymerization of microtubules and their alignment into a solid phragmoplast facilitates the delivery of vesicles at the cell division plane [18,19]. During the TVN and TN stages, even distribution of microtubules is observed over the wavy, membrane disk. The centrifugal expansion of cell plate development coincides with the timely disappearance of phragmoplast microtubules from the centre, leading to a ring phragmoplast [8,20] (Fig. 2). This ring continues to expand and grow along the direction of cell plate expansion (Fig. 2). Thus, the cell plate itself contains a gradient of stages ranging from the most mature at the cell plate centre to newly accumulated membranes at the leading edge. As the cell plate docks at the plasma membrane, a discontinuous ring phragmoplast is formed (Fig. 2).

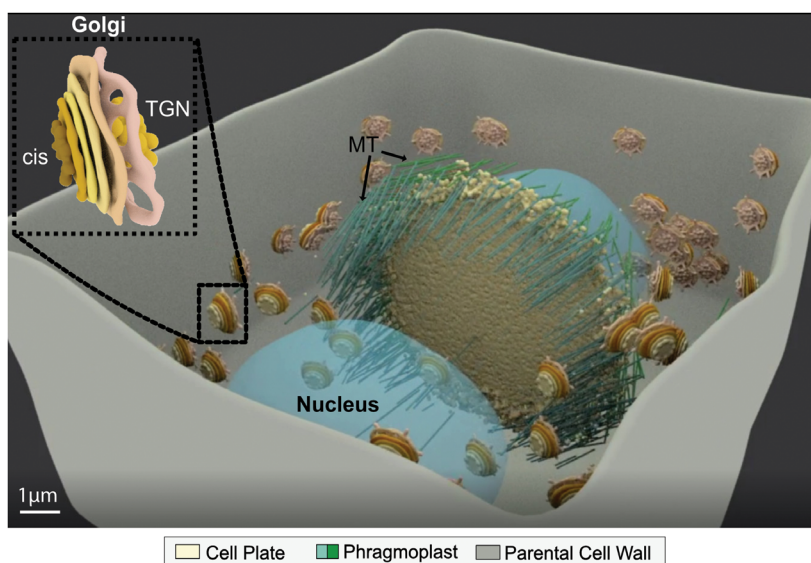
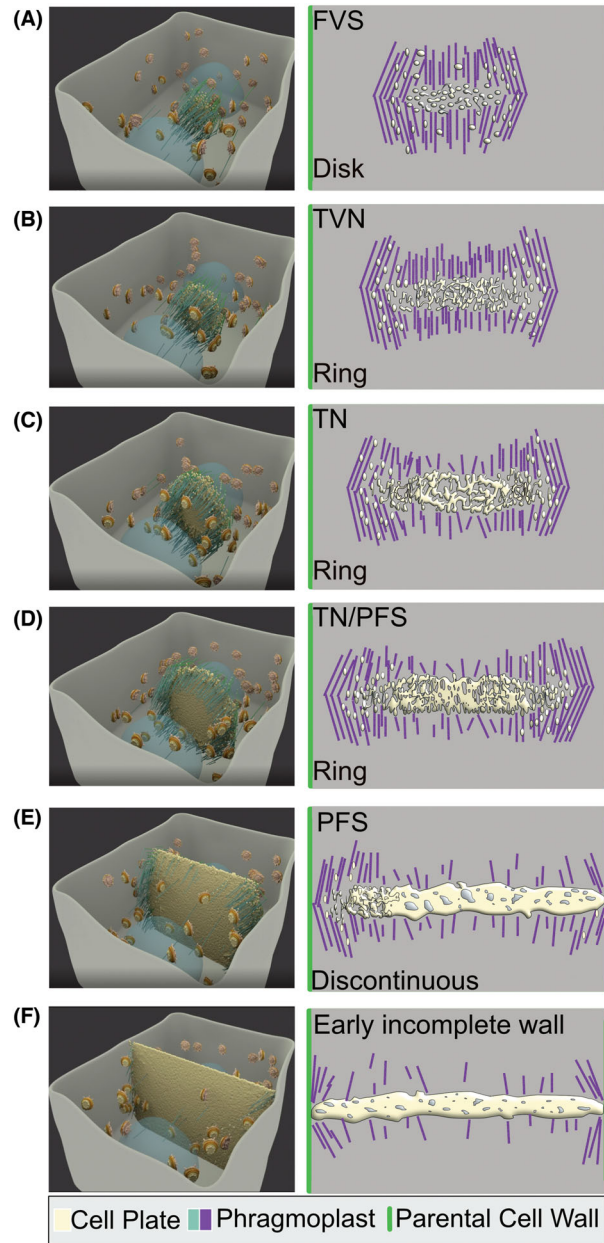


**Fig. 1.** Schematic representation of cytokinesis, summarizing cell plate formation. Still image excerpt from Video S1, S2. MT (microtubules). TGN (*trans*-Golgi network). Scale bar represents 1  $\mu\text{m}$ .



## Molecular components involved in cytokinesis

### Cytoskeletal array in cytokinesis

During cytokinesis, the cytoskeleton is organized into the phragmoplast that guides the delivery of cytokinetic vesicles to the ribosome-excluding cell plate assembly matrix (CPAM) at the division plane. This requires the coordination of microtubules and microfilaments, along with many microtubule-associated proteins (MAPs) and actin-binding proteins (ABPs),

**Fig. 2.** Schematic representation of cell plate assembly and phragmoplast organization. Cell plate assembly occurs in four stages. On the left snapshots of the animation, represent different cytokinetic stages. Nucleus (blue), Golgi stacks (variegated orange), cytokinetic vesicles (yellow) and phragmoplast microtubules (teal/green) in their arrangement around the developing cell plate are shown. To the right is a simplified representation of this process showing membrane organization (yellow) and the phragmoplast (purple) to further illustrate the simultaneous maturation and naming mechanics. (A) During the FVS stage, cytokinetic vesicles guided by the phragmoplast accumulate at the centre of the dividing cell, the cell plate assembly matrix, where fusion starts to occur. This represents a disk-like tight bundling of the phragmoplast microtubules. (B, C) Vesicles undergo fusion and fission and conformational changes, resulting in TVN (B). The phragmoplast continues to expand with the membrane material expanding at the centre while microtubules depolymerize at the sites where TVN – TN is formed. This leads to a ring-like phragmoplast conformation (C). (D) Transition from TN to PFS. The membrane structures are beginning to close and create the PFS. The membrane network further expands to a continuous PFS taking up the majority of the cell plate. The fenestrae left open are often sites of plasmodesmata formation. (E) As the cell plate docks at the plasma membrane, a discontinuous ring phragmoplast is formed. (F) The remaining end continues to mature until it fuses to the parental cell wall completing cytokinesis.

including kinesin and myosin motors. These motor proteins deliver cargo to the cell plate and support its expansion and maturation [10,11,21,22]. Early in the G2 stage of mitosis, the division plane and phragmoplast orientation are determined by the preprophase band (PPB) [23]. Proper PPB assembly and establishment of the division plane require the TON1/TRM/PP2A complex [24].

Once the division plane has been established, the expansion of the phragmoplast requires a suite of proteins including: myosin VIII [25], three myosin XI members (1, 2, K) [26], Kinesin-12 POK1 and POK2 [27], TAN1 and AIR9 and two PHGAPs [28,29]. Three IQ67 DOMAIN (IQD) proteins physically interact with POKs and PHGAPs, likely providing a scaffold for division plane maintenance [30]. During cytokinesis, the phragmoplast expands from the cell centre to the cell cortex, while its shape transforms from a disc of microtubules to a ring, and then to a wide discontinuous ring until it disassembles (Fig. 2). The microtubule severing complex KATANIN1 (KTN1) and its interactors, microtubule-binding protein MACET4/CORD4, function in phragmoplast organization and expansion [31,32].

### Vesicle fusion and membrane organization

Cytokinetic vesicles contribute membrane material and deliver cargo for the biogenesis of the cell plate.

Cytokinetic vesicles are primarily Golgi/*trans* Golgi network (TGN) derived [15] with contributions from endosomal populations. The ARF GEFs (BIG1-4) assist in the delivery of newly synthesized proteins and endocytosed cargo to the forming cell plate [33].

SNARE proteins regulate vesicle docking and fusion at the CPAM. In Arabidopsis, two kinds of SNARE complexes involving the cytokinesis-specific SNARE KNOLLE act redundantly during cytokinesis [34]: (a) KNOLLE and its partners Qbc-SNARE SNAP33 and either R-SNAREs VAMP721/VAMP722, or (b) KNOLLE and its partners Qb-SNARE NPSN11, Qc-SNARE SYP71 and also R-SNAREs VAMP721/VAMP722 [35–37]. Inactive cytokinetic SNARE complexes are assembled at the ER and are transformed into fusogenic SNARE complexes after passage through the Golgi/TGN to the cell division plane [38]. The cytokinesis-specific KNOLLE [34] is widely used as a marker to identify mitotic cells. The localization of KNOLLE is tightly regulated and degraded in the vacuole at the end of cytokinesis [37]. This regulation includes the AP-1 adaptor subunits at the TGN [39], which are essential for the trafficking of KNOLLE to the cell plate [40,41] and sterol-dependent endocytosis, further facilitating the correct localization of the syntaxin at the cell plate [42]. Sec1/Munc18 (SM) proteins, such as KEULE, assist in SNARE complex formation, essential for vesicle fusion during cytokinesis [43] (Fig. 3).

The action of Rab GTPases and tethering factors brings in close proximity the cytokinetic vesicles with the target membrane at the cell plate. Different GTPases recognize classes of trafficking machinery

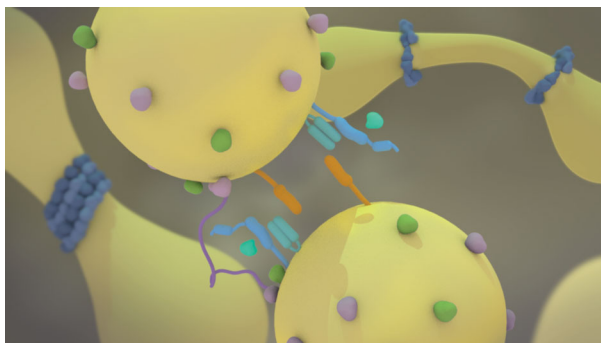


**Fig. 3.** Vesicle fusion. During the early stages of cell plate assembly, cytokinetic vesicles regulated by molecular switches, such as RAB GTPases (green and light purple) undergo fusion. Vesicle fusion is mediated SNAREs (blue and orange) assisted by regulatory proteins and tethering complexes (dark purple). Dynamin rings (dark blue) assemble around the vesicles and stretch the fused membrane, creating the dumbbell-like structures and tubulations.

and provide directionality in vesicle transport. Among the Arabidopsis small GTPases, RABA2 and RABA3 preferentially localize to the leading edge of the cell plate, indicating a role in the delivery and incorporation of new material into the assembling cell plate [44]. A complete roadmap of the different GTPases and their overlapping and complementary functions in cytokinesis is still unknown. Several RABA1 members are recruited to the cell plate during cytokinesis [45–48]. The TGN/early endosome-resident RABA1d has been implicated in the recycling of material from the plasma membrane (PM) to the growing plate [48]. Further, the RABA2a and RABA1e vesicles display a different spatiotemporal pattern during cytokinesis [47]. In addition to RABAs, RABE1 localizes to the cell plate and interacts with the Stomatal Cytokinesis-Defective (SCD) complex that regulates trafficking to the cell plate and potentially activates RABE1 [49,50].

The attachment of vesicles to the target membrane over a distance is facilitated by tethering complexes [51]. The tethering complexes, TRAPP1 and exocyst are sequentially regulating cell plate assembly, expansion and maturation. TRAPP1—predominantly assists in vesicle fusion inside the CPAM [52], while the exocyst complex functions at the onset of cytokinesis and during cell plate maturation [51–53]. Tethering factors act as guanine nucleotide exchange factors (GEFs) on GTPases, mediating their activation. Recent proteomic and large-scale interaction studies indicate that TRAPP1 likely acts on the RABA2 GTPase [54]. Notably, the TRAPP1 complex is involved in sorting exocyst subunits, demonstrating synergistic activities between the two tethering complexes or their subunits during cytokinesis [52]. Furthermore, the DENN domain SCD1 and 2 proteins also functionally interact with subunits of the exocyst tethering complex and RabE1, regulating post-Golgi trafficking to the plasma membrane and the cell plate [49].

During cytokinesis, it is estimated that ~70% of excess membrane material is recycled, via clathrin-coated vesicles (CCVs) throughout the TN to PFS stages [6,16] (Fig. 4). The presence of the Clathrin Light Chain, Dynamin-Related Proteins, SCD1 and 2, Epsin-like adaptors, and the adaptin-like T-PLATE at the cell plate, support the role of clathrin-mediated recycling of excess membrane material from the cell plate [12,55–60].

## Cell-wall construction

The primary cell wall comprises a dynamic network of cellulose microfibrils embedded in a network of

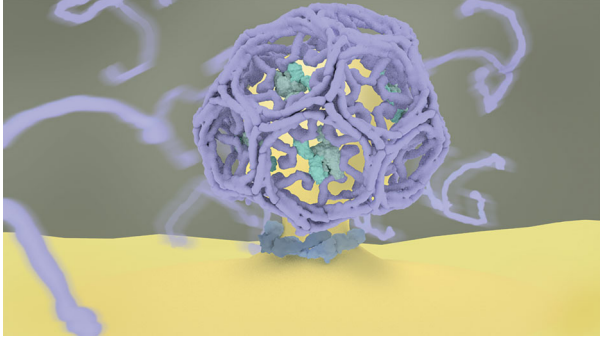


**Fig. 4.** Clathrin-coated vesicles (CCVs). Cartoon representation of clathrin coated vesicles. Clathrin triskelion cage (purple) assisted by adaptor protein complexes (teal) encapsulates cell plate membrane (yellow). Dynamin ring (blue) facilitates CCV fission.

hemicellulose, pectin, glycoproteins and other macromolecules [61]. The deposition and assembly of polysaccharides into a new cell wall during cytokinesis is a gradual process; however, a detailed study has been mostly impeded by the technical limitations to perform live imaging of polysaccharides (Box 1).

### Callose and cellulose

Callose and cellulose are polysaccharides that are synthesized by biosynthetic enzymes at the cell plate membrane (Fig. 5). Callose, a  $\beta$ -(1,3)-linked glucan is transiently deposited during cell plate development. Its accumulation starts at the TVN stage and peaks at the TN and PFS stages [6]. It has been proposed that

callose stabilizes the fragile membrane network and assists in the expansion of the cell plate to a fenestrated sheet [6]. Callose synthases, also known as glucan synthase-like proteins (CALS/GSL), are responsible for callose biosynthesis. Of the 12 family members only one, CalS10/GSL8 has been shown to be necessary for cytokinesis through genetic evidence, exhibiting distinct mutant phenotypes including cell plate stubs and seedling lethality [62–64]. CalS1/GSL6 has also been implicated [65] in cell plate development, but its role in cytokinesis has not been genetically supported. GSL8 interacts with GSL10 but this interaction remains to be investigated at the cell plate [66]. The trafficking pathway of GSL8 to the cell plate is mediated via post-Golgi vesicles, which is supported by its detection in proteomic analyses of TGN/EE compartments [67,68]. The transient accumulation of callose is achieved by the calcium activation of the callose synthase, followed by the timely removal of the polysaccharide via hydrolytic enzymes, once the new cell wall is stabilized [69–71]. The role of transient deposition of callose in polysaccharide assembly is still unknown. It is plausible that callose could serve as a scaffold into which other more permanent polysaccharides and proteins are later deposited [72]. The *Arabidopsis* genome contains 50 (1,3)- $\beta$ -glucanases [73,74], however, no specific member has been so far assigned for callose degradation at the cell plate.

The mechanisms underlying the complex transition from a vesicle membrane network (TN) to a fenestrated sheet and a mature cell plate, and the contribution of polysaccharides such as callose in this

#### Box 1. Primary cell-wall components.

Term	Location of synthesis	Detected at the cell plate	Structure
Callose	Plasma membrane	[6]	$\beta$ -(1,3)-linked glucan
Cellulose	Plasma membrane	[6] [81]	$\beta$ -(1,4)-linked glucan
Xyloglucan	Golgi apparatus	[87]	$\beta$ -(1,4)-linked glucan backbone that is further substituted with xylosyl, galactosyl, fucosyl residues
Pectin	Golgi apparatus and TGN	[52,87,99]	A family of galacturonic acid-rich polysaccharides that includes homogalacturonan, rhamnogalacturonan I and the substituted galacturonans rhamnogalacturonan II (RG-II) and xylogalacturonan (XGA)
Glycoproteins	ER and Golgi	[52,104]	Structural proteins with oligosaccharide chains (glycans) attached to polypeptide (5 classes based on their enriched amino acids)

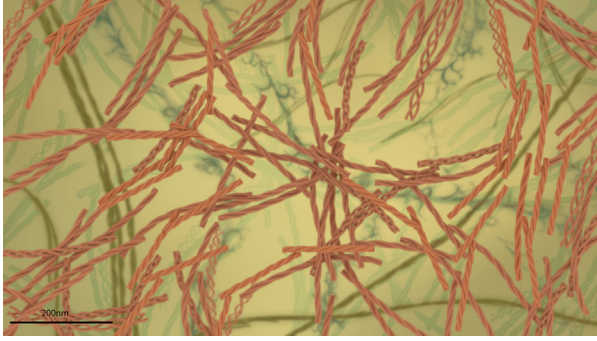


**Fig. 5.** Callose-containing cell plate. Cartoon representation of proposed callose conformations in helical structured fibres. Callose (orange-red helical structures). The background in pale colours represents other cell wall components. Scale bar represents 200 nm.

transition are not well understood. Overcoming the lethality hurdles in genetic studies associated with the GSL family [62–64], a modelling approach was implemented. Cell plate sub-structures were approximated with testable shapes. The free energy of cell plate structures and their combination in a network was modelled by adopting the Helfrich energy that examines the elastic properties of lipid bilayers [75]. The Helfrich energy model was further modified with the addition of a novel term, the spreading force, possibly derived by polysaccharide deposition [76]. To reach a mature cell plate, the proposed model requires the onset of a two-dimensional spreading/stabilizing force, coupled with a concurrent loss of spontaneous curvature. The absence of a spreading/stabilizing force predicts failure of maturation [76]. The transient accumulation of callose, coinciding with the predicted stages requiring this spreading force is consistent with the proposed model's concept, lending support for the proposed role of callose in cell plate maturation. Further, a specific cytokinetic callose chemical inhibitor, Endosidin7 (ES7), has been instrumental to better understand the necessity for callose at the cell plate [77]. Notably, ES7 does not inhibit wound or stress-induced callose. The cytokinetic defects resulting from ES7 application both in higher plants and algae support the evolutionarily conserved role of the polymer in cytokinesis [77,78]. The failure of cell plate maturation with ES7 application indicates that callose is likely a contributor to the stabilizing or spreading force as predicted by modelling [76] (Fig. 5). Similarly, The *P. patens saber* mutant has cytokinesis defects that are caused by abnormal ER-cell plate connections, and delayed/ aberrant callose accumulation [79]. A plausible hypothesis is that calcium levels necessary for callose synthase activity are mediated via ER-cell plate

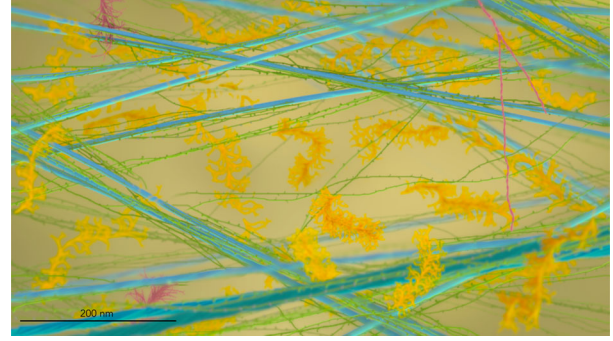


**Fig. 6.** Primary cell wall. Cartoon representation of primary cell wall of dicot plants and organization of its constituents. Cellulose (blue), pectin (yellow) and xyloglucan (green), structural proteins (pink). Scale bar represents 200 nm.

interactions and are affected in the *P. patens saber* mutant, highlighting the importance of callose during cytokinesis and a potential ER-mediated regulation. The junction of the cell plate with the parental cell wall is also rich in callose [6], although the contributions of different polysaccharides and the flux of polysaccharides and biosynthetic enzymes at this location remain to be characterized.

The cell wall develops with the deposition of permanent polysaccharides such as cellulose, cross-linking glycans and glycoproteins [58] (Fig. 6). Deposition of cellulose, a  $\beta$ -(1,4)-linked glucan, at the cell plate, coincides with the flattening and stiffening of the cell plate at the late TN and PFS stages concomitant with the reduction of callose [6]. Cellulose synthase complexes (CSC) are responsible for cellulose biosynthesis. For an in depth analysis of cellulose deposition at the cell plate, we refer to an excellent recent review [80]. Live imaging of cellulose synthase suggested the appearance of the enzyme and the product as early as the TVN [81]. However, the limited resolution of light microscopy in the study does not allow for the precise dissection of the cell plate stage. In addition to cellulose synthases (CESAs), a member of the Cellulose Synthase Like-D family (CSLD5), supports the construction of the new cell wall [82]. The direct product of CSLD5 has not been yet identified, but similar to the product of CSLD3, it is likely a  $\beta$ -(1,4)-glucan polysaccharide [83], providing a scaffold for crystalline cellulose.

### Non-cellulosic polysaccharides and glycoproteins

Hemicelluloses and pectins, also known as matrix polysaccharides or cross-linking glycans are synthesized in the Golgi apparatus and are transported via

vesicles to the developing the cell plate. Hemicelluloses bind to cellulose microfibrils while pectin forms a soft network with extensive but weak contacts to cellulose and xyloglucan in mature cell wall [84], thus their timely deposition and assembly are essential for a functional cell wall network. Our current understanding of the delivery and assembly of these polysaccharides into the developing cell plate and cell wall is limited and mostly derived from studies using electron microscopy coupled with immunolocalization with polysaccharide specific antibodies [85–91]. Hemicellulose in dicot plants, known as xyloglucan (XyG), consists of a  $\beta$ -1,4 glucan backbone featuring a regular pattern of substitutions [92]. Most Golgi localized enzymes involved in the biosynthesis of XyG are well characterized [92,93]. In red clover (*Trifolium pretense* L.) roots, XyG has been observed both in secretory vesicles and the developing cell plate, likely starting at the TVN stage with its presence most abundant upon completion of the new cell wall [87].

Pectin structure is comprised of a galacturonic acid-based backbone, with subgroups determining its diversification and classification into four main types: homogalacturonan (HG), rhamnogalacturonan I (RG-I), rhamnogalacturonan II (RG-II) and substituted galacturonans [94]. While several pectin biosynthetic and modifying enzymes have been identified, due to the complexity of the molecules, many enzymes are still awaiting identification [94–96]. Pectin biosynthesis likely starts at the *cis*-Golgi with non-esterified RGI and HG present in the *cis* and medial cisternae, while arabinose-containing side chains of RGI are detected only in the TGN, following a compartmentalized assembly line [97]. While pectins are synthesized and secreted in a methyl esterified form at the cell wall, they are de-esterified by pectin methyl esterases, leading to their acidification and allowing for further cross-linking [61,98]. The presence of methyl esterified pectin at the cell plate has been detected in different systems including *Arabidopsis* and *Nicotiana tabacum* Bright-Yellow-2 (BY-2) dividing cells [52,99]. The absence of RGI in the cell plate but presence in the middle lamella of red clover (*Trifolium pretense* L.) suggests that acidification of the polysaccharide occurs at later stages [87]. RG-II, a more complex form of pectin, serves as the site of borate cross-linking within pectin to facilitate gel formation. Notably, RGII has been detected at the cell plate as shown using immunoelectron microscopy in tobacco BY-2 cells, suggesting that complex pectin structures are deposited at the cell plate [100]. The complexity of the matrix polysaccharides and the various degrees of modification complicates the task of dissecting their trafficking

and assembly at the cell plate and the developing cell wall.

The polysaccharide content of the TGN SYP61-positive vesicle populations was characterized by combining vesicle isolation using the SNARE SYP61 as bait and a large-scale polysaccharide detection using a collection of  $\sim 150$  antibodies against cell wall polysaccharides [101]. Interestingly, both xyloglucan and pectin glycans were present in the isolated vesicles and carried various degrees of substitution. This suggests that diverse glycan populations are carried in the apoplast for their final assembly. Adoption of glycomic analysis methodology for the identification of cytokinetic vesicles with the aid of specific markers for vesicle isolation can shed light on the specific types of polysaccharide structures transported to the cell plate.

Beyond polysaccharides, glycoproteins also constitute important structural components of the cell wall, although they do not possess catalytic activity [61,102,103]; their presence at the cell plate has been detected with the aid of monoclonal antibodies [52,104]. EXTENSIN3, a hydroxyproline-rich glycoprotein is associated with cell plate development, is enriched at the junctions with the parental cell wall, and is proposed to provide a scaffold for polysaccharide organization [105,106].

## Challenges and emerging technologies

Cell plate development is a dynamic process that involves the coordination of the cytoskeleton, vesicle trafficking, polysaccharide deposition and assembly with constant remodelling to develop a new cell wall separating the two daughter cells. Given this complexity, there are significant challenges in dissecting this process.

The different stages of cell plate development occur simultaneously in an expanding cell plate; thus, their dissection in both time and space requires advanced technologies and modalities including four-dimensional (4D), high-resolution, long-term imaging in a biologically relevant (multicellular) system. The synchronization of cytokinesis in a multicellular system is not trivial because it occurs mostly in tissues with high meristematic activity. Embryo or seedling lethality is a landmark in cytokinesis mutants, hence the inability to take full advantage of a genetic approach in their dissection.

The dissection of polysaccharide deposition at the cell wall is currently not easily amenable to live imaging as most of the specific probes are monoclonal antibodies against polysaccharide epitopes [107], requiring immunodetection methods in fixed cells. Many

proteins involved in cell plate formation, such as callose synthases, are multi-spanning membrane proteins that are difficult to fluorescently tag or recombinantly express to characterize their localization and function.

Since the early studies of plant cytokinesis, the development of new technologies and approaches continues to provide means of dissecting complex processes.

Chemical biology using ES7 and SMIFH2 informed the role of callose and formins, respectively, in cytokinesis [77,78,108] and can be instrumental in dissecting different aspects of cytokinesis at a spatiotemporal level while overcoming lethality.

Advanced imaging technologies, such as Lattice Light Sheet (LLS) microscopy, enables long term 4D imaging without photobleaching [109] which has been used to analyse mitotic cells in mammalian cells [110] and is a promising approach for plants. Further, Light Sheet [111] and vertical imaging [112] are gaining more traction in plants and can provide cell division patterns that take the effect of gravity into account. Structured illumination microscopy has been instrumental to better understand CESA dynamics at the PM [113]. The application of live super-resolution microscopy can help dissect protein dynamics at different cell plate stages.

Advanced image-processing tools [114] and biophysical modelling [76] enable the development of models that can provide insights into the contribution of individual components in cytokinesis. The developed model [76] can be used to interrogate the biomechanical contribution of polysaccharides in cell plate maturation. Additionally, the application of Brillouin microscopy that assesses stiffness through the thickness of the wall [115] or atomic force microscopy (AFM)-based analysis that can assess external topography and elasticity of plant cells [116] could be used to biologically interrogate proposed models. Such synergy of information can help inform how cell plate expansion and maturation are regulated based on different polysaccharides and genetic backgrounds. Similarly, cell shape analysis coupled with modelling can facilitate the prediction of division-plane orientations and aid in the characterization of contributing proteins [117].

The generation of probes that allow live imaging of the cell wall [118], such as Pontamine Fast Scarlet 4B for cellulose [119], aniline blue fluorochrome for callose, fluorophore-functionalized chitosan oligosaccharides (COS) and metabolic click-mediated labelling for pectin [120–122], are critical to better understand polysaccharide deposition and assembly in the cell wall. Overcoming the major bottleneck of live

polysaccharide imaging along with the biosynthetic enzymes during cytokinesis can help understand the complex regulation of polysaccharide transport, deposition and assembly into the cell plate and new cell wall.

Established cell culture systems, such as BY-2 cultures [123] or algae [78], are amenable to synchronization and can be used to establish quick pipelines for interrogation. Conditional mutants, such as the temperature sensitive *tplate* mutant, can overcome many of the challenges with canonical cytokinesis mutants [124]. Biochemical analysis of isolated cytokinetic vesicles [101] can reveal the nature of diverse cargo transported at the cell plate.

## Conclusions and perspectives

While recent advances have provided a better understanding of cell plate formation [11] many questions remain, some of which are listed here. (a) What is the cargo of cytokinetic vesicles? (b) How many types of cytokinetic vesicles exist and how is their cargo separated? (c) Which motor proteins specifically facilitate the transport of cytokinetic vesicles along microtubules regulating membrane and cargo delivery? (d) What is the stoichiometry and organization/orientation of organelles during cell plate assembly and expansion? (e) What are the signalling mechanisms that coordinate transitions of the cell-plate membrane and phragmoplast expansion? (f) What is the timing of polysaccharide deposition and how is this regulated? (g) How do specific polysaccharides, such as callose, contribute to the two-dimensional spreading force necessary for cell plate expansion and maturation? (h) What are the mechanisms that regulate the fusion of the cell plate with the parental cell wall?

Continuing on recent discoveries, and armed with emerging technologies, the mysteries of this fundamental aspect of plant life will certainly be unravelled in the near future.

## Acknowledgements

The authors sincerely apologize to colleagues whose relevant work could not be discussed because of length limitations. The authors are extremely grateful to Professors Bo Liu, Lacey Samuels, Sebastian Bednarek and Marisa Otegui for their critical comments during the preparation of the animation. The authors are grateful to the anonymous reviewers for their constructive criticism. This work was supported by NSF Grant MCB 1818219 and by the Department of Agriculture Hatch (CA-D-PLS-2132-H).

## References

- 1 Sablowski R, Gutierrez C. Cycling in a crowd: coordination of plant cell division, growth, and cell fate. *Plant Cell*. 2022;**34**:193–208.
- 2 Rasmussen CG, Bellinger M. An overview of plant division-plane orientation. *New Phytol*. 2018;**219**:505–12.
- 3 Yi P, Goshima G. Division site determination during asymmetric cell division in plants. *Plant Cell*. 2022;**34**:2120–39.
- 4 Drakakaki G. Polysaccharide deposition during cytokinesis: challenges and future perspectives. *Plant Sci*. 2015;**236**:177–84.
- 5 Jurgens G. Cytokinesis in higher plants. *Annu Rev Plant Biol*. 2005;**56**:281–99.
- 6 Samuels AL, Giddings TH Jr, Staehelin LA. Cytokinesis in tobacco BY-2 and root tip cells: a new model of cell plate formation in higher plants. *J Cell Biol*. 1995;**130**:1345–57.
- 7 Staehelin LA, Hepler PK. Cytokinesis in higher plants. *Cell*. 1996;**84**:821–4.
- 8 Smertenko A, Assaad F, Baluska F, Bezanilla M, Buschmann H, Drakakaki G, et al. Plant cytokinesis: terminology for structures and processes. *Trends Cell Biol*. 2017;**27**:885–94.
- 9 Buschmann H, Müller S. Update on plant cytokinesis: rule and divide. *Curr Opin Plant Biol*. 2019;**52**:97–105.
- 10 Lee YJ, Liu B. Microtubule nucleation for the assembly of acentrosomal microtubule arrays in plant cells. *New Phytol*. 2019;**222**:1705–18.
- 11 Gu Y, Rasmussen CG. Cell biology of primary cell wall synthesis in plants. *Plant Cell*. 2022;**34**:103–28.
- 12 McMichael CM, Bednarek SY. Cytoskeletal and membrane dynamics during higher plant cytokinesis. *New Phytol*. 2013;**197**:1039–57.
- 13 Muller S, Jurgens G. Plant cytokinesis-no ring, no constriction but centrifugal construction of the partitioning membrane. *Semin Cell Dev Biol*. 2016;**53**:10–8.
- 14 McFarlane HE, Doring A, Persson S. The cell biology of cellulose synthesis. *Annu Rev Plant Biol*. 2014;**65**:69–94.
- 15 Segui-Simarro JM, Austin JR, White EA, Staehelin LA. Electron tomographic analysis of somatic cell plate formation in meristematic cells of Arabidopsis preserved by high-pressure freezing. *Plant Cell*. 2004;**16**:836–56.
- 16 Otegui MS, Mastroratte DN, Kang BH, Bednarek SY, Staehelin LA. Three-dimensional analysis of syncytial-type cell plates during endosperm cellularization visualized by high resolution electron tomography. *Plant Cell*. 2001;**13**:2033–51.
- 17 Ahn G, Kim H, Kim DH, Hanh H, Yoon Y, Singaram I, et al. SH3 domain-containing protein 2 plays a crucial role at the step of membrane Tubulation during cell plate formation. *Plant Cell*. 2017;**29**:1388–405.
- 18 Lee YR, Giang HM, Liu B. A novel plant kinesin-related protein specifically associates with the phragmoplast organelles. *Plant Cell*. 2001;**13**:2427–39.
- 19 Euteneuer U, McIntosh JR. Polarity of midbody and phragmoplast microtubules. *J Cell Biol*. 1980;**87**:509–15.
- 20 Murata T, Sano T, Sasabe M, Nonaka S, Higashiyama T, Hasezawa S, et al. Mechanism of microtubule array expansion in the cytokinetic phragmoplast. *Nat Commun*. 2013;**4**:1967.
- 21 Lee YR, Liu B. The rise and fall of the phragmoplast microtubule array. *Curr Opin Plant Biol*. 2013;**16**:757–63.
- 22 Smertenko A, Hewitt SL, Jacques CN, Kacprzyk R, Liu Y, Marcec MJ, et al. Phragmoplast microtubule dynamics – a game of zones. *J Cell Sci*. 2018;**131**:jcs203331.
- 23 Van Damme D, Vanstraelen M, Geelen D. Cortical division zone establishment in plant cells. *Trends Plant Sci*. 2007;**12**:458–64.
- 24 Spinner L, Gadeyne A, Belcram K, Goussot M, Moison M, Duroc Y, et al. A protein phosphatase 2A complex spatially controls plant cell division. *Nat Commun*. 2013;**4**:1863.
- 25 Wu SZ, Bezanilla M. Myosin VIII associates with microtubule ends and together with Actin plays a role in guiding plant cell division. *Elife*. 2014;**3**:e03498.
- 26 Abu-Abied M, Belausov E, Hagay S, Peremyslov V, Dolja V, Sadot E. Myosin XI-K is involved in root organogenesis, polar auxin transport, and cell division. *J Exp Bot*. 2018;**69**:2869–81.
- 27 Müller S, Livanos P. Plant Kinesin-12: Localization Heterogeneity and Functional Implications. *Int J Mol Sci*. 2019;**20**:4213.
- 28 Buschmann H, Dols J, Kopischke S, Peña EJ, Andrade-Navarro MA, Heinlein M, et al. Arabidopsis KCBP interacts with AIR9 but stays in the cortical division zone throughout mitosis via its MYTH4-FERM domain. *J Cell Sci*. 2015;**128**:2033–46.
- 29 Stöckle D, Herrmann A, Lipka E, Lauster T, Gavidia R, Zimmermann S, et al. Putative ROPGAPs impact division plane selection and interact with kinesin-12 POK1. *Nat Plants*. 2016;**2**:16120.
- 30 Kumari P, Dahiya P, Livanos P, Zergiebel L, Kölling M, Poeschl Y, et al. IQ67 DOMAIN proteins facilitate preprophase band formation and division-plane orientation. *Nat Plants*. 2021;**7**:739–47.
- 31 Sasaki T, Tsutsumi M, Otomo K, Murata T, Yagi N, Nakamura M, et al. A novel katanin-tethering machinery accelerates cytokinesis. *Curr Biol*. 2019;**29**:4060–4070.e3.
- 32 Panteris E, Kouskouveli A, Pappas D, Adamakis IS. Cytokinesis in fra2 *Arabidopsis thaliana* p60-katanin

- mutant: defects in cell plate/Daughter Wall formation. *Int J Mol Sci.* 2021;**22**:1405.
- 33 Richter S, Kientz M, Brumm S, Nielsen ME, Park M, Gavidia R, et al. Delivery of endocytosed proteins to the cell-division plane requires change of pathway from recycling to secretion. *Elife.* 2014;**3**:e02131.
  - 34 Lauber MH, Waizenegger I, Steinmann T, Schwarz H, Mayer U, Hwang I, et al. The Arabidopsis KNOLLE protein is a cytokinesis-specific syntaxin. *J Cell Biol.* 1997;**139**:1485–93.
  - 35 El Kasmi F, Krause C, Hiller U, Stierhof YD, Mayer U, Conner L, et al. SNARE complexes of different composition jointly mediate membrane fusion in Arabidopsis cytokinesis. *Mol Biol Cell.* 2013;**24**:1593–601.
  - 36 Zhang L, Zhang H, Liu P, Hao H, Jin JB, Lin J. Arabidopsis R-SNARE proteins VAMP721 and VAMP722 are required for cell plate formation. *PLoS one.* 2011;**6**:e26129.
  - 37 Jurgens G, Park M, Richter S, Touihri S, Krause C, El Kasmi F, et al. Plant cytokinesis: a tale of membrane traffic and fusion. *Biochem Soc Trans.* 2015;**43**:73–8.
  - 38 Karnahl M, Park M, Mayer U, Hiller U, Jürgens G. ER assembly of SNARE complexes mediating formation of partitioning membrane in Arabidopsis cytokinesis. *Elife.* 2017;**6**:e25327.
  - 39 Yan X, Wang Y, Xu M, Dahhan DA, Liu C, Zhang Y, et al. Cross-talk between clathrin-dependent post-Golgi trafficking and clathrin-mediated endocytosis in Arabidopsis root cells. *Plant Cell.* 2021;**33**:3057–75.
  - 40 Park M, Song K, Reichardt I, Kim H, Mayer U, Stierhof YD, et al. Arabidopsis  $\mu$ -adaptin subunit AP1M of adaptor protein complex 1 mediates late secretory and vacuolar traffic and is required for growth. *Proc Natl Acad Sci USA.* 2013;**110**:10318–23.
  - 41 Teh OK, Shimono Y, Shirakawa M, Fukao Y, Tamura K, Shimada T, et al. The AP-1  $\mu$  adaptin is required for KNOLLE localization at the cell plate to mediate cytokinesis in Arabidopsis. *Plant Cell Physiol.* 2013;**54**:838–47.
  - 42 Boutté Y, Frescatada-Rosa M, Men S, Chow CM, Ebine K, Gustavsson A, et al. Endocytosis restricts Arabidopsis KNOLLE syntaxin to the cell division plane during late cytokinesis. *EMBO J.* 2010;**29**:546–58.
  - 43 Assaad FF, Huet Y, Mayer U, Jurgens G. The cytokinesis gene KEULE encodes a Sec1 protein that binds the syntaxin KNOLLE. *J Cell Biol.* 2001;**152**:531–43.
  - 44 Chow CM, Neto H, Foucart C, Moore I. Rab-A2 and Rab-A3 GTPases define a trans-golgi endosomal membrane domain in Arabidopsis that contributes substantially to the cell plate. *Plant Cell.* 2008;**20**:101–23.
  - 45 Qi X, Zheng H. Rab-A1c GTPase defines a population of the trans-Golgi network that is sensitive to endosidin1 during cytokinesis in Arabidopsis. *Mol Plant.* 2013;**6**:847–59.
  - 46 Qi X, Kaneda M, Chen J, Geitmann A, Zheng H. A specific role for Arabidopsis TRAPP II in post-Golgi trafficking that is crucial for cytokinesis and cell polarity. *Plant J.* 2011;**68**:234–48.
  - 47 Davis DJ, McDowell SC, Park E, Hicks G, Wilkop TE, Drakakaki G. The RAB GTPase RABA1e localizes to the cell plate and shows distinct subcellular behavior from RABA2a under Endosidin 7 treatment. *Plant Signal Behav.* 2016;**11**:e984520.
  - 48 Berson T, von Wangenheim D, Taka T, Amajova O, Rosero A, Ove Ka M, et al. Trans -Golgi network localized small GTPase RabA1d is involved in cell plate formation and oscillatory root hair growth. *BMC Plant Biol.* 2014;**14**:252.
  - 49 Mayers JR, Hu T, Wang C, Cardenas JJ, Tan Y, Pan J, et al. SCD1 and SCD2 form a complex that functions with the exocyst and RabE1 in exocytosis and cytokinesis. *Plant Cell.* 2017;**29**:2610–25.
  - 50 McMichael CM, Reynolds GD, Koch LM, Wang C, Jiang N, Nadeau J, et al. Mediation of clathrin-dependent trafficking during cytokinesis and cell expansion by Arabidopsis stomatal cytokinesis defective proteins. *Plant Cell.* 2013;**25**:3910–25.
  - 51 Vukasinovic N, Zarsky V. Tethering complexes in the Arabidopsis endomembrane system. *Front Cell Dev Biol.* 2016;**4**:46.
  - 52 Rybak K, Steiner A, Synek L, Klaeger S, Kulich I, Facher E, et al. Plant cytokinesis is orchestrated by the sequential action of the TRAPP II and exocyst tethering complexes. *Dev Cell.* 2014;**29**:607–20.
  - 53 Fendrych M, Synek L, Pecenkova T, Toupalova H, Cole R, Drdova E, et al. The Arabidopsis exocyst complex is involved in cytokinesis and cell plate maturation. *Plant Cell.* 2010;**22**:3053–65.
  - 54 Kalde M, Elliott L, Ravikumar R, Rybak K, Altmann M, Klaeger S, et al. Interactions between transport protein particle (TRAPP) complexes and Rab GTPases in Arabidopsis. *Plant J.* 2019;**100**:279–97.
  - 55 Fujimoto M, Arimura S, Ueda T, Takanashi H, Hayashi Y, Nakano A, et al. Arabidopsis dynamin-related proteins DRP2B and DRP1A participate together in clathrin-coated vesicle formation during endocytosis. *Proc Natl Acad Sci USA.* 2010;**107**:6094–9.
  - 56 Fujimoto M, Arimura S, Nakazono M, Tsutsumi N. Arabidopsis dynamin-related protein DRP2B is co-localized with DRP1A on the leading edge of the forming cell plate. *Plant Cell Rep.* 2008;**27**:1581–6.
  - 57 Konopka CA, Backues SK, Bednarek SY. Dynamics of Arabidopsis dynamin-related protein 1C and a clathrin light chain at the plasma membrane. *Plant Cell.* 2008;**20**:1363–80.

- 58 Konopka CA, Bednarek SY. Comparison of the dynamics and functional redundancy of the Arabidopsis dynamin-related isoforms DRP1A and DRP1C during plant development. *Plant Physiol.* 2008;**147**:1590–602.
- 59 Damme DV, Gadeyne A, Vanstraelen M, Inzé D, Montagu MCEV, Jaeger GD, et al. Adaptin-like protein TPLATE and clathrin recruitment during plant somatic cytokinesis occurs via two distinct pathways. *Proc Natl Acad Sci USA.* 2011;**108**: 615–20.
- 60 Song K, Jang M, Kim SY, Lee G, Lee GJ, Kim DH, et al. An a/ENTH domain-containing protein functions as an adaptor for clathrin-coated vesicles on the growing cell plate in Arabidopsis root cells. *Plant Physiol.* 2012;**159**:1013–25.
- 61 Albersheim P, Darvill A, Roberts K, Sederoff R, Staehelin LA. Plant cell walls. New York: Garland Science; 2011.
- 62 Thiele K, Wanner G, Kindziarski V, Jurgens G, Mayer U, Pachel F, et al. The timely deposition of callose is essential for cytokinesis in Arabidopsis. *Plant J.* 2009;**58**:13–26.
- 63 Chen XY, Liu L, Lee E, Han X, Rim Y, Chu H, et al. The Arabidopsis Callose synthase gene *GSL8* is required for cytokinesis and cell patterning. *Plant Physiol.* 2009;**150**:105–13.
- 64 Guseman JM, Lee JS, Bogenschutz NL, Peterson KM, Virata RE, Xie B, et al. Dysregulation of cell-to-cell connectivity and stomatal patterning by loss-of-function mutation in Arabidopsis *chorus* (glucan synthase-like 8). *Development.* 2010;**137**:1731–41.
- 65 Hong Z, Delauney AJ, Verma DP. A cell plate-specific callose synthase and its interaction with phragmoplastin. *Plant Cell.* 2001;**13**:755–68.
- 66 Saatian B, Austin RS, Tian G, Chen C, Nguyen V, Kohalmi SE, et al. Analysis of a novel mutant allele of *GSL8* reveals its key roles in cytokinesis and symplastic trafficking in Arabidopsis. *BMC Plant Biol.* 2018;**18**:295.
- 67 Heard W, Sklenar J, Tome DF, Robatzek S, Jones AM. Identification of regulatory and cargo proteins of endosomal and secretory pathways in *Arabidopsis thaliana* by proteomic dissection. *Mol Cell Proteomics.* 2015;**14**:1796–813.
- 68 Drakakaki G, van de Ven W, Pan S, Miao Y, Wang J, Keinath NF, et al. Isolation and proteomic analysis of the SYP61 compartment reveal its role in exocytic trafficking in Arabidopsis. *Cell Res.* 2012;**22**:413–24.
- 69 Him JLK, Pelosi L, Chanzy H, Putaux JL, Bulone V. Biosynthesis of (1 → 3)-beta-D-glucan (callose) by detergent extracts of a microsomal fraction from *Arabidopsis thaliana*. *Eur J Biochem.* 2001;**268**:4628–38.
- 70 Hepler PK. The role of calcium in cell division. *Cell Calcium.* 1994;**16**:322–30.
- 71 Wolniak SM, Hepler PK, Jackson WT. Detection of the membrane-calcium distribution during mitosis in *Haemanthus endosperm* with chlorotetracycline. *J Cell Biol.* 1980;**87**:23–32.
- 72 Stone BA, Clarke AE. Chemistry and biology of (1 → 3)-β-glucans. Melbourne, Vic.: La Trobe University Press; 1992.
- 73 Doxey AC, Yaish MW, Moffatt BA, Griffith M, McConkey BJ. Functional divergence in the Arabidopsis beta-1,3-glucanase gene family inferred by phylogenetic reconstruction of expression states. *Mol Biol Evol.* 2007;**24**:1045–55.
- 74 Levy A, Guenoune-Gelbart D, Epel BL. Beta-1,3-Glucanases: Plasmodesmal gate keepers for intercellular communication. *Plant Signal Behav.* 2007;**2**:404–7.
- 75 Helfrich W. Elastic properties of lipid bilayers: theory and possible experiments. *Z Naturforsch C.* 1973;**28**:693–703.
- 76 Jawaid MZ, Sinclair R, Bulone V, Cox DL, Drakakaki G. A biophysical model for plant cell plate maturation based on the contribution of a spreading force. *Plant Physiol.* 2022;**188**:795–806.
- 77 Park E, Diaz-Moreno SM, Davis DJ, Wilkop TE, Bulone V, Drakakaki G. Endosidin 7 specifically arrests late cytokinesis and inhibits Callose biosynthesis, revealing distinct trafficking events during cell plate maturation. *Plant Physiol.* 2014;**165**:1019–34.
- 78 Davis DJ, Wang M, Sørensen I, Rose JKC, Domozych DS, Drakakaki G. Callose deposition is essential for the completion of cytokinesis in the unicellular alga *Penium margaritaceum*. *J Cell Sci.* 2020;**133**:jcs249599.
- 79 Cheng X, Bezanilla M. SABRE populates ER domains essential for cell plate maturation and cell expansion influencing cell and tissue patterning. *Elife.* 2021;**10**: e65166.
- 80 Chen HW, Persson S, Grebe M, McFarlane HE. Cellulose synthesis during cell plate assembly. *Physiol Plant.* 2018;**164**:17–26.
- 81 Miart F, Desprez T, Biot E, Morin H, Belcram K, Hofte H, et al. Spatio-temporal analysis of cellulose synthesis during cell plate formation in Arabidopsis. *Plant J.* 2014;**77**:71–84.
- 82 Gu F, Bringmann M, Combs JR, Yang J, Bergmann DC, Nielsen E. Arabidopsis CSLD5 functions in cell plate formation in a cell cycle-dependent manner. *Plant Cell.* 2016;**28**:1722–37.
- 83 Yang J, Bak G, Burgin T, Barnes WJ, Mayes HB, Peña MJ, et al. Biochemical and genetic analysis identify CSLD3 as a beta-1,4-glucan synthase that functions during plant Cell Wall synthesis. *Plant Cell.* 2020;**32**:1749–67.
- 84 Cosgrove DJ. Building an extensible cell wall. *Plant Physiol.* 2022:kiac184. <https://doi.org/10.1093/plphys/kiac184> Online ahead of print.

- 85 Lynch MA, Staehelin LA. Domain-specific and cell type-specific localization of two types of cell wall matrix polysaccharides in the clover root tip. *J Cell Biol.* 1992;**118**:467–79.
- 86 Moore PJ, Darvill AG, Albersheim P, Staehelin LA. Immunogold localization of xyloglucan and rhamnogalacturonan I in the cell walls of suspension-cultured sycamore cells. *Plant Physiol.* 1986;**82**:787–94.
- 87 Moore PJ, Staehelin LA. Immunogold localization of the cell-wall-matrix polysaccharides rhamnogalacturonan I and xyloglucan during cell expansion and cytokinesis in *Trifolium pratense* L.; implication for secretory pathways. *Planta.* 1988;**174**:433–45.
- 88 Moore PJ, Swords KM, Lynch MA, Staehelin LA. Spatial organization of the assembly pathways of glycoproteins and complex polysaccharides in the Golgi apparatus of plants. *J Cell Biol.* 1991;**112**:589–602.
- 89 Kang BH, Nielsen E, Preuss ML, Mastrorarde D, Staehelin LA. Electron tomography of RabA4b- and PI-4Kbeta1-labeled trans Golgi network compartments in *Arabidopsis*. *Traffic.* 2011;**12**:313–29.
- 90 McFarlane HE, Young RE, Wasteneys GO, Samuels AL. Cortical microtubules mark the mucilage secretion domain of the plasma membrane in *Arabidopsis* seed coat cells. *Planta.* 2008;**227**:1363–75.
- 91 Young RE, McFarlane HE, Hahn MG, Western TL, Haughn GW, Samuels AL. Analysis of the Golgi apparatus in *Arabidopsis* seed coat cells during polarized secretion of pectin-rich mucilage. *Plant Cell.* 2008;**20**:1623–38.
- 92 Pauly M, Keegstra K. Biosynthesis of the plant Cell Wall matrix polysaccharide xyloglucan. *Annu Rev Plant Biol.* 2016;**67**:235–59.
- 93 Zabolina OA, Zhang N, Weerts R. Polysaccharide biosynthesis: glycosyltransferases and their complexes. *Front Plant Sci.* 2021;**12**:625307.
- 94 Atmodjo MA, Hao ZY, Mohnen D. Evolving views of pectin biosynthesis. *Annu Rev Plant Biol.* 2013;**64**:747.
- 95 Engle KA, Amos RA, Yang JY, Glushka J, Atmodjo MA, Tan L, et al. Multiple *Arabidopsis* galacturonosyltransferases synthesize polymeric homogalacturonan by oligosaccharide acceptor-dependent or de novo synthesis. *Plant J.* 2022;**109**:1441–56.
- 96 Anderson CT. We be jammin’: an update on pectin biosynthesis, trafficking and dynamics. *J Exp Bot.* 2016;**67**:495–502.
- 97 Zhang GF, Staehelin LA. Functional compartmentation of the Golgi apparatus of plant cells : immunocytochemical analysis of high-pressure frozen- and freeze-substituted sycamore maple suspension culture cells. *Plant Physiol.* 1992;**99**:1070–83.
- 98 Caffall KH, Mohnen D. The structure, function, and biosynthesis of plant cell wall pectic polysaccharides. *Carbohydr Res.* 2009;**344**:1879–900.
- 99 Toyooka K, Goto Y, Asatsuma S, Koizumi M, Mitsui T, Matsuoka K. A mobile secretory vesicle cluster involved in mass transport from the Golgi to the plant cell exterior. *Plant Cell.* 2009;**21**:1212–29.
- 100 Zhou Y, Awano T, Kobayashi M, Matcho T, Takabe K. Immunocytochemical detection of rhamnogalacturonan II on forming cell plates in cultured tobacco cells. *Biosci Biotechnol Biochem.* 2017;**81**:899–905.
- 101 Wilkop T, Pattathil S, Ren G, Davis DJ, Bao W, Duan D, et al. A hybrid approach enabling large-scale Glycomic analysis of post-Golgi vesicles reveals a transport route for polysaccharides. *Plant Cell.* 2019;**31**:627–44.
- 102 Silva J, Ferraz R, Dupree P, Showalter AM, Coimbra S. Three decades of advances in arabinogalactan-protein biosynthesis. *Front Plant Sci.* 2020;**11**:610377.
- 103 Showalter AM, Basu D. Extensin and arabinogalactan-protein biosynthesis: glycosyltransferases, research challenges, and biosensors. *Front Plant Sci.* 2016;**7**:814.
- 104 Yu M, Zhao J. The cytological changes of tobacco zygote and proembryo cells induced by beta-glucosyl Yariv reagent suggest the involvement of arabinogalactan proteins in cell division and cell plate formation. *BMC Plant Biol.* 2012;**12**:126.
- 105 Cannon MC, Terneus K, Hall Q, Tan L, Wang Y, Wegenhart BL, et al. Self-assembly of the plant cell wall requires an extensin scaffold. *Proc Natl Acad Sci USA.* 2008;**105**:2226–31.
- 106 Hall Q, Cannon MC. The cell wall hydroxyproline-rich glycoprotein RSH is essential for normal embryo development in *Arabidopsis*. *Plant Cell.* 2002;**14**:1161–72.
- 107 Pattathil S, Avci U, Baldwin D, Swennes AG, McGill JA, Popper Z, et al. A comprehensive toolkit of plant cell wall glycan-directed monoclonal antibodies. *Plant Physiol.* 2010;**153**:514–25.
- 108 Zhang L, Smertenko T, Fahy D, Koteyeva N, Moroz N, Kuchařová A, et al. Analysis of formin functions during cytokinesis using specific inhibitor SMIFH2. *Plant Physiol.* 2021;**186**:945–63.
- 109 Chen BC, Legant WR, Wang K, Shao L, Milkie DE, Davidson MW, et al. Lattice light-sheet microscopy: imaging molecules to embryos at high spatiotemporal resolution. *Science.* 2014;**346**:1257998.
- 110 Aguet F, Upadhyayula S, Gaudin R, Chou YY, Cocucci E, He K, et al. Membrane dynamics of dividing cells imaged by lattice light-sheet microscopy. *Mol Biol Cell.* 2016;**27**:3418–35.
- 111 Ovečka M, Sojka J, Tichá M, Komis G, Basheer J, Marchetti C, et al. Imaging plant cells and organs

- with light-sheet and super-resolution microscopy. *Plant Physiol.* 2021;**188**:683–702.
- 112 Glanc M, Fendrych M, Friml J. Mechanistic framework for cell-intrinsic re-establishment of PIN2 polarity after cell division. *Nat Plants.* 2018;**4**:1082–8.
- 113 Duncombe SG, Chethan SG, Anderson CT. Super-resolution imaging illuminates new dynamic behaviors of cellulose synthase. *Plant Cell.* 2022;**34**:273–86.
- 114 van Oostende-Triplet C, Guillet D, Triplet T, Pandzic E, Wiseman PW, Geitmann A. Vesicle dynamics during plant cell cytokinesis reveals distinct developmental phases. *Plant Physiol.* 2017;**174**:1544–58.
- 115 Prevedel R, Diz-Munoz A, Ruocco G, Antonacci G. Brillouin microscopy: an emerging tool for mechanobiology. *Nat Methods.* 2019;**16**:969–77.
- 116 Braybrook SA. Measuring the elasticity of plant cells with atomic force microscopy. *Methods Cell Biol.* 2015;**125**:237–54.
- 117 Martinez P, Allsman LA, Brakke KA, Hoyt C, Hayes J, Liang H, et al. Predicting division planes of three-dimensional cells by soap-film minimization. *Plant Cell.* 2018;**30**:2255–66.
- 118 Voiniciuc C, Pauly M, Usadel B. Monitoring polysaccharide dynamics in the plant Cell Wall. *Plant Physiol.* 2018;**176**:2590–600.
- 119 Anderson CT, Carroll A, Akhmetova L, Somerville C. Real-time imaging of cellulose reorientation during cell wall expansion in Arabidopsis roots. *Plant Physiol.* 2010;**152**:787–96.
- 120 DeVree BT, Steiner LM, Głazowska S, Ruhnnow F, Herburger K, Persson S, et al. Current and future advances in fluorescence-based visualization of plant cell wall components and cell wall biosynthetic machineries. *Biotechnol Biofuels.* 2021;**14**:78.
- 121 Anderson CT, Wallace IS, Somerville CR. Metabolic click-labeling with a fucose analog reveals pectin delivery, architecture, and dynamics in Arabidopsis cell walls. *Proc Natl Acad Sci USA.* 2012;**109**:1329–34.
- 122 Ropitiaux M, Hays Q, Baron A, Fourmois L, Boulogne I, Vauzeilles B, et al. Dynamic imaging of cell wall polysaccharides by metabolic click-mediated labeling of pectins in living elongating cells. *Plant J.* 2022;**110**:916–24.
- 123 Maeda K, Higaki T. Cell cycle synchronization and time-lapse imaging of cytokinetic tobacco BY-2 cells. *Methods Mol Biol.* 2022;**2382**:245–52.
- 124 Wang J, Yperman K, Gronos P, Jiang Q, Dragwidge J, Mylle E, et al. Conditional destabilization of the TPLATE complex impairs endocytic internalization. *Proc Natl Acad Sci USA.* 2021;**118**:e2023456118.

## Supporting information

Additional supporting information may be found online in the Supporting Information section at the end of the article.

**Video S1.** Animation of cytokinesis, summarizing cell plate formation. Non narrated cytokinesis animation with audio. Soundtrack “At the secret seashore” by Mikis Theodorakis.

**Video S2.** Narrated cytokinesis animation by Destiny Davis. For clarity, actin filaments and several organelles including endoplasmic reticulum and different endosomal populations are not shown in the animation.

## **Chapter 2. A biophysical model for plant cell plate maturation based on the contribution of a spreading force**

This chapter is published in a manuscript describing the development of a biophysical model for cell plate formation and the potential role of a spreading force, possibly contributed by callose, in cell plate expansion. The model was tested by inhibiting cytokinetic callose, which exhibited traits consistent with those proposed by the model, both phenotypically and temporally. I contributed to all the experimental aspects of the manuscript.

A Biophysical Model For Plant Cell Plate Maturation Based On The Contribution Of A Spreading Force.

Jawaid MZ, Sinclair R, Bulone V, Cox DL, Drakakaki G. A biophysical model for plant cell plate maturation based on the contribution of a spreading force. *Plant Physiol.* 2022 Feb 4;188(2):795–806. doi: 10.1093/plphys/kiab552. PMID: 34850202; PMCID: PMC8825336.



# A biophysical model for plant cell plate maturation based on the contribution of a spreading force

Muhammad Zaki Jawaid,<sup>1</sup> Rosalie Sinclair ,<sup>2</sup> Vincent Bulone,<sup>3,4</sup> Daniel L. Cox,<sup>1,†</sup> and Georgia Drakakaki ,<sup>2,\*†</sup>

<sup>1</sup> Department of Physics and Astronomy, University of California, Davis, California, USA

<sup>2</sup> Department of Plant Sciences, University of California, Davis, California, USA

<sup>3</sup> School of Food, Agriculture and Wine, The University of Adelaide, Waite Campus, Adelaide SA 5064, Australia

<sup>4</sup> Department of Chemistry, Division of Glycoscience, KTH Royal Institute of Technology, Stockholm, Sweden

\*Author for communication: [gdrakakaki@ucdavis.edu](mailto:gdrakakaki@ucdavis.edu)

†Senior authors.

D.C. and G.D. designed and analyzed research. M.Z.J. did computational work and R.S. did experimental work. M.Z.J. wrote the article, with significant revisions from D.C., G.D. and input from R.S. and V.B. R.S. contributed to the “Materials and methods”, the experimental data presented and the relevant analysis and interpretation, as well as figure illustrations and captions. All authors read and approved the final version of the manuscript.

The authors responsible for distribution of materials integral to the findings presented in this article in accordance with the policy described in the Instructions for Authors (<https://academic.oup.com/plphys/pages/general-instructions>) are G. Drakakaki ([gdrakakaki@ucdavis.edu](mailto:gdrakakaki@ucdavis.edu)) and D.L. Cox ([cox@physics.ucdavis.edu](mailto:cox@physics.ucdavis.edu)).

## Abstract

Plant cytokinesis, a fundamental process of plant life, involves de novo formation of a “cell plate” partitioning the cytoplasm of dividing cells. Cell plate formation is directed by orchestrated delivery, fusion of cytokinetic vesicles, and membrane maturation to form a nascent cell wall by timely deposition of polysaccharides. During cell plate maturation, the fragile membrane network transitions to a fenestrated sheet and finally a young cell wall. Here, we approximated cell plate sub-structures with testable shapes and adopted the Helfrich-free energy model for membranes, including a stabilizing and spreading force, to understand the transition from a vesicular network to a fenestrated sheet and mature cell plate. Regular cell plate development in the model was possible, with suitable bending modulus, for a two-dimensional late stage spreading force of 2–6 pN/nm, an osmotic pressure difference of 2–10 kPa, and spontaneous curvature between 0 and 0.04 nm<sup>-1</sup>. With these conditions, stable membrane conformation sizes and morphologies emerged in concordance with stages of cell plate development. To reach a mature cell plate, our model required the late-stage onset of a spreading/stabilizing force coupled with a concurrent loss of spontaneous curvature. Absence of a spreading/stabilizing force predicts failure of maturation. The proposed model provides a framework to interrogate different players in late cytokinesis and potentially other membrane networks that undergo such transitions. Callose, is a polysaccharide that accumulates transiently during cell plate maturation. Callose-related observations were consistent with the proposed model’s concept, suggesting that it is one of the factors involved in establishing the spreading force.

## Introduction

Cytokinesis is a fundamental process of plant life that is different from animal cell cytokinesis. In plants, formation of

a cell plate develops into the new cell wall, partitioning the cytoplasm of the dividing cell. Cell plate formation involves highly orchestrated vesicle accumulation, fusion, and

Received August 13, 2021. Accepted October 27, 2021. Advance access publication November 27, 2021

© The Author(s) 2021. Published by Oxford University Press on behalf of American Society of Plant Biologists.

This is an Open Access article distributed under the terms of the Creative Commons Attribution License (<https://creativecommons.org/licenses/by/4.0/>), which permits unrestricted reuse, distribution, and reproduction in any medium, provided the original work is properly cited.

**Open Access**

membrane transformation concurrent with the time-specific deposition of polysaccharides such as callose, cellulose, and cross-linking glycans along with glycoproteins (Figure 1). This development requires choreographed accumulation of post-Golgi vesicles via the phragmoplast, an assembly of microtubules and microfilaments that help organize vesicle delivery to the cell plate assembly matrix, at the division plane (Lee and Liu, 2013).

Cell plate expansion is centrifugal, led by the accumulation and fusion of cytokinetic vesicles to the leading edge and maturation of the membrane network from the center (Samuels et al., 1995; Segui-Simarro et al., 2004; Lee and Liu, 2013; Smertenko et al., 2017). Cell plate development takes place in morphologically defined stages (Figure 1). It starts with initial fusion of Golgi vesicles stage, in which cytokinetic vesicles are guided by the phragmoplast to the cell plate assembly matrix (Figure 1A). Fused vesicles are transformed into dumbbells that undergo conformational changes to form a tubulo-vesicular network (TVN) (Figure 1B), which transitions to a tubular network (TN) (Figure 1C). The TN expands into a planar fenestrated sheet (PFS). As the gaps in the fenestrated sheet are gradually closing, this leads to the formation of the young cell wall sandwiched between two parallel plasma membranes that fuses with the parental cell wall (Figure 1D) (Samuels et al., 1995; Segui-Simarro et al., 2004). Excess membrane material is recycled concurrently, along with the accumulation of different polysaccharide materials. Based on elegant electron tomography studies, it is estimated that 70% of membrane material is removed during the transition of the cell plate from TVN to TN and PFS (Segui-Simarro et al., 2004). Analysis of vesicle dynamics support electron microscopy studies showing an initial vesicle delivery with fast expansion, followed by slower expansion phase (van Oostende-Triplet et al., 2017). It is notable that the multiple stages exist simultaneously (Figure 1), adding complexity in dissecting them (Drakakaki, 2015).

During cell plate expansion and maturation, membrane remodeling and network expansion are highly coordinated with the deposition of polysaccharides, providing an opportunity to study membrane morphology changes. The molecular basis of vesicle delivery at the cell plate has been extensively studied (McMichael and Bednarek, 2013; Boruc and Van Damme, 2015; Jurgens et al., 2015) with key components such as RAB GTPases, soluble *N*-ethylmaleimide-sensitive factor attachment protein receptor, tethering complexes, dynamin rings, and accessory proteins receiving attention (McMichael and Bednarek, 2013; Jurgens et al., 2015; Smertenko et al., 2017). However, the factors contributing to stage transition from a vesicular network to a fenestrated sheet, leading to cell plate maturation, are largely unknown. Dynamin rings and clathrin coated vesicles contribute to recycling of excess material (McMichael and Bednarek, 2013), while the deposition of polysaccharides likely contributes to transition into a mature cell plate. Hemicelluloses and pectins are deposited via Golgi derived vesicles. Callose and cellulose are directly synthesized at the

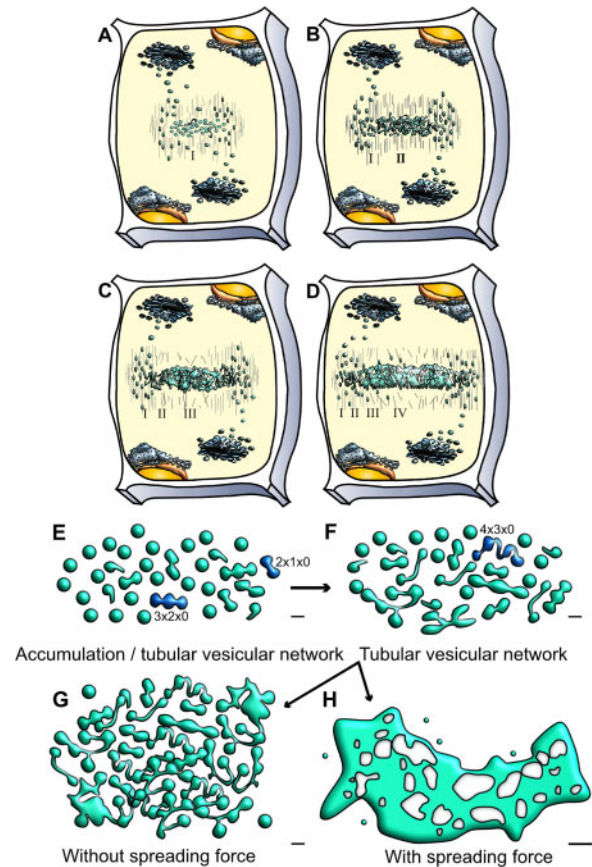


**Figure 1** Schematic representation of cell plate development stages and the potential role of a spreading force in cell plate maturation. A–D, Cell plate development occurs centrifugally in multiple stages. A, During the first stage (I), cytokinetic vesicles guided by the phragmoplast accumulate at the center of the dividing cells, at the cell plate assembly matrix. B, Vesicles undergo fusion and fission and conformational changes resulting in TVN (Stage II). C, Interconnected membrane structures transition to a TN. At this stage high callose deposition occurs (Stage III). D, The membrane network further expands to an almost continuous fenestrated membrane sheet (PFS) (Stage IV). Deposition of additional polysaccharides helps transition to a new cell wall, separating the two daughter cells. Note that different stages can occur simultaneously, images are not to scale. This simplified representation emphasizes on cell plate membranes (Samuels et al., 1995; Segui-Simarro et al., 2004). E–H, Schematic representation of cell plate development describing the role of a spreading force. E, Early stages of vesicle accumulation and fusion and F, TVN and TN structures are shown. Two different possibilities are projected for stage transition (1) Incomplete/arrested cell plate G. In the absence of a spreading force G, tubular and fenestrated structures accumulate, and there is a lack of maturation towards a single, complete cell plate structure. (2) Normal cell plate transition H. In our calculations, we discover that for expansion/maturation to occur as in D, the presence of a spreading force is required, along with the decrease of spontaneous curvature to a threshold value. This allows for a sheet-like cell plate (SCP) structure to form. The structures in this schematic description are adapted from data collected from EM tomography (Segui-Simarro et al., 2004) with bars in E–G = 50 nm, H = 0.25  $\mu$ m. Dark blue vesicles denote those labeled by the mathematical naming schema as described in Figure 2. Whereas in E,  $2 \times 1 \times 0$  denotes two oblate spheroids, one tubular connection, and zero holes.

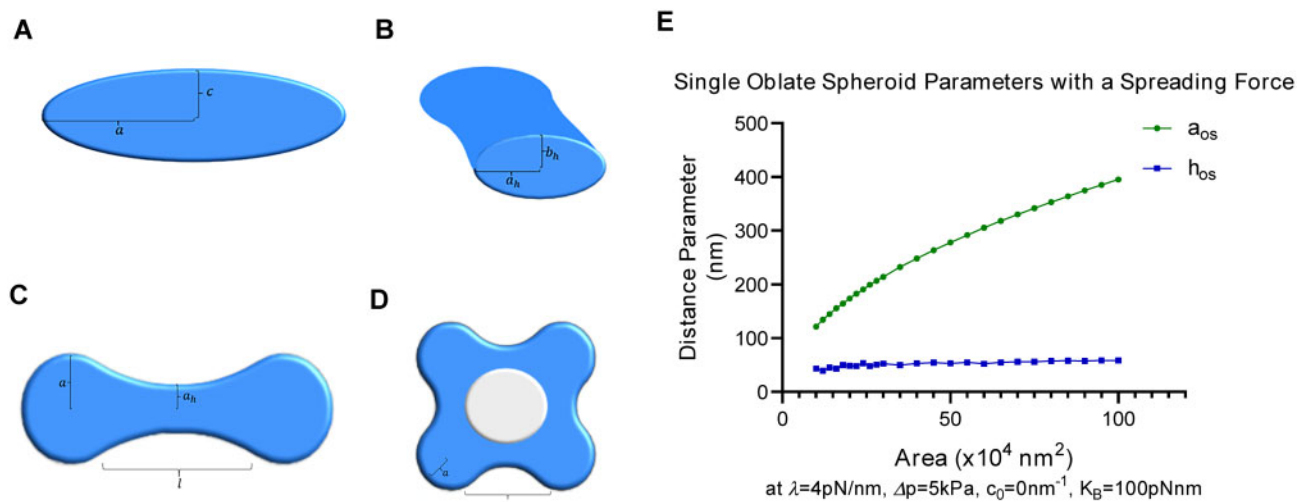


**Figure 2** Approximating cell plate structures using a variational approach. A–D, Examples of membrane structure parameterizations used for modeling. A, Cross-section of an oblate spheroid through the polar axis. The major axis radius is labeled  $a$  and the minor axis radius is labeled  $c$ . This structure is used to model vesicles, or mature cell plate structures in the case where  $a \gg c$ . B, Cross-section of an elliptic hyperboloid at its center, showing the skirt radii. The hyperboloid can be parameterized by its length  $l$  and its skirt radius in the equatorial plane  $a_h$ , the skirt radius in the axial plane is given by  $b_h$ , which can be written as a function of the other parameters listed as shown in [Supplemental Equation S3](#). C, An example of a tubulo-vesicular structure parameterized by two oblate spheroids connected by a single elliptic hyperboloid (referred to as a  $2 \times 1 \times 0$  structure). Only the top view is shown. D, An example of a  $4 \times 4 \times 1$  conformation that models a transition to a fenestrated network with genus  $g = 1$  (one gap). E, Evolution of single oblate spheroid parameters in the presence of a spreading force. In the presence of a spreading force, the thickness of the oblate spheroid remains in the 40–80 nm range despite the increase in area. This reflects the thicknesses and growth patterns found in intermediate cell plate stages ([Samuels et al., 1995](#)). Here,  $h_{os} = 2c$  ( $a_{os}$ ,  $c$  shown in A), represents the overall height, or thickness, of the oblate spheroid. In the absence of a spreading force,  $h_{os}$ , or the thickness, is estimated to grow in values that are not observed experimentally. For reference, an area of  $10^4 \text{ nm}^2$  is roughly equal to that of a single vesicle.

cell plate ([Miart et al., 2014](#); [Chen et al., 2018](#)). Callose, a  $\beta$ -1-3 glucan is a dominant polysaccharide transiently synthesized at the cell plate. Structural glycoproteins such as extensins are part of the newly formed cell plate ([Cannon et al., 2008](#)) and can contribute to cell plate maturation. Given the complexity of cell plate development and the concurrent presence of different stages, a biophysical model can be used as a framework for interrogation of individual components that can provide insights and guide future research.

In this study, we used biophysical modeling to dissect the transition between the vesicular network stage to a fenestrated sheet and a mature cell plate. We tested the hypothesis that a time-dependent spreading and stabilizing force is necessary for cell plate maturation. We could model this force by adding a phenomenological “areal pressure” term to the Helfrich model free energy for the cell plate surface. Furthermore, we monitored its influence by adopting a variational approach to locally minimize the model free energy in time, assuming the process is sufficiently slow to consider the system close to thermodynamic equilibrium. The quasi-equilibrium is constantly redefined as vesicles are added at the cell plate boundary. This enables us to use the total cell plate surface area as a proxy for time. We demonstrate semi-quantitatively that by assuming a late time onset of this spreading and stabilizing force, followed by the reduction of membrane spontaneous curvature, we can reproduce the observed morphological time dependent transition of the cell plate morphology.

## Results

We took a modeling approach to generate tools to dissect better membrane network transition during cell plate maturation. Due to the complexity of cell plate development, we decided to look for energy minima within a parameterized restrictive geometry basis set, thereby adopting a restricted variational approach within testable approximated structures. We found that existing general adaptive mesh approaches, such as Surface Evolver, while in principle more accurate, were not amenable for application in our study, due to their inability to incorporate the spreading/stabilizing force into such a large-scale system ([Brakke, 1996](#)).

### Shape approximation

First, we approximated subcellular structures with testable shapes that could be used in a model. As shown in [Figure 1](#), the cell plate, during its different transitional stages, contains cytokinetic vesicles, fused vesicles stretched to dumbbells, TVNs and fenestrated structures that finally mature to a complete cell plate and a new cell wall. These structures can be modeled using a combination of oblate spheroids and elliptical hyperboloids ([Figures 1 and 2](#)). Namely, cytokinetic vesicles can be approximated using oblate spheroids, where the two defining radii can be used as variational parameters as shown in [Figure 2A](#). The oblate spheroid can also be used to model the expanded/late-stage

cell plate close to completion, as a very large oblate spheroid with  $a \gg c$ .

Similarly, structures found within the fenestrated sheet and the TVN stages can be approximated using a combination of elliptic hyperboloids and oblate spheroids, such that the hyperboloids are continuous at the oblate spheroid boundaries. These elliptic hyperboloids can be parameterized by their length, hereafter referred to as  $l$ , and their skirt radius in the equatorial plane, hereafter referred to as  $a_h$ . The other parameters needed to define an elliptic hyperboloid can be written as a function of these two parameters due to boundary conditions that arise from mandating continuity. [Figure 2B](#) shows a cross-section of an elliptic hyperboloid, while [Figure 2C](#) shows an example of two vesicles joined by a single tube.

### Naming convention of different approximated conformations

The naming convention for different conformations follows the example: A shape that is labeled as  $6 \times 7 \times 2$ , represents a conformation that has six oblate spheroids (or vesicles), seven hyperboloids (or tubes), and two gaps (or fenestrations, with  $g = 2$ ). A  $2 \times 1 \times 0$  conformation, can approximate dumbbell structures found in early TNs, where two vesicles join via a single tube ([Figure 2C](#)). An example of a  $4 \times 4 \times 1$  conformation with a single fenestration, which can be used to approximate early fenestrated structures, is shown in [Figure 2D](#).

### Energy minimization

The area of any given conformation was calculated by numerical integration methods, and a corresponding parameter space of a given area was found. For simplicity, we analyzed conformations that shared the same parameters for each of the oblate spheroids, and each of the hyperboloids with examples shown in [Figure 2](#). We found a four-dimensional parameter space ( $a, c, a_h, l$ ) that corresponded to a given area up to an error tolerance ( $< 0.01\%$ ) for each conformation of interest, and then calculated the energies of [Equation 1](#) within that parameter space. The energy minimum was then extrapolated from that parameter space. Additional information about the four-dimensional parameter space as well as the calculation of the area elements used in the numerical integration methods is given in the [supplemental information](#) ([Supplemental Eq. S1–S4, S10 and S11](#)), and the full list of the parameters involved are shown in [Supplemental Figure S1](#).

### Modified Helfrich energy

In order to identify contributing factors for cell plate maturation beyond the vesicle network stage, we modeled the free energy for the cell plate surface by adopting the Helfrich energy ([Helfrich, 1973](#)) with the addition of a novel term to model the presence of a spreading/stabilizing force. The free energy is defined as follows:

$$E = E_{\text{bending}} + E_{\text{pressure}} + E_{\text{tension}} + E_{\text{gaussian}} + E_{\text{spreading}} \quad (1)$$

Each of the components is described in detail in the [supplemental information](#) corresponding to [Supplemental Equations S5–S9](#).

The terms describe (1) the bending energy over the closed membrane surface(s) of the cell plate, which depends on the local curvature or the spontaneous curvature of the membrane, given by  $c_0$ , and the bending modulus, given by  $K_B$ , (2) the pressure energy which results from the difference in osmotic pressure between the inside and the outside of the cell plate, represented by  $\Delta p$ , (3) the energy associated with the surface tension of the membrane, which depends on the local surface tension, given by  $\gamma$ , (4) the Gaussian bending energy, and (5) the novel term of spreading/stabilizing force.

The novel spreading force term is analogous to a two-dimensional pressure acting against the periphery of the cell plate structure along the equatorial plane. It is dependent on  $\lambda$ , which parameterizes the spreading/stabilizing force, having units of force/length. We allow for  $\lambda$  to be time-dependent, which would represent the “turning on” of polymer production in an expanding plate. We also allow for  $c_0$  to be time-dependent, accounting for differences in spontaneous curvature that may arise from changes in membrane composition during cell plate evolution.

This methodology can also be used to provide a basis for the quantitative assessment of membrane structures found in the endoplasmic reticulum and the Golgi apparatus which are so far limited in a large-scale view using Helfrich theory. Earlier work ([Shemesh et al., 2014](#)) examined possible morphologies as a function of curvature modifying proteins using full minimization of the free energy via the Surface Evolver finite element approach ([Brakke, 1996](#)). However, these finite element methods were unable to consider the spreading/stabilizing force required in [Supplemental Equations S6–S9](#) in any such available code. To establish a testable and functional model, we adopted the variational approach including multiple connected surfaces with negative curvature tubulations as a reasonable compromise approach to explore the quasi-equilibrium stabilities of different morphologies that are fully representative of the observed structures.

### Model parameter ranges and the need of a spreading/stabilizing force

We first minimized the modified Helfrich energy ([Eq. 1](#)) for multiple conformations (vesicular, tubular, and fenestrated) to determine a range of parameters that would match the experimentally observed cell plate sizes/thicknesses. From electron tomography cryo-EM images of developing cell plates, we determined that the thickness of a cell plate in various stages of development was  $\sim 40$ – $120$  nm ([Segui-Simarro et al., 2004](#)). Therefore, we tuned the free parameters in our energy model such that conformations’ thickness across the equatorial plane was in the range of  $40$ – $120$  nm. We determined that, depending on the choice of the

**Table 1** Model parameter ranges

Parameter	Value
Bending modulus $K_B$	62.5–200 pNnm
Spontaneous curvature $c_o$	0–0.04 nm <sup>-1</sup>
Pressure difference $\Delta p$	2–10 kPa
Spreading force parameter $\lambda$	2–6 pN/nm
Surface tension parameter $\gamma$	1.6 pN/nm
Gaussian bending modulus $K_G$	-0.8 $K_B$

The terms describe (1) the bending energy over the closed membrane surface(s) of the cell plate, which depends on the local curvature or the spontaneous curvature of the membrane, given by  $c_o$ , and the bending modulus, given by  $K_B$ , (2) the pressure energy which results from the difference in osmotic pressure between the inside and the outside of the cell plate, represented by  $\Delta p$ , (3) the energy associated with the surface tension of the membrane, which depends on the local surface tension, given by  $\gamma$ , (4) the Gaussian bending energy, and (5) the term of spreading/stabilizing force.

bending modulus, the allowed values of the spreading/stabilizing force parameter  $\lambda$  should be between 0.0 and 6.0 pN/nm, the spontaneous curvature  $c_o$  between 0 and 0.04 nm<sup>-1</sup>, and a finite pressure difference  $\Delta p$  around 2–10 kPa. A deviation from these ranges results in structures that are either too thick or too thin to exist in intermediate stages of cell plate development based on literature. An example of how we tuned the parameters to fit the experimental sizes and shapes is given in Figure 2E, in which a single oblate spheroid evolves with the area increase with given parameter values while maintaining the experimentally observed thickness. It is notable that a spreading force is necessary to achieve the desired values. A summary of the full range of parameter values are given in Table 1 and a full description of these parameters is provided in the supplemental information.

Although the range of values for the pressure difference and the planar spreading force parameter were phenomenologically determined, they are within reasonable bounds. For instance, the solute concentration difference between the interior and the exterior of the cell plate by employing the van't Hoff equation, which yields a solute concentration difference between  $8 \times 10^{-4}$  mol/l and  $4 \times 10^{-3}$  mol/l, comparable to protein solute concentration differences in higher plant cells. The spreading force required for cell plate maturation over a length of a nanometer is around 2–6 pN, which is comparable to the polymerization ratchet forces of a microtubule (Kent and Lele, 2017).

### A spreading force is required for cell plate maturation while its absence energetically favors the accumulation of tubular and vesicular networks

Our goal was to assess within the modeled free energy of Eq. (1), whether a spreading force is essential for the necessary transitions from a combination of TVN to a fenestrated sheet and finally to a single mature cell plate structure. Applying Equation 1, we compared the energy minima compared to that of a mature cell plate (Figure 3A). From an energy perspective, we identified that in the absence of a spreading

force, tubulo-vesicular and fenestrated structures have a lower value of energy at minima and are more stable than a single late-stage cell plate structure (resembled by a single oblate spheroid) of the same area. Figure 3A shows the energy minima of tubular and fenestrated structures ( $7 \times 6 \times 0, \dots$ ) compared to those of a single oblate spheroid ( $1 \times 0 \times 0$ ).  $\Delta E_{\min}$  represents the difference of the energy minima value of the labelled structure with that of a single oblate spheroid, so that  $\Delta E_{\min}(2 \times 1 \times 0) = E_{\min}(1 \times 0 \times 0) - E_{\min}(2 \times 1 \times 0)$ . Thus, positive  $\Delta E_{\min}$  indicate the relative stability of the labelled conformation. Our simulations indicate that in the absence of a spreading force, increased tubularity is preferred with the increase in area (Figure 1G and 3A). Furthermore, in the absence of a spreading force, some fenestrated structures ( $4 \times 4 \times 1, 6 \times 7 \times 2$ ) are also energetically stable and are therefore likely to accumulate.

We then examined the possibility of a transition from TVNs to a single oblate spheroid or a fully mature cell plate in the presence of a spreading force (Figure 3B). Within the theory and the variational approach, we find that this is possible if the spontaneous curvature decreases to a threshold value ( $\sim 0.015$  nm<sup>-1</sup>) with larger cell plate area, that is, in the presence of a spreading force. From an energy perspective, this suggests that TVNs, TNs, as well as fenestrated sheets, should be unstable as compared to a single oblate spheroid, and thus transition of their morphology to one without tubes or fenestrations. While a finite spontaneous curvature is necessary to explain the origin of stability of the incoming vesicles (Jung et al., 2001), a change in the spontaneous curvature of the membrane is predictable due to the expected changes in membrane composition and protein activity that occurs during cell plate development (McMahon and Boucrot, 2015).

Figure 3B shows the relative instability of selected tubular and fenestrated structures compared to a single oblate spheroid in the presence of a spreading force and zero spontaneous curvature. Less tubular structures are now energetically favorable than highly tubular or fenestrated structures, with a single, complete structure being the most favorable. For structures without fenestrations or gaps (such as  $2 \times 1 \times 0$  or  $3 \times 2 \times 0$ ), we can also map a path to a single oblate spheroid if we relax the parameter restrictions that were initially imposed during the variational calculation. Figure 3B shows results with the parameter restrictions in place. Supplemental Figure S2 shows data for a fenestrated structure in the absence (Supplemental Figure S2A) and the presence (Supplemental Figure S2B) of a spreading/stabilizing force, leading to gap shrinkage with the parameter restrictions in place.

To better represent a biological system, we compared an ensemble of  $2 \times 1 \times 0$  structures (approximating accumulated fused vesicles forming a network) to a single oblate spheroid of the same combined area. Similar to our earlier calculations, we find that in the absence of a spreading force, a single oblate spheroid is less stable, as shown in

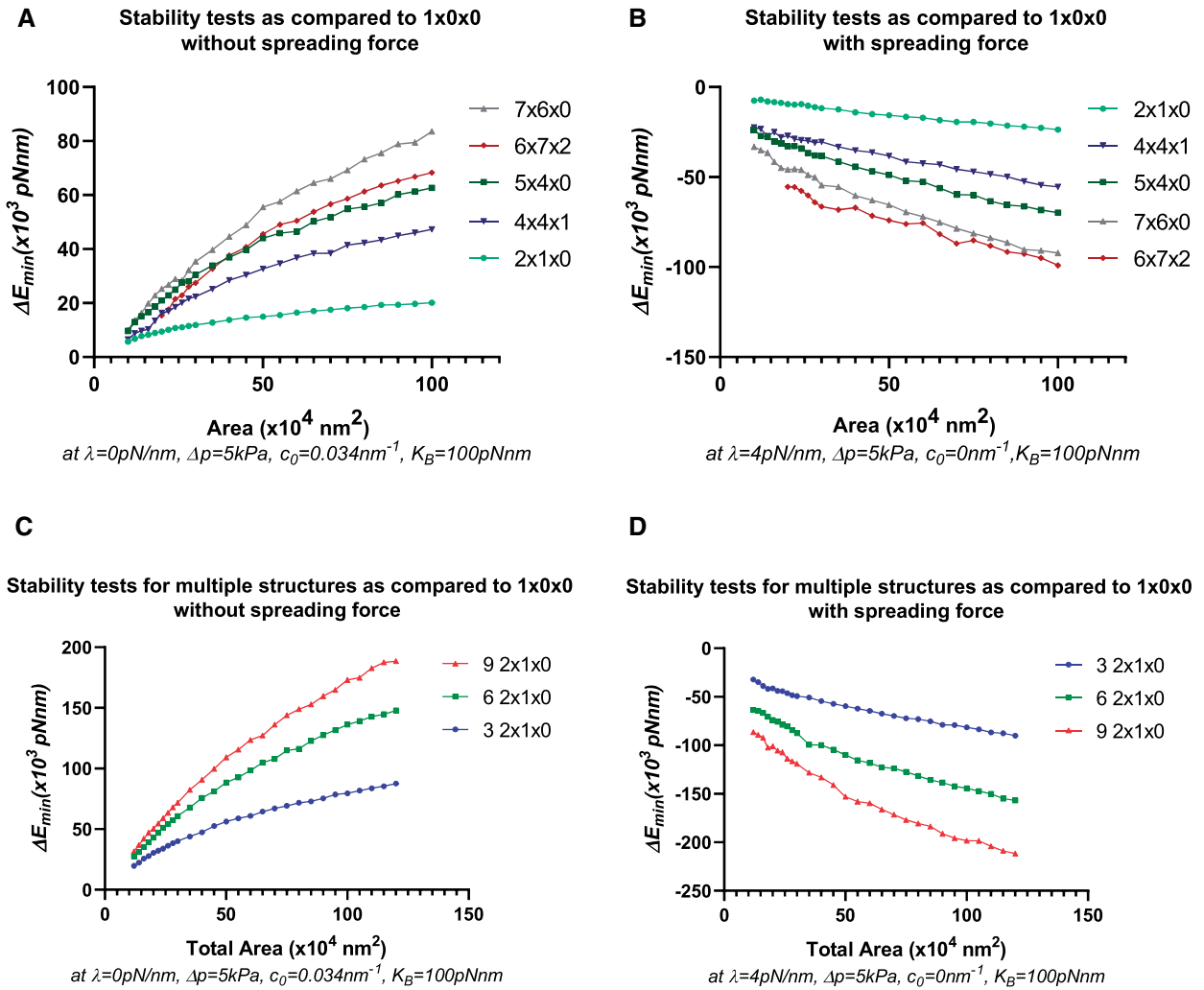


**Figure 3** Stability tests to determine the role of a spreading force in different shape conformations. A and B, Stability tests determined by  $\Delta E_{\min}$  versus Area for different conformations compared to a single oblate spheroid at the labelled area. A positive value of  $\Delta E_{\min}$  indicates relative stability of the labelled conformation as compared to a single oblate spheroid ( $1 \times 0 \times 0$ ). A, Relative stability of tubular ( $2 \times 1 \times 0$ ,  $5 \times 4 \times 0$ ,  $7 \times 6 \times 0$ ) and fenestrated ( $4 \times 4 \times 1$ ,  $6 \times 7 \times 2$ ) structures in the absence of a spreading force with a finite spontaneous curvature. B, Stability of a single oblate spheroid over tubular and fenestrated structures in the presence of a spreading force and with zero spontaneous curvature. Note that in (B) a decrease of spontaneous curvature to a threshold value close to  $0.015 \text{ nm}^{-1}$  yields similar results. C and D, Stability test for multiple  $2 \times 1 \times 0$  structures compared to a single oblate spheroid at the labeled area. C, Relative stability of multiple  $2 \times 1 \times 0$  structures compared to a single oblate spheroid in the absence of a spreading force. At a labeled area, a larger number of structures have collectively a higher, more positive value of  $\Delta E_{\min}$ , thereby indicating that in the absence of a spreading force, tubular, as well as emerging fenestrated/network structures (as inferred by the results of A and B) are energetically favorable and tend to accumulate as shown in [Figure 1G](#). D, Stability of a single oblate spheroid compared to multiple  $2 \times 1 \times 0$  structures in the presence of a spreading force and with zero spontaneous curvature. In the presence of a spreading force, at a labeled area, a larger number of structures have a lower, more negative value of  $\Delta E_{\min}$  collectively, thereby indicating the energetic favorability of structures fusing to form larger, more mature structure(s).

[Figure 3C](#). The relative instability is magnified with the increase of area, and with the increase in the number of tubular structures. In the presence of a spreading force and a decreased spontaneous curvature, as in [Figure 3D](#), the inverse is true, favoring fewer complex structures. When comparing multiple structures to a single mature structure of the same area, there is no need to enforce the decrease in spontaneous curvature. However, for consistency, results with a zero spontaneous curvature in the presence of a spreading force, and a finite spontaneous curvature in the absence of a spreading force are shown.

Our simulations also showed that a stiffer membrane, for example, one that is represented by a larger bending modulus, requires a stronger spreading force in addition to a higher pressure difference to transition to a mature cell plate structure as shown in [Supplemental Figures S3–S7](#). However, regardless of the choice of the bending modulus that may arise in different regions of the cell plate due to varying thickness and rigidity, a spreading force is necessary (see [Supplemental Figures S3–S7](#)). We also show calculations for larger, highly tubulated fenestrated structures (i.e.  $10 \times 13 \times 4$ ) in [Supplemental Figures S8 and S9](#), which

are stable in the absence of a spreading force, but unstable compared to a single oblate spheroid in the presence of a spreading force, further supporting our model. In [Supplemental Figures S10 and S11](#), we animate the 3D evolution and transition of cell plate structures in the presence and the absence of a spreading force as predicted by our model.

### Exploring polysaccharide deposition as a contributing factor to cell plate maturation and model prediction

There are several potential contributing factors during cell plate maturation including cell wall polysaccharides. Given that the model examines the specific transition between TN to a fenestrated sheet and a mature cell plate, the timing of the contributing sources at the lagging zone is critical. Among the different polysaccharides we first examined callose.

Live staining of callose in dividing *Arabidopsis thaliana* roots showed a prominent and transient accumulation of the polysaccharide at the lagging zone, starting from the center ([Figure 4, B–D](#)). Treatment with Endosidin7 (ES7), which inhibits cytokinetic callose deposition ([Park et al., 2014](#)), caused failure of the cell plate to mature into a cross wall. [Figure 4, E–G](#) shows an example of arrested cell plate development in the absence of callose, in contrast to normal gradual cell plate maturation concomitant with callose deposition as in [Figure 4, A–D](#). This is consistent with the model's prediction in the absence of a spreading force, where planar fenestrated and tubular structures accumulate, but do not mature into a stable cross-wall like structure.

Given the loadbearing role of cellulose, we then examined the effect of cellulose compared to callose inhibition in our experimental conditions. Cellulose inhibition by isoxaben (IXB) treatment led to strong reduction of root growth ([Scheible et al., 2001](#); [Worden et al., 2015](#)) and a root swollen phenotype compared to ES7 ([Supplemental Figure S12](#)). However, while cytokinesis defects in the form of cell plate stubs, were observed with ES7 treatment ([Figure 5, E](#) and [Supplemental Figure S12, E and J](#)), this effect was not detectable in IXB treatment ([Figure 5](#) and [Supplemental Figure S12, G–J](#)). ES7 treatment caused binucleate cells as a result of failed cytokinesis ([Figure 5F](#)); however, this phenotype was not pronounced in the IXB treatment ([Figure 5J](#)).

We then included a treatment with the myosin inhibitor 2,3-butanedione monoxime (BDM), interfering with actin-based organelle transport ([Samaj et al., 2000](#); [Tominaga et al., 2000](#); [Higaki et al., 2008](#)). Unlike ES7 ([Figure 5, P–R](#)), a 20-mM BDM treatment for 2 h led to inhibition of RABA2a trafficking [Figure 5, S–X](#), but not cell plate fragmentation, showing an effect on endomembrane trafficking, that in turn could impact cell plate development.

### Estimating the required polysaccharide synthesis rates for a stabilizing/spreading force

We note that the spreading/stabilizing force can be described by the mean square end-to-end excursion within the Flory

self-avoiding polymer theory in two-dimensions ([Schulmann et al., 2013](#)). If we assume reasonable values of polymer persistence length and areal density, we require a rate of polysaccharide synthesis close to  $\frac{dN}{dt} \sim 1.75 \times 10^6 \text{ s}^{-1}$  to obtain the spreading force parameter of  $\lambda = 4 \frac{\mu N}{nm}$ . The modeled  $dN/dt$  is biologically achievable given an estimated cellular value of  $1.8 \times 10^5 \cdot \text{s}^{-1}$  based on in vitro callose synthase activity ([Him et al., 2001](#)) and an average protein concentration in eukaryotic cells ([Albe et al., 1990](#); [Milo, 2013](#)). However, in-vitro experimental systems of the relevant polymer(s) synthase(s) in artificial vesicles are required to test this hypothesis. A full description of this derivation is given in the [supplemental information](#) corresponding to [Supplemental Equations S12–S17](#).

## Discussion

Although several proteins have been identified that regulate cell plate formation ([McMichael and Bednarek, 2013](#); [Smertenko et al., 2017](#), [Gu and Rasmussen, 2021](#)), the mechanisms underlying the complex transition from a vesicle membrane network (TN) to a fenestrated sheet and a mature cell plate are not well understood.

To circumvent these hurdles and to better dissect cell plate maturation, we used biophysical modeling. We developed a model based on the Helfrich free energy for the cell plate surface with the incorporation of a spreading/stabilizing force as an “areal pressure” (force per unit distance). From an energy minimization analysis, we have shown that a planar spreading/stabilizing force is vital for cell plate to transition from vesicle membrane network to a fenestrated sheet and late stage/mature cell plate. We also show that in the absence of a spreading/stabilizing force, the addition of membrane material yields stable TN structures, but that those structures are unable to mature beyond this stage. As shown by different simulations, the need for this spreading/stabilizing force is magnified when we compare a single mature cell plate to multiple smaller vesicle network structures of the same total area. We do not have the detailed molecular scale mechanisms behind the spreading/stabilizing force, but we show that a simple model based upon the expansion of a quasi-two-dimensional self-avoiding polymer captures the correct form ([Supplemental Figure S13](#)).

To reach a mature cell plate, our model requires the late-stage onset of the spreading force coupled with a concurrent loss of spontaneous curvature. This raises the intriguing possibility of a common origin to the decrease in spontaneous curvature and onset of a spreading/stabilizing force. In the model, the spreading force is relevant when there is sufficient connection of individual oblate spheroidal vesicles, and it is at this stage that we shut off the spontaneous curvature. The nanoscale surface topography can potentially serve as a direct biochemical signal to activate this process ([Lou et al., 2019](#)). The possible tethering of polysaccharides or glycoproteins to the membrane could concomitantly induce spreading and reduce spontaneous curvature by modifying the membrane mechanics. Notably, inhibition of long

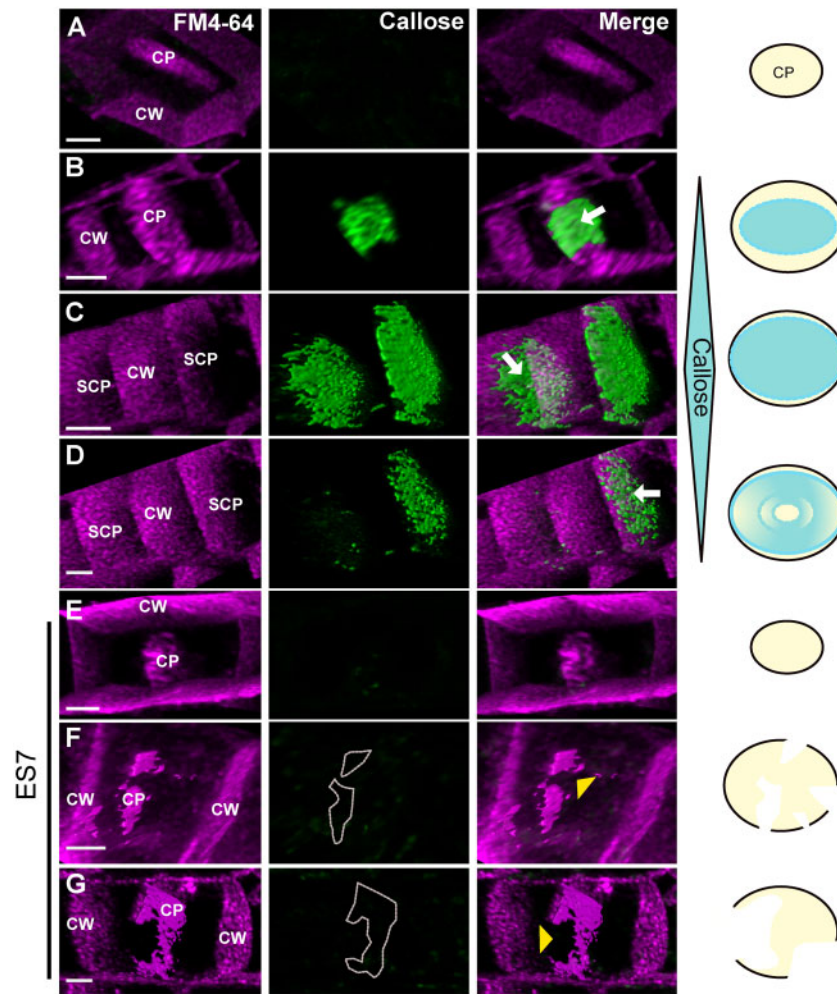


**Figure 4** Progression of the cell plate in the presence and absence of callose. A–D, Cell plate progression in the presence of callose. A, It shows an early stage cell plate before the accumulation of callose, while (B–D) represent later cell plate stages including SCP as indicated in [Figure 1D](#). FM4–64 staining (magenta) is used to stain plasma membrane and the cell plate, while Aniline Blue fluorochrome (green) staining shows callose accumulation. Note the transient accumulation of callose in later stages leading to the maturation of cell plate during normal cytokinesis (B–D). C and D represent two snapshots of a time series. C, Two cell plates can be observed, and as maturation continues to D, callose is eliminated from one cell plate indicating its transient nature. Arrows indicate callose accumulation at the cell plate. E–G, Progression of cytokinesis under ES7 treatment for 2 h that inhibits callose deposition. Note that early cell plate development is not affected with ES7 treatment as shown in earlier studies ([Park et al., 2014](#)) (E). However, in late stages of cell plate development under ES7 treatment, the absence of callose prevents the transition into a stable mature single structure, leading to characteristic “cell plate stubs” (F and G). CP indicates cell plate, SCP indicates SCP as depicted in [Figure 1](#). CW indicates cell wall. Yellow arrowheads denote lack of callose at cell plate breakage points. Dotted lines in F, G outline the position where callose should be deposited. Images are 3D reconstructions from Z-stacks of live confocal imaging and show single timepoints. C and D are snapshots of a time series. Figures are representative of root tips from a minimum of 10 *Arabidopsis* seedlings. A schematic representation on the right indicates the accumulation of callose in relation to cell plate development. White gaps at the bottom indicate cell plate fragmentation. Bars = 3  $\mu$ m.

chain fatty acid affects cell plate maturation ([Bach et al., 2011](#)). It is plausible that membrane microdomains control both spontaneous curvature and the onset of a spreading force at the cell plate.

Curvature-stabilizing proteins are active at the cross-sections of tubules and sheet edges of endoplasmic reticulum ([Shemesh et al., 2014](#); [Schweitzer et al., 2015](#)). While force generating proteins are involved in the tubulation and membrane material recycling processes ([Otegui et al., 2001](#); [Ahn et al., 2017](#)), no proteins have been identified with properties of membrane expansion at the cell plate.

The phragmoplast-driven vesicle delivery is a dynamic and complex process ([Buschmann and Müller, 2019](#)) that with the aid of motor proteins can be considered as a spreading/stabilizing force during cell plate maturation. For example, Myosin VIII plays a role in guiding phragmoplast expansion ([Wu and Bezanilla, 2014](#)), while several kinesins are involved in the functional organization of the phragmoplast ([Buschmann and Müller, 2019](#)). Microtubule directed vesicle delivery occurs at the leading edge; however, it is followed by microtubule depolymerization at the lagging zone, which is the transitional stage that the model describes ([Lee and](#)

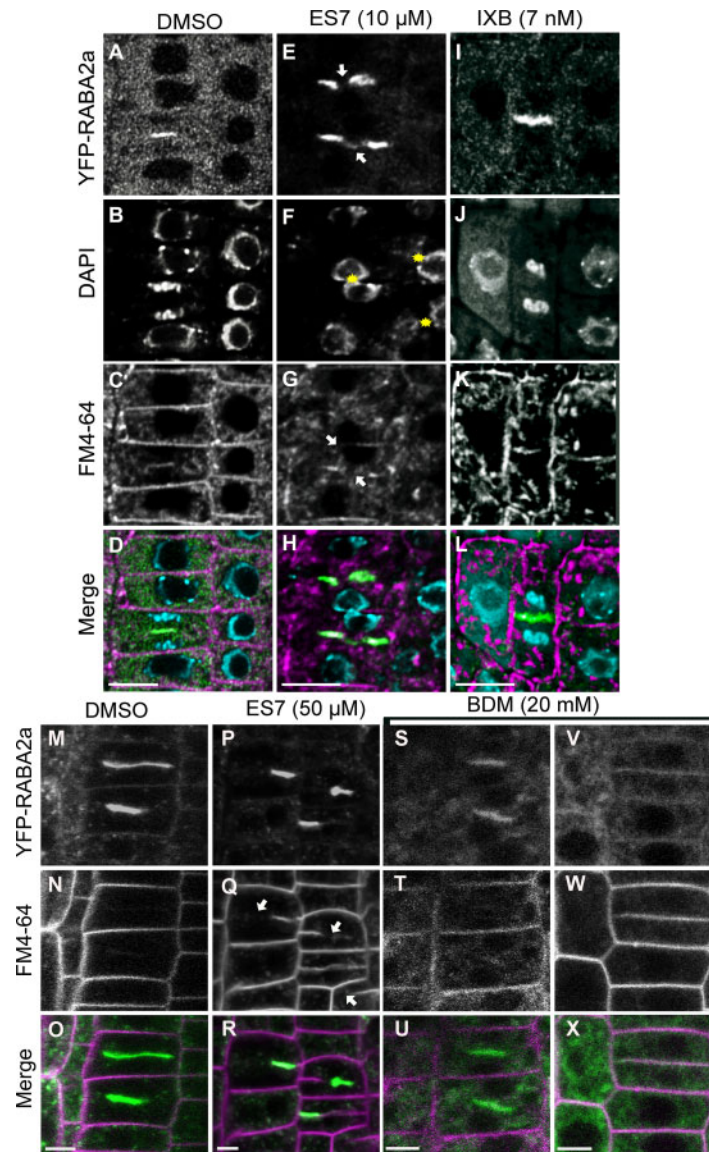


**Figure 5** Comparison of chemical inhibitors of cellulose, callose and myosin on cytokinesis. A–L, Evaluation of cytokinesis inhibition under 5 day chemical treatment in Arabidopsis root tips. Under control DMSO treatment normal cytokinesis is observed (A–D). Under ES7 treatment typical cytokinesis defects are observed with the cytokinesis marker RABA2a (E), multinucleate cells (F) are shown by DAPI staining. Under IXB treatment cell plate progression was observed (I) without discernable cytokinetic defects in the form of binucleate cells (J) or cell plate stubs (I, K, and L). Please note cell swelling under IXB treatment. The cytokinesis marker RABA2a is shown in green, while FM4–64 staining of plasma membrane is shown in magenta. Nuclei staining by DAPI are indicated in blue. Samples were stained with FM4–64FX, fixed and stained post fixation for DAPI. Results were observed in at least six roots for each drug treatment. Samples are single scans of fixed cells. Bars = 10 μm. M–X, Effect of 2 h short-term (50 μM) ES7 and the putative myosin inhibitor 2,3-butanedione 2-monoxime (20 mM BDM) treatment in cytokinesis. Under DMSO control treatment normal progression of cytokinesis is observed (M–O). Under ES7 treatment, characteristic cell plate stubs were observed with RABA2a and the plasma membrane stain FM4–64 (P–R). Under BDM treatment, a reduction of RABA2a signal was observed with increase in cytoplasmic pattern (S–X). The cytokinesis marker RABA2a is shown in green, while FM4–64 staining of plasma membrane is shown in magenta. Samples are single scans of live cell confocal imaging. Results were observed in at least six roots for each drug treatment. Bars = 5 μm.

Liu, 2013). Furthermore, inhibition of myosin causes a broader effect on cell plate expansion, as it is involved in general vesicle delivery (Figure 5). Therefore, it is challenging to assign a specific function of motor proteins to cell plate maturation at the lagging zone. Time-lapse experiments directed at the role of motor proteins at the lagging zone will shed light on their contribution to the stabilizing and spreading force that the model predicts.

It is plausible that polysaccharide deposition serves as this stabilizing and spreading role. The matrix polysaccharides hemicellulose and pectin are synthesized in the Golgi apparatus and delivered via vesicles from the beginning of cytokinesis (Moore and Staehelin, 1988; Toyooka et al., 2009; Rybak et al., 2014). Thus, these classes of polysaccharides are unlikely the major players as they do not overlap with the predicted onset of the spreading/stabilizing force, although

experimental verification awaits. Callose and cellulose are synthesized directly at the plasma membrane and are excellent candidates for exploration. Our data showed that pharmacological inhibition of cellulose at the root tip inhibited cell elongation in general, while inhibition of callose deposition led to cytokinesis defects consistent with the conformations predicted by the model in the absence of a spreading force. Callose accumulation peaks at the intermediate TN stage, a transitional stage that coincides with loss of membrane volume (Samuels et al., 1995; Segui-Simarro et al., 2004). The timing of callose deposition in late stages when the overall cell plate membrane network “flattens” (Samuels et al., 1995; Segui-Simarro et al., 2004) is consistent with the need of callose in providing a lateral spreading/stabilizing force. Furthermore, the predicted required values of callose deposition are within biological thresholds (Him et al., 2001; Pelosi et al., 2003). Notably, a study by Thiele et al. (2009) indicates that callose is required to establish the connection between the nascent cross-wall and the parental cell wall, rather than stabilizing the young cell plate (Thiele et al., 2009), so that further analysis on the role of callose in the proposed model awaits verification. It is plausible that callose could serve as a scaffold into which other more permanent polysaccharides and proteins are later deposited (Stone and Clarke, 1992; Him et al., 2001). Potential transient interaction with cellulose or other glucans (Miart et al., 2014; Gu et al., 2016; Abou-Saleh et al., 2018) can contribute to a composite that supports the stability of the cell plate and helps the attachment to the parental cell wall. Structural glycoproteins such as extensins (Cannon et al., 2008) can provide a scaffold for polysaccharide deposition, and these altogether can generate the desired spreading/stabilizing force proposed by the model. Further (challenging) experiments are necessary to determine how the possible conformations of different polysaccharides and proteins or their combinations, synthesized *in vitro* in an artificial membrane setup, can contribute to different magnitudes of spreading/stabilizing force in lipid vesicle networks.

A unique element in the study was the approximation of cellular compartments with testable shapes such as vesicles and complete cell plates with oblate spheroids, fused vesicles and tubular structures with elliptical hyperboloids and their combination in a network. Approximating vesicles, tubulations and their networks in the current model has the potential of a wider application and can be adopted during quantitative assessment of membrane dynamics. It can be used as a basis for addressing the equilibrium of vesiculation (oblate spheroids) and tubulation (elliptic hyperboloids) and applied to ER-intermediate compartments, Golgi, and endosomes in all eukaryotic cells.

In conclusion, our model provides a framework for understanding how membrane structures evolve in the presence of a spreading/stabilizing force and will likely shed light in such transitions that occur beyond cytokinesis.

## Materials and methods

A full description of our model development, parameter set up, plant growth, chemical treatment, and analysis is presented in the [supplemental material](#).

## Supplemental data

### Supplemental Text S1.

**Supplemental Figure S1.** Parameters visualized on a representative  $2 \times 1 \times 0$  structure.

**Supplemental Figure S2.** Effect of a spreading force visualized in a  $8 \times 10 \times 3$  conformation.

**Supplemental Figure S3.** Evolution of single oblate spheroid parameters in the presence of a spreading force.

**Supplemental Figure S4.** Stability tests of various configurations under different bending modulus in the absence of a spreading force.

**Supplemental Figure S5.** Stability tests of various configurations under different bending modulus in the presence of a spreading force and with zero spontaneous curvature.

**Supplemental Figure S6.** Stability tests of multiple  $2 \times 1 \times 0$  structures as compared to a single oblate spheroid in the absence of a spreading force and with finite spontaneous curvature.

**Supplemental Figure S7.** Stability tests of multiple  $2 \times 1 \times 0$  structures as compared to a single oblate spheroid in the presence of a spreading force and with zero spontaneous curvature.

**Supplemental Figure S8.** Stability tests of tubular/fenestrated structures as compared to a single oblate spheroid in the absence of a spreading force.

**Supplemental Figure S9.** Stability tests of tubular/fenestrated structures as compared to a single oblate spheroid in the presence of a spreading force.

**Supplemental Figure S10.** Evolution/transition of a cell plate structure in the absence of a spreading force as predicted by the model.

**Supplemental Figure S11.** Evolution/transition of a final cell plate structure from [Figure S10](#) in the presence of a spreading force as predicted by the model.

**Supplemental Figure S12.** Effect of IXB and ES7 on cellular organization and root growth.

**Supplemental Figure S13.** Proposed model of polymer deposition generating a two-dimensional spreading force.

**Supplemental Video S1.** Evolution/transition of a cell plate structure in the absence of a spreading force as predicted by the model.

**Supplemental Video S2.** Evolution/transition of a final cell plate structure from [Figure S10](#) in the presence of a spreading force as predicted by the model.

## Acknowledgments

We would also like to thank the members of the Drakakaki lab, particularly Drs. Destiny Davis, Michel Ruiz Rosquete,

Minmin Wang for useful discussions and Dr. Shuxiao Zhang for help with statistical analysis. We thank Anika Sagar and Alexander Zhou for help with quantification.

## Funding

This work was supported by NSF Grant MCB 1818219 to G.D. and D.C. G.D. was additionally, partially supported by the Department of Agriculture Hatch (CA-D-PLS-2132-H).

*Conflict of interest statement.* None declared.

## References

- Abou-Saleh RH, Hernandez-Gomez MC, Amsbury S, Paniagua C, Bourdon M, Miyashima S, Helariutta Y, Fuller M, Budtova T, Connell SD, et al.** (2018) Interactions between callose and cellulose revealed through the analysis of biopolymer mixtures. *Nat Commun* **9**: 4538
- Ahn G, Kim H, Kim DH, Hanh H, Yoon Y, Singaram I, Wijesinghe KJ, Johnson KA, Zhuang X, Liang Z, et al.** (2017) SH3 domain-containing protein 2 plays a crucial role at the step of membrane tubulation during cell plate formation. *Plant Cell* **29**: 1388–1405
- Albe KR, Butler MH, Wright BE** (1990) Cellular concentrations of enzymes and their substrates. *J Theor Biol* **143**: 163–195
- Bach L, Gissot L, Marion J, Tellier F, Moreau P, Satiat-Jeunemaitre B, Palauqui JC, Napier JA, Faure JD** (2011) Very-long-chain fatty acids are required for cell plate formation during cytokinesis in *Arabidopsis thaliana*. *J Cell Sci* **124**: 3223–3234
- Boruc J, Van Damme D** (2015) Endomembrane trafficking overarching cell plate formation. *Curr Opin Plant Biol* **28**: 92–98
- Brakke KA** (1996) The surface evolver and the stability of liquid surfaces. *Philos Trans Royal Soc Mathe Phys Eng Sci* **354**: 2143–2157
- Buschmann H, Müller S** (2019) Update on plant cytokinesis: rule and divide. *Curr Opin Plant Biol* **52**: 97–105
- Cannon MC, Terneus K, Hall Q, Tan L, Wang Y, Wegenhart BL, Chen L, Lampport DT, Chen Y, Kieliszewski MJ** (2008) Self-assembly of the plant cell wall requires an extensin scaffold. *Proc Natl Acad Sci USA* **105**: 2226–2231
- Chen HW, Persson S, Grebe M, McFarlane HE** (2018) Cellulose synthesis during cell plate assembly. *Physiol Plant* **164**: 17–26
- Drakakaki G** (2015) Polysaccharide deposition during cytokinesis: challenges and future perspectives. *Plant Sci* **236**: 177–184
- Gu F, Bringmann M, Combs JR, Yang J, Bergmann DC, Nielsen E** (2016) *Arabidopsis* CSLD5 functions in cell plate formation in a cell cycle-dependent manner. *Plant Cell* **28**: 1722–1737
- Gu Y, Rasmussen CG** (2021) Cell biology of primary cell wall synthesis in plants. *Plant Cell* koab249;doi:10.1093/plcell/koab249
- Helfrich W** (1973) Elastic properties of lipid bilayers - theory and possible experiments. *Z Naturforsch C* **28**: 693–703
- Higaki T, Kutsuna N, Sano T, Hasezawa S** (2008) Quantitative analysis of changes in actin microfilament contribution to cell plate development in plant cytokinesis. *BMC Plant Biol* **8**: 80
- Him JLK, Pelosi L, Chanzy H, Putaux JL, Bulone V** (2001) Biosynthesis of (1 → 3)-beta-D-glucan (callose) by detergent extracts of a microsomal fraction from *Arabidopsis thaliana*. *Eur J Biochem* **268**: 4628–4638
- Jung HT, Coldren B, Zasadzinski JA, Iampietro DJ, Kaler EW** (2001) The origins of stability of spontaneous vesicles. *Proc Natl Acad Sci USA* **98**: 1353–1357
- Jurgens G, Park M, Richter S, Touhri S, Krause C, El Kasmi F, Mayer U** (2015) Plant cytokinesis: a tale of membrane traffic and fusion. *Biochem Soc Trans* **43**: 73–78
- Kent IA, Lele TP** (2017) Microtubule-based force generation. *Wiley Interdiscip Rev Nanomed Nanobiotechnol* **9**: 10.1002/wnan.1428
- Lee YRJ, Liu B** (2013) The rise and fall of the phragmoplast microtubule array. *Curr Opin Plant Biol* **16**: 757–763
- Lou HY, Zhao W, Li X, Duan L, Powers A, Akamatsu M, Santoro F, McGuire AF, Cui Y, Drubin DG, et al.** (2019) Membrane curvature underlies actin reorganization in response to nanoscale surface topography. *Proc Natl Acad Sci USA* **116**: 23143–23151
- McMahon HT, Boucrot E** (2015) Membrane curvature at a glance. *J Cell Sci* **128**: 1065–1070
- McMichael CM, Bednarek SY** (2013) Cytoskeletal and membrane dynamics during higher plant cytokinesis. *New Phytol* **197**: 1039–1057
- Miart F, Desprez T, Biot E, Morin H, Belcram K, Hofte H, Gonneau M, Vernhettes S** (2014) Spatio-temporal analysis of cellulose synthesis during cell plate formation in *Arabidopsis*. *Plant J* **77**: 71–84
- Milo R** (2013) What is the total number of protein molecules per cell volume? A call to rethink some published values. *BioEssays* **35**: 1050–1055
- Moore PJ, Staehelin LA** (1988) Immunogold localization of the cell-wall-matrix polysaccharides rhamnogalacturonan I and xyloglucan during cell expansion and cytokinesis in *Trifolium pratense* L.; implication for secretory pathways. *Planta* **174**: 433–445
- Otegui MS, Mastrorade DN, Kang BH, Bednarek SY, Staehelin LA** (2001) Three-dimensional analysis of syncytial-type cell plates during endosperm cellularization visualized by high resolution electron tomography. *Plant Cell* **13**: 2033–2051
- Park E, Diaz-Moreno SM, Davis DJ, Wilkop TE, Bulone V, Drakakaki G** (2014) Endosidin 7 specifically arrests late cytokinesis and inhibits callose biosynthesis, revealing distinct trafficking events during cell plate maturation. *Plant Physiol* **165**: 1019–1034
- Pelosi L, Imai T, Chanzy H, Heux L, Buhler E, Bulone V** (2003) Structural and morphological diversity of (1 → 3)-beta-D-glucans synthesized in vitro by enzymes from *Saprolegnia monoica*. Comparison with a corresponding in vitro product from blackberry (*Rubus fruticosus*). *Biochemistry* **42**: 6264–6274
- Rybak K, Steiner A, Synek L, Klaeger S, Kulich I, Facher E, Wanner G, Kuster B, Zarsky V, Persson S, et al.** (2014) Plant cytokinesis is orchestrated by the sequential action of the TRAPP II and exocyst tethering complexes. *Dev Cell* **29**: 607–620
- Samaj J, Peters M, Volkmann D, Baluska F** (2000) Effects of myosin ATPase inhibitor 2,3-butanedione 2-monoxime on distributions of myosins, F-actin, microtubules, and cortical endoplasmic reticulum in maize root apices. *Plant Cell Physiol* **41**: 571–582
- Samuels AL, Giddings TH Jr, Staehelin LA** (1995) Cytokinesis in tobacco BY-2 and root tip cells: a new model of cell plate formation in higher plants. *J Cell Biol* **130**: 1345–1357
- Scheible WR, Eshed R, Richmond T, Delmer D, Somerville C** (2001) Modifications of cellulose synthase confer resistance to isoxaben and thiazolidinone herbicides in *Arabidopsis lxr1* mutants. *Proc Natl Acad Sci USA* **98**: 10079–10084
- Schulmann N, Meyer H, Kreer T, Cavallo A, Johnner A, Baschnagel J, Wittmer JP** (2013) Strictly Two-Dimensional Self-Avoiding Walks: Density Crossover Scaling. *Polym Sci Ser C* **55**: 181–211
- Schweitzer Y, Shemesh T, Kozlov MM** (2015) A model for shaping membrane sheets by protein scaffolds. *Biophys J* **109**: 564–573
- Segui-Simarro JM, Austin JR, White EA, Staehelin LA** (2004) Electron tomographic analysis of somatic cell plate formation in meristematic cells of *Arabidopsis* preserved by high-pressure freezing. *Plant Cell* **16**: 836–856
- Shemesh T, Klemm RW, Romano FB, Wang S, Vaughan J, Zhuang X, Tukachinsky H, Kozlov MM, Rapoport TA** (2014) A model for the generation and interconversion of ER morphologies. *Proc Natl Acad Sci USA* **111**: E5243–E5251
- Smertenko A, Assaad F, Baluska F, Bezanilla M, Buschmann H, Drakakaki G, Hauser MT, Janson M, Mineyuki Y, Moore I, et al.** (2017) Plant cytokinesis: terminology for structures and processes. *Trends Cell Biol* **27**: 885–894
- Stone BA, Clarke AE** (1992) *Chemistry and Biology of 1,3-β-Glucans*, La Trobe University Press, Victoria, Australia

- Thiele K, Wanner G, Kindzierski V, Jurgens G, Mayer U, Pahl F, Assaad FF** (2009) The timely deposition of callose is essential for cytokinesis in *Arabidopsis*. *Plant J* **58**: 13–26
- Tominaga M, Yokota E, Sonobe S, Shimmen T** (2000) Mechanism of inhibition of cytoplasmic streaming by a myosin inhibitor, 2,3-butanedione monoxime. *Protoplasma* **213**: 46–54
- Toyooka K, Goto Y, Asatsuma S, Koizumi M, Mitsui T, Matsuoka K** (2009) A mobile secretory vesicle cluster involved in mass transport from the Golgi to the plant cell exterior. *Plant Cell* **21**: 1212–1229
- van Oostende-Triplet C, Guillet D, Triplet T, Pandzic E, Wiseman PW, Geitmann A** (2017) Vesicle dynamics during plant cell cytokinesis reveals distinct developmental phases. *Plant Physiol* **174**: 1544–1558
- Worden N, Esteve VE, Domozych DS, Drakakaki G** (2015) Using chemical genomics to study cell wall formation and cell growth in *Arabidopsis thaliana* and *Penium margaritaceum*. *Methods Mol Biol* **1242**: 23–39
- Wu SZ, Bezanilla M** (2014) Myosin VIII associates with microtubule ends and together with actin plays a role in guiding plant cell division. *Elife* **3**: e03498

### **Chapter 3. Quantitative cell plate development and identification of robust transition points between growth phases**

This chapter, as part of a published manuscript, describes the use of four-dimensional imaging by lattice light sheet microscopy (LLSM) to address cell plate development. By developing a pipeline to quantitatively extract cell plate dynamics, it enabled us to dissect robustly transition phases during cell plate formation. This further allowed us to elucidate the point in which callose is critical for membrane transition as proposed by our model described in chapter 2.

Rosalie Sinclair, Minmin Wang, Muhammad Zaki Jawaid, Toshisangba Longkumer, Jesse Aaron, Blair Rossetti, Eric Wait, Kent McDonald, Daniel Cox, John Heddleston, Thomas Wilkop, Georgia Drakakaki, Four-dimensional quantitative analysis of cell plate development using lattice light sheet microscopy identifies robust transition points between growth phases, *Journal of Experimental Botany*, 2024;, erae091, <https://doi.org/10.1093/jxb/erae091>

## RESEARCH PAPER

4D quantitative analysis of cell plate development using by LLSM

Sinclair *et al.*

# Four-dimensional quantitative analysis of cell plate development using lattice light sheet microscopy identifies robust transition points between growth phases

Rosalie Sinclair<sup>1</sup>, Minmin Wang<sup>1</sup>, Muhammad Zaki Jawaid<sup>3</sup>, Toshisangba Longkumer<sup>1</sup>, Jesse Aaron<sup>4</sup>, Blair Rossetti<sup>4</sup>, Eric Wait<sup>4, 5</sup>, Kent McDonald<sup>6</sup>, Daniel Cox<sup>3</sup>, John Heddleston<sup>4</sup>, Thomas Wilkop<sup>2</sup>, and Georgia Drakakaki<sup>1,\*</sup>

<sup>1</sup> Department of Plant Sciences, University of California Davis, Davis, CA, USA

<sup>2</sup> Department of Molecular Cellular Biology, Light Microscope Core, University of California Davis, Davis, CA, USA

<sup>3</sup> Department of Physics and Astronomy, University of California Davis, Davis, CA, USA

<sup>4</sup> Janelia Research Campus, Ashburn, VA, USA

<sup>5</sup> Current address :Elephas Biosciences, Madison, WI, USA

<sup>6</sup> Electron Microscopy Facility, University of California, Berkeley, CA, USA

\* Correspondence: gdrakakaki@ucdavis.edu

### Highlight

Employing lattice light sheet 4D microscopy, we dissected plant cytokinesis, a multistage process involving orchestrated delivery of membranes and polysaccharides. Quantitative analysis revealed phase shifts, that disappeared through inhibition of callose deposition.

## **Abstract**

Cell plate formation during cytokinesis entails multiple stages occurring concurrently and requiring orchestrated vesicle delivery, membrane remodelling, and timely deposition of polysaccharides, such as callose. Understanding such a dynamic process requires dissection in time and space; this has been a major hurdle in studying cytokinesis. Using lattice light sheet microscopy (LLSM), we studied cell plate development in four dimensions, through the behavior of yellow fluorescent protein (YFP)-tagged cytokinesis-specific GTPase RABA2a vesicles. We monitored the entire duration of cell plate development, from its first emergence, with the aid of YFP–RABA2a, in both the presence and absence of cytokinetic callose. By developing a robust cytokinetic vesicle volume analysis pipeline, we identified distinct behavioral patterns, allowing the identification of three easily trackable cell plate developmental phases. Notably, the phase transition between phase I and phase II is striking, indicating a switch from membrane accumulation to the recycling of excess membrane material. We interrogated the role of callose using pharmacological inhibition with LLSM and electron microscopy. Loss of callose inhibited the phase transitions, establishing the critical role and timing of the polysaccharide deposition in cell plate expansion and maturation. This study exemplifies the power of combining LLSM with quantitative analysis to decode and untangle such a complex process.

**Keywords:** Callose, cell plate, cytokinesis, 4D imaging, lattice light sheet microscopy, plant cell division, quantitative image analysis, RABA2a.

**Abbreviations:** AIC, Advanced Imaging Center; CSL, cellulose synthase-like protein; ES7, Endosidin 7; FVS, fusion of vesicles stage; GSL, glucan synthase like; LLSM, lattice light sheet microscopy; MS, Murashige and Skoog; PFS, planar fenestrated sheet; ROI, region of interest; TN, tubular network; TVN, tubular–vesicular network YFP, yellow fluorescent protein.

## Introduction

Cytokinesis is a fundamental process in life, determining growth, development, and differentiation. In plant cytokinesis, a process fundamentally different from cytokinesis in animals and fungi (Samuels *et al.*, 1995; Stachelin and Hepler, 1996; Jürgens, 2005; Drakakaki, 2015; Gu and Rasmussen, 2022; Sinclair *et al.*, 2022), *de novo* formation of a cell plate partitions the cytoplasm of the dividing cell. Cell plate development occurs in multiple stages. It requires the directed and choreographed accumulation of post-Golgi vesicles via the phragmoplast (a structure composed of cytoskeletal polymers, associated proteins, and membranes) at the division plane (Smertenko, 2018)(Lee and Liu, 2013).

Cell plate expansion is centrifugal, led by the accumulation and fusion of vesicles arriving at the leading edge. Various morphologically determined cell plate developmental stages exist simultaneously during cytokinesis (Samuels *et al.*, 1995; Seguí-Simarro *et al.*, 2004). First, during the fusion of vesicle stage (FVS), cytokinetic vesicles guided by the phragmoplast arrive at the division plane where fusion occurs. Upon vesicle fusion and fission, membrane tubulation, primarily due to the activity of dynamin-related proteins (Otegui *et al.*, 2001; Seguí-Simarro *et al.*, 2004), helps the transition to a tubular–vesicular network (TVN) (Samuels *et al.*, 1995; Seguí-Simarro *et al.*, 2004). The membrane morphology evolves through the expansion of the network to a smoother tubular network (TN). The polysaccharide callose is predominantly

deposited at this stage (Samuels *et al.*, 1995). The excess membrane material is recycled via clathrin-coated vesicles (Otegui *et al.*, 2001). As the cell plate smoothens and expands, it transitions to a planar fenestrated sheet (PFS). The cell plate stiffens with the deposition of polysaccharides, leading to the formation of a cross-wall. As the phragmoplast expands centrifugally, delivering vesicles to the leading edge of the cell plate, the center matures with the removal of excess membranes and deposition of polysaccharides. Thus, at any given time, the cell plate contains a gradient of developmental stages. A recent review (Sinclair *et al.*, 2022) includes an animated overview of cytokinesis.

The synchronous and timed deposition of membrane material and polysaccharides control the cell plate's expansion, stability, and maturation into a new cross-wall (Drakakaki, 2015; Smertenko *et al.*, 2017; Gu and Rasmussen, 2022). However, little is known about how these mechanisms are orchestrated (Drakakaki, 2015; Smertenko *et al.*, 2017). Many GTPases are localized at the cell plate (Chow *et al.*, 2008; Geldner *et al.*, 2009; Qi *et al.*, 2011; Qi and Zheng, 2013; Berson *et al.*, 2014; Mayers *et al.*, 2017; Shi *et al.*, 2023), including the Rab-related GTPase RABA2a, which is involved in the delivery of *trans*-Golgi network-derived vesicles to the leading edge of the cell plate. As such, RABA2a is considered a good marker for cytokinetic vesicle accumulation directing cargo to the cell plate (Chow *et al.*, 2008). Necessary, vesicular fusion events during Arabidopsis cell plate formation are mediated by SNARE complexes that involve KNOLLE and its partners (El Kasmi *et al.*, 2013).

Our current insights into cell plate formation are based on two-dimensional, electron (Samuels *et al.*, 1995; Seguí-Simarro *et al.*, 2004) and *in vivo* fluorescence micrographs, with only minimal contributions from multidimensional spatiotemporal data (reviewed in Drakakaki, 2015; Smertenko *et al.*, 2017; Sinclair *et al.*, 2022; Geitmann, 2023). During the TN stage,

callose, a  $\beta$ -1,3-glucan polysaccharide, is temporally integrated into the cell plate (Samuels *et al.*, 1995). It is proposed that callose contributes a spreading force in the stabilization and maturation of the cell plate (Jawaid *et al.*, 2022). However, its timely delivery and contribution to the stage progression of cytokinesis remain elusive. Dissecting the dynamic behavior of components such as callose and other polysaccharides, and the overall phragmoplast machinery, is essential for a comprehensive understanding of their contributions. Even with the advancement in many technologies, research into cell plate development is hindered by the fact that mutations in cytokinesis, such as those of callose synthase/glucan synthase like (GSL8), are often lethal (Desprez *et al.*, 2007; Chen *et al.*, 2009; Thiele *et al.*, 2009), making a genetic approach to the underlying questions unfeasible. Therefore, imaging modalities that allow observation of the whole cytokinesis process in space and over time, with high image quality, are required to improve our understanding.

So far, confocal-based modalities are not ideal as they exhibit significant photobleaching, making it very challenging to capture with high temporal resolution the entire process of cell plate formation from initiation to maturation. In order to identify a region in the seedling where cell plates will develop requires a dedicated marker that labels the phragmoplast, such as TUA6 (Ueda *et al.*, 2003), and/or a nuclear stain suitable for live cell imaging. For a cytokinetic vesicle marker, such as RABA2a, the presence of an already initiated cell plate is required to set up the image acquisition, which in turn compromises early-stage observations. Additional challenges include: balancing field of view with temporal resolutions and inherent growth motion of the seedling laterally and axially. In the absence of automated tracking algorithms, manual adjustments in  $x$ ,  $y$ , and  $z$  are often required. These go hand in hand with extensive post-data processing, including concatenation and alignment.

Recent technological and methodological advances are now allowing four-dimensional (4D, *XYZT*), *in vivo* fluorescence microscopy, which can provide more biologically relevant quantitative information. The development of lattice light sheet microscopy (LLSM) enables lengthy image acquisitions with significantly minimized photobleaching. LLSM is a promising avenue in dissecting mitosis across different biological systems. It is allowing for easier acquisition of multiple cytokinesis events simultaneously, from their earliest detection, while decreasing the constant need to manually track the cell plate during acquisition (Chen *et al.*, 2014; Aguet *et al.*, 2016). In plants, LLSM has been employed to reveal the spatiotemporal accumulation of Annexin 1 – green fluorescent protein (ANN1-GFP) around the nuclear envelope of elongating trichoblasts (Tichá *et al.*, 2020), the dynamic subcellular localization of ROOT HAIR DEFECTIVE 2 (GFP–RHD2), as well as the observation of fine actin filaments in young root hairs (Ovecka *et al.*, 2022). However, while LLSM is an enabling modality, it has not yet been adopted to study cytokinesis in plants, potentially in part due to the efforts required to establish an imaging and quantitative analysis routine.

In this study, we adopted LLSM to study cytokinesis in plants. Taking advantage of the unique capabilities of LLSM, we investigated cell plate dynamics using the cytokinesis marker yellow fluorescent protein (YFP)–RABA2a coupled with pharmacological inhibition of callose. Quantitative analysis revealed the presence of distinct phases, with easily identifiable transition points during cell plate development, which were altered by inhibition of callose. The here presented imaging pipeline together with the identified stage transition can help further unravel the complex process of cytokinesis and interrogate the biological role of its components.

## Materials and methods

### Plant materials and growth

All *Arabidopsis* (*Arabidopsis thaliana*) seedlings were grown as described previously (Park *et al.*, 2014). Briefly, seeds were sterilized for 10 min in a solution containing 10% (v/v) sodium hypochlorite (NaOCl)/80% (v/v) ethanol/10% (v/v) water, followed by three washes in 90% (v/v) ethanol for 1 min, and subsequently air dried. Seeds were germinated on square plates containing Murashige and Skoog (MS) medium (Sigma; one-quarter strength), supplemented with 1% (w/v) Suc, pH 5.7, solidified with 0.5% (w/v) phytigel (Sigma) and designated chemicals. Plates were incubated at 10° off the vertical in a growth room with a 16 h light/8 h dark photoperiod for 3–5 d. Transgenic lines expressing YFP–RABA2a (Chow *et al.*, 2008) were used to observe cell plate development with or without chemical treatment (Park *et al.*, 2014).

### Chemical treatment and staining procedures

For microscopy, seedlings were grown as described above for 3 d and then transferred to 48-well plates containing 2 ml of liquid MS medium supplemented with 390 mM DMSO (Sigma), 50  $\mu$ M Endosidin 7 (ES7) (ChemBridge) (or otherwise indicated concentration) and allowed to grow for 2 h as pulse treatment. Chemicals were diluted to their working concentrations from 1000 $\times$  stock solutions. FM4-64 (5  $\mu$ M) diluted 1:1000 from a stock solution, applied for 5 min, was used to stain the plasma membrane. Aniline blue fluorochrome (Biosupplies) was used to detect callose at 0.1 mg ml<sup>-1</sup> in water, diluted from 1 mg ml<sup>-1</sup> stock. Staining was performed directly on imaging slides.

### Transmission electron microscopy

Four-day-old *Arabidopsis* seedlings, treated with 50  $\mu$ M ES7 for 1 h, were analyzed by transmission electron microscopy (TEM). Root tips (1 mm) were excised and fixed using high-pressure freezing methods as described earlier (McDonald, 2014; Otegui, 2020). Excised root tips were placed in a type B freezing planchette containing yeast paste as a filler/cryoprotectant

and frozen under high pressure in a high-pressure freezing unit (BAL-TEC HPM 010). Freeze substitution was performed in 1% OsO<sub>4</sub> and 0.1% uranyl acetate in acetone, followed by infiltration and embedding in Epon resin as described earlier (McDonald and Webb, 2011; McDonald, 2014). Thin sections (70 nm) were cut on a Leica Ultracut E ultramicrotome, picked up on Formvar-coated slot or 100 mesh grids, and post-stained for 7 min in 2% uranyl acetate in 70% methanol, followed by 4 min staining in Reynold's lead citrate. Images were taken with a Gatan Ultrascan 1000 camera on a FEI Tecnai-12 electron microscope operating at 120 kV.

## Confocal/high resolution microscopy

### Image acquisition

A Zeiss Airyscan 980 or a Leica SP8 was used for confocal imaging. The Leica SP8 was used to image YFP-RABA2a seedlings co-stained with FM4-64 (5 μM) utilizing a ×100/1.4 NA oil objective (HC PL APO CS2) employing a high resonant scanning with line averaging set to 15. Excitation at 512 nm was used for both YFP-RABA2a and FM4-64, with emissions collected at 520–558 nm and 650–800 nm for YFP and FM4-64, respectively. For the time-lapse series, Z-stacks were collected at intervals of ~1 min for 30–45 min. Images are representatives of five biological replicates (independent seedlings).

The Zeiss 980 was used to image YFP-RABA2a seedlings co-stained with aniline blue at single time points, using Airyscan CO 8Y mode. The fluorescent signal of YFP-RABA2a was excited using a 514 nm laser at 25% power, and aniline blue fluorochrome was excited using the 405 nm laser at 15% power. All images were collected using the LD LCI Plan-Apochromat ×40/1.2 NA (Korr DIC M27) water objective. Images are representatives of five biological replicates (independent seedlings).

The Zeiss 980 was used to image Arabidopsis seedlings treated for 2 h with 50  $\mu$ M ES7 or DMSO and co-stained with 5  $\mu$ M FM4-64. The fluorescent signal of FM4-64 was excited using a 514 nm laser at 10% power. All images were collected using the LD LCI Plan-Apochromat  $\times$ 40/1.2 NA (Korr DIC M27) water objective. Images are representatives of 20 biological replicates (independent seedlings).

### Image processing

Leica SP8 data were deconvolved using classic maximum likelihood estimation (CMLE), manually adjusting for background with a maximum of 20 iterations and corrected for XYZ drift using Huygens (SVI). Collected images from the Zeiss 980 Airyscan were processed using the Zeiss built-in Airyscan processing software employing automated settings. All data were exported to Imaris (Oxford Instruments) for segmentation and 3D or 4D visualization. Figures were assembled using Affinity Designer (Serif).

### Lattice light sheet microscopy

#### Imaging

Imaging was performed using the lattice light sheet microscope at the Advanced Imaging Center (AIC) on the Janelia Research Campus, following sample preparation and imaging procedures as previously described ([Chen \*et al.\*, 2014](#)). Arabidopsis seedlings at 3–4 d old were mounted on a 5 mm coverslip [Warner Instruments Cat. No 64-0700 (CS-5R)]. One seedling was mounted per coverslip within a thin layer of 0.5% low melting agarose (w/v) in water. The cover slip was clipped to the end of a long extension of the sample holder and submerged in a bath filled with 8.5 ml of 1/4-strength MS liquid medium. The opposite end of the coverslip holder was bolted to the sample piezo ([Chen \*et al.\*, 2014](#)). YFP–RABA2a plants were stained with FM4-64, and both

fluorophores were excited using a 488 MPB fiber laser. A two-camera system, 2× Hamamatsu Orca Flash 4.0 v2 sCMOS, was used to acquire the images of the two fluorophores.

## Lattice light sheet microscopy image processing

All data were acquired in the dithered mode and were deconvolved by using a Richardson–Lucy algorithm adapted to run on a graphics processing unit (GPU) (NVIDIA, GeForce GTX TITAN), using an experimentally measured point spread function (PSF) for each emission wavelength.

Before visualization, all 3D datasets acquired via sample scan in the  $x$ ,  $y$ , and  $z$  coordinated system were transformed (‘deskewed’) to the more conventional  $x$ ,  $y$ , and  $z$  coordinates using a GPU.

## Selection of points of interest for channel alignment and image stabilization

### Channel alignment

The BigStitcher plugin in ImageJ was used to process datasets before quantitative analysis. All files using BigStitcher were converted to .xml to register how the data are stored and track any internal processing following the pipeline described in the AIC guidelines:

<https://knowledge.aicjanelia.org/posts/20200730-stabilize-roi-selection/>. One .xml file was generated per time-lapse dataset. For our experiments, the metadata denoted FM4-64 as channel 0 and YFP–RABA2a as channel 1.

Once a file was generated, channel alignment was applied first, followed by drift correction (movement in the field of view). Note that the drift correction can lead to misalignment if processing is conducted in this sequence. Channel alignment followed a similar routine to the drift correction, as described in AIC guidelines:

<https://knowledge.aicjanelia.org/posts/20200730-stabilize-roi-selection/> with the following modifications. (i) In the Multiview Explorer window, the first time point was selected for

channel 0 (FM4-64), and the command ‘Detect Interest Points’ was used for navigation to the interest points ‘Difference-of-Gaussian’ with no other restrictions selected. This was repeated for channel 1 (YFP–RABA2a). (ii) Then the parameters used to identify the points of interest were refined using the sigma and threshold sliders. The minimum threshold was used to detect the space within each cell, enabling the individual selections of interest for each cell. Sigma values were set to a range of 8–9 to obtain detectable points/regions inside each cell that can be used for the alignment. Adjustments were made to create the best recognizable points common between the two channels to facilitate the best alignment in the next step. (iii) The points of interest were registered using a precise descriptor-based (translation-invariant) algorithm to align the two channels and validate them through the viewer window 3D function. The transformation model is rigid, with an allowed error for random sample consensus iterative methodology known as RANSAC (px) of 7–8. This was repeated for various sigma thresholds until the two channels overlapped. (iv) Once complete, the BigStitcher windows were closed, and in the plugins menu the following sequence was selected: Multiview Reconstruction→Batch Processing→Tools→Duplicate Transformations. Transform one-time points to other time points. The selected transformation was then applied to all time points across the dataset.

## Drift correction

Following channel alignment, drift correction was applied using the steps below as described in the AIC guidelines: <https://knowledge.aicjanelia.org/posts/20200730-stabilize-roi-selection/>.

Note the significant differences from the channel alignment steps: (i) the use of all time points in one channel, instead of the first time point and (ii) the adjustment of Gaussian values to identify the cell wall corners across the time points, instead of the space inside the cells that was used for

channel alignment. The threshold was set to the maximum, while the sigma value was set to a range from 7.5 to 9.5.

### Create a bounding box for the region of interest

Region of interest (ROI) selection and export as 3D .tiffs were used to decrease file size and obtain workable files by following the steps ‘Create Bounding Box for Region of Interest’ as outlined in AIC guidelines: <https://knowledge.aicjanelia.org/posts/20200730-stabilize-roi-selection/>.

### Image stack assembly and bleach correction

The .tiff files generated from the bounding box ROI step were then separated into folders by each channel and concatenated into a full-time series using ImageJ. The time series were then bleach-corrected using histogram matching. Finally, processed data were first exported into individual .tiffs and subsequently into the .ims format using the Imaris file converter. Before converting, settings were adjusted for the voxel dimension, *XYZT* frame, and image acquisition time points. Files were finalized and imported into Imaris for 4D volumetric rendering. All time series at this step contained two datasets, one for ‘raw’ data and one for the histogram-matched bleach-corrected data.

. Representative datasets used in the study are available on Zenodo at [10.5281/zenodo.10515765](https://zenodo.org/record/10515765)

### Imaris segmentation

Surface rendering of individual cell plates was performed with the surface creation tool using Imaris X64 9.6.0 in conjunction with object tracking as outlined by user guidelines,

<https://qbi.uq.edu.au/research/facilities/microscopy-facility/image-analysis-user-guides/analysis-software/imiris/creating-surface-imiris>, with the following modifications. (i) In the first step of

the surface creation, a bounding box was drawn to enable the separation of a specific region to reduce the working file size. (ii) Surface segmentation was performed using the ‘new surfaces’ function. The appropriate channel (histogram corrected) was used. Surface detail was set to 0.1  $\mu\text{m}$ , and thresholding was based on background subtraction with the values set based on the diameter of the largest sphere fitting the object. To obtain these values, the diameter of the largest shape was measured in the 2D view under the slice mode. (iii) During the next step, the image histogram was adjusted to best fit the objects of interest. Multiple surfaces/segmentations could be used for different cell plates and different time points for statistical analysis. (iv) In the next step, a preview was generated by Imaris, with the final surfaces bounding all the objects that were detected in the ROI. Objects were filtered based on voxel count to better define the observed objects. In general, a voxel count of 20 throughout the dataset allowed for the best observation. Surfaces were tracked throughout the time course with autoregression motion selected, and the maximum travel distance between time points was set to 4  $\mu\text{m}$ . The maximum gap size for surfaces in consecutive frames in a track was set to 3. (v) Following surface rendering, individual cell plates were segmented by selecting their corresponding subsurfaces, rebuilding the cell plate individual tracks, and connecting the subtracks together. Surfaces and volumes of cell plates were extracted, uniquely named, and quantitatively analyzed.

We note that working with different channels separately leads to manageable file sizes matching better the computer processing power. As the different channels are aligned, they can be later combined after further processing. (vi) Cell plate diameter values were recorded manually for each time point during cell plate formation by measuring the largest distance of YFP–RABA2a. The FM4-64 plasma membrane stain was employed to determine the predicted cross-wall width and was used to normalize the diameters, accounting for cell size variations (Chow *et al.*, 2008;

van Oostende-Triplet *et al.*, 2017). Finally, normalized diameter values were averaged at their respective time points across cell plates.

## Quantification and statistical analysis

The data generated from the intensity-based Imaris segmentation were compiled in Excel files and further analyzed (Supplementary tables S1 & S2). The Origin 2021 software (Origin, 2003. Origin 7.5. OriginLab Corp., Northampton, MA, USA) was used to normalize the data to their maximum volume or area. To determine an approximate rate of change of measured volumes/areas, the data were fitted to a polynomial (adjusted  $R^2$   $0.69 \pm 0.03$ ), from which derivatives were calculated. For visualization purposes, the derivatives were linearly shifted, creating a time when all rates passed through zero. However, raw datasets were considered for fitness comparison and any further statistical analysis differences.

## Binning approach for further statistical analysis

For statistical comparison of volume accumulation between control and ES7 treated samples, the data were divided into five groups (bins) for further statistical analysis. These bins correspond to the normalized volume changes based on the following approach: bin 1 (increasing values from 0 to  $0.33 \mu\text{m}^3$ ), bin 2 (increasing values from  $0.33 \mu\text{m}^3$  to  $0.66 \mu\text{m}^3$ ), bin 3 (increasing values from  $0.66 \mu\text{m}^3$  to  $1 \mu\text{m}^3$ ), bin 4 (decreasing values from  $1 \mu\text{m}^3$  to  $0.66 \mu\text{m}^3$ ), bin 5 (decreasing values from  $0.66 \mu\text{m}^3$  to  $0.33 \mu\text{m}^3$ ), and bin 6 (decreasing values from  $0.33 \mu\text{m}^3$  until reaching the final minimal YFP-RABA2a cell plate volume). The width of the bins, as well as the divide between increasing and decreasing values, were chosen for simplicity. The derived rates from each of the volume bins were then averaged. These averages were statistically analyzed using two-tailed pairwise *t*-tests (GraphPad) and then were plotted .

*P*-values for diameter studies were additionally calculated using a second binning approach. The normalized diameter values were averaged across cell plates at their respective time points. For comparisons, The ES7 time points were laterally adjusted such that the averaged ES7 values at the starting point matched the corresponding control value. *P*-values were then calculated using pairwise *t*-tests (GraphPad).

## Results

### Development of a 4D lattice light sheet microscopy image acquisition and processing pipeline to study plant cytokinesis

Cell plate assembly, expansion, and maturation are regulated in space and time over an extended period. Therefore, 4D imaging is necessary to examine in depth the membrane and cell plate expansion dynamics. We first used laser scanning confocal microscopy with a resonance scanner, maximizing acquisition speeds, to follow cytokinesis over extended periods of time. Using YFP-RABA2a (Chow *et al.*, 2008) as a cytokinesis marker, high resolution imaging of cell plate development was possible (Fig. 1). Time-lapse imaging showed centrifugal expansion of the cell plate. This approach, however, was not sustainable for the dissection of a large number of cytokinesis events. With confocal microscopy, one could only manually track developing cell plates, one at a time, limiting its scalability. Further, using this approach, only already sufficiently assembled cell plates could be imaged since their presence was necessary to set up the acquisition.

To circumvent these hurdles and capture full cell plate events, while improving throughput, we used LLSM. LLSM affords imaging at much faster rates and with less light exposure of the sample, minimizing photobleaching and phototoxicity (Chen *et al.*, 2014). LLSM helps to extend the observation time, while affording higher axial resolution with similar lateral

resolutions to those obtained with confocal microscopy. Using LLSM, we recorded the marker YFP–RABA2a in the root tips of 3-day-old *A. thaliana* seedlings. We generated 4D data capturing the complete process of cell plate development with minimal photobleaching, allowing the acquisition of datasets amenable to in-depth quantitative analysis. The cell membrane and cellular architecture dye, FM4-64, was used to provide a reference for overall cell shape and cell plate expansion perspective. Once image acquisition was completed, a pipeline was developed primarily using open-source software for image processing followed by quantitative analysis (Fig. 2, see more details in the Materials and methods). In brief, this involved image deskewing, aligning the two fluorescence channels, correcting for (*XYZ*) drift, and selection of an ROI to obtain a manageable data size. Once data were exported into readable formats (.tiff), they were concatenated into time series stacks for each channel. The image files were bleach-corrected by histogram matching across time points for the whole stack (Fig. 2B, C). Segmentation of developing cell plates was performed using an intensity value-based algorithm in IMARIS, followed by quantitative analysis of cell plate volume, surface area, and diameter (Fig. 2D).

### Quantification of cell plate dynamics shows three distinct developmental stages based on YFP–RABA2a accumulation patterns

With the adoption of LLSM, cell plate growth from its point of origin at the vesicle accumulation stage (FVS) until completion of cytokinesis can be observed, a time frame that was not previously established with confocal and electron microscopy (Seguí-Simarro *et al.*, 2004; Higaki *et al.*, 2008; van Oostende-Triplet *et al.*, 2017; Geitmann, 2023). An example is presented in Fig. 3A, a pink segmented surface, in which volume and area change and rates are tracked by a bold blue line in Fig. 3B–E. As shown in Fig. 3A, B, completion of cytokinesis takes place within 20–30 min. Within this time window, cell plate volume peaked during the first 8 min

(Fig. 3A). Then the cell plate expanded laterally and flattened, with the gradual reduction of the vesicle accumulation marker dispersing at the cell plate rim and finally disappearing (Supplementary Video S1), probably representing transitions to discontinuous phragmoplast stages (Smertenko *et al.*, 2017; Sinclair *et al.*, 2022). With LLSM, observation of multiple cytokinetic events within the same root tip was possible. Each observed cytokinetic event was unique. Events in the same root tip did not exhibit over-reaching similarity.

A quantitative analysis of segmented cell plates based on the cytokinetic marker was performed to better understand the spatiotemporal dynamics of vesicle accumulation and cell plate expansion. Normalized volumes of developing cell plates were fitted to a polynomial regression, allowing accumulation trends to be observed across biological samples (Fig. 3B). As mentioned above, the cell plate volume accumulation based on YFP–RABA2a peaked within ~8 min, followed by a rapid reduction over the following 8 min. The rates of volume ( $1.5 \times 10^3$ – $9.5 \times 10^3 \mu\text{m}^3 \text{min}^{-1}$ ) accumulation determined by the first-order derivative showed a net positive addition of YFP–RABA2a vesicle/membrane material for the first 8 min (Fig. 3C). Within this period, a short interval exhibits linear growth. The first 8 min marked a turning point at which the rates of volume accumulation switched to a net negative value (Fig. 3C, asterisk). The negative rate values probably represent recycling of large amounts of material during cell plate expansion and maturation, as postulated from electron microscopy analysis (Otegui *et al.*, 2001; Seguí-Simarro *et al.*, 2004). We also quantified the bounding surface area corresponding to the segmented cell plates. The time course of the YFP–RABA2a bounding surface areas and their corresponding rates (Fig. 3D, E) showed an overall similar trend in line with the volume accumulation. Without overinterpretation of the data, one can note that peak values are slightly deviating, which might be indicative for geometrical changes—thinning or thickening.

In summary, three distinct phases became apparent based on our quantification: phase I, a rapid phase of cytokinetic vesicle material delivery with a positive YFP–RABA2a cell plate volume rate, followed by a substantial volume reduction (phase II). Finally, a third phase (phase III) of minimal cytokinetic vesicle presence at the rim of the cell plate took place before joining the parental cell wall.

To correlate the dynamic behavior of YFP–RABA2a cytokinetic vesicles with that of the cell plate membrane, we quantitated both volumes and bounding surface areas. The membrane was visualized by staining with the endocytic lipophilic dye FM4-64. The segmentation of FM4-64-stained membranes throughout cytokinesis is not a trivial task, given that the staining is very much prone to indiscriminate staining of all membranes over time and/or bleaching. The inherently fluctuating time point for cell plate formation after the initiation of the staining is an additional challenge and limits available datasets. The temporal behavior of the YFP–RABA2a volumes and stained cell membranes for selected samples observed via LLSM ([Supplementary Fig. S1A–D](#)) and laser scanning confocal microscopy is shown in [Supplementary Fig. S1, Table S3](#).

The normalized and polynomial fitted data for both the YFP–RABA2a volume and membrane volume follow a similar pattern. Both exhibit a distinct and rapid growth phase of volume accumulation that, after reaching its zenith, is followed by a reduction at somewhat lower rates. The peaks for both YFP–RABA2a and the FM4-64 membrane occur at similar times. It is noteworthy, that the FM4-64 membrane removal dynamics exhibit higher dispersion, compared with the very coherent rates of the YFP–RABA2a volume. One can only speculate on the causative factors for this, with varying rates of membrane removal or incomplete FM4-64 staining (stain exhaustion) being possible reasons. Bounding surfaces follow similar trends for

both YFP–RABA2a and FM4-64 staining (Supplementary Fig. S1C, D). Confocal data show a very similar pattern to that observed for the LLSM data. Both YFP–RABA2a volumes and FM4-64 membrane volumes follow similar dynamics, with distinct peaks at similar times (Supplementary Fig. S1E, F).

These data highlight the suitability of our global analysis of membrane volumes during cell plate development as a mechanism to decipher progression of cell plate formation consistent with earlier predictions based on electron microscopy (Otegui *et al.*, 2001; Seguí-Simarro *et al.*, 2004). In future studies, the use of the cytokinesis-specific SNARE KNOLLE (Lukowitz *et al.*, 1996) might be a useful alternative for charting the membrane kinetics.

## **Inhibition of callose deposition arrests cytokinesis and induces aberrant membrane accumulation patterns**

Our data show that while vesicle volume accumulation is a very rapid process, the expansion and maturation phase is lengthier. The latter stages are accompanied by a significant loss of cell plate volume, probably due to the recycling of membrane material. During the transition of the cell plate from a membrane network to a fenestrated sheet, the accumulation of the polysaccharide callose is implicated in stabilizing this network and providing a spreading force for expansion and maturation (Samuels *et al.*, 1995; Jawaid *et al.*, 2022). To better understand the role of callose during these dynamic cell plate transitions, we applied ES7, a small molecule that has shown inhibition of cytokinetic callose deposition and callose synthase activity in microsome assays (Drakakaki *et al.*, 2011; Park *et al.*, 2014). As observed by confocal microscopy, YFP–RABA2a accumulation was not affected by the 2 h ES7 pulse treatment. However, the cell plate expansion and maturation were impaired, leading to stagnation, as shown by the cytokinesis marker YFP–RABA2a and FM4-64 staining (Fig. 4). Quantification of cell plate stubs on

seedlings stained with FM4-64 averaged three stubs per seedlings, while DMSO controls showed zero to rarely one cell plate stub (Supplementary Fig. S2A–C). We then used TEM on high-pressure-fixed root tips to resolve changes induced by ES7 at the ultrastructural level. Consistent with our confocal observations, no cell plate stubs were observed in DMSO controls (Supplementary Fig. S2D) while irregular cell plate structures were observed in ES7-treated roots (Supplementary Fig. S2E). As shown in Supplementary Fig. S2F, the structure of cytokinetic vesicles was not affected during the accumulation stage, and no discernible aberrations in the vesicle or Golgi morphology were observed. However, irregular cell plate stubs were observed in later stages of cytokinesis (Supplementary Fig. S2G, arrows) in contrast to normally expanding cell plates as previously reported in *Arabidopsis* (Samuels *et al.*, 1995), corroborating our light microscopy observations.

## Membrane transition between cytokinetic stages is affected by the chemical inhibition of callose

While informative, confocal and electron microscopy were not ideal for studying the dynamic nature of cell plate development under ES7 treatment. Thus, we again employed LLSM. The use of LLSM still allowed imaging of various cytokinetic events, facilitating quantification and providing an analysis of the impact of callose inhibition. It is worth noting that the observed events took longer compared with untreated plants.

In contrast to the untreated seedlings (Fig. 3), the cell plates subjected to a 2 h ES7 pulse treatment (Fig. 5) exhibited a notable accumulation of YFP–RABA2a volume that persisted beyond 15 min without significant expansion in the cell plate itself. Meanwhile, the marker maintained a condensed structure, eventually fragmenting throughout the lifetime of the imaged cell plates (Fig. 5A; Supplementary Video S2, cell plates shown in blue). Another ES7-induced

phenotype, though less frequent, showed relative expansion in the cell plate, but also eventually fragmented in an erratic pattern (shown in pink in [Supplementary Video S3](#)). Overall, the relative expansion did not match that observed in untreated samples, as further discussed below. Under the influence of ES7, the attempted cell plate development ran longer than in the controls, averaging  $35 \pm 13.7$  min compared with the 20–30 min in untreated samples. The variation in ES7-induced phenotypes was probably due to the timing of the drug's effect at different cytokinetic stages, as multicellular root tips are not synchronized.

Quantifying YFP–RABA2a cell plate volumes ([Fig. 5B](#)) and their corresponding rates of change ([Fig. 5C](#)) under a 2 h ES7 pulse treatment showed an initial phase of rapid volume growth, followed by a slower to stagnant accumulation of YFP–RABA2a membrane material, leading to a plateau of retained volume over a longer time frame. This prolonged plateau contributes to the increased average division time compared with the untreated plants ([Fig. 5B, C](#)). Similarly, the bounding surface area of the cell plates exhibited very similar dynamics and behavior, with a broad plateau of surface area over time and a severely depressed rate of surface area change ([Fig. 5D, E](#)). Overall, the phenotypic observations and quantifications of cell plate characteristics demonstrate a stark difference between ES7-treated and control cell plates. While the control cell plates followed distinct, consistent growth phases based on volume changes, marked by a transition from positive to negative rates, no apparent pattern changes in ES7-treated volumes, corresponding to discernible phase transitions, were observed.

In order to assess the impact of ES7, the volume growth rates of both control and ES7-treated cell plates were divided into equidistant volume intervals using 20% intervals (six 'bins') for statistical analysis. We focused on five bins, as the sixth bin at the end of the collection showed high variability. The first three intervals (bins 1–3) correspond to the normalized

increasing volumes in the control, ranging from 0 to  $0.33 \mu\text{m}^3$ ,  $0.33 \mu\text{m}^3$  to  $0.66 \mu\text{m}^3$ , and  $0.66 \mu\text{m}^3$  to  $1 \mu\text{m}^3$ , respectively. Intervals 4 and 5 represent reducing volumes ranging between  $1 \mu\text{m}^3$  and  $0.66 \mu\text{m}^3$  and between  $0.66 \mu\text{m}^3$  and  $0.33 \mu\text{m}^3$ , respectively (Fig. 6F). Bin 1 (Fig. 6A) corresponds to the interval with maximum volume accumulation, which is similar between the control and ES7 (Figs 3, 5). Intervals 2, 3, and 5 exhibited statistically significant differences between the control and ES7 treatments (Fig. 6B–C, E). The most pronounced difference was observed in interval 5 (Fig. 6E), in which ES7-treated cell plates showed minimal growth reduction and maintained a positive average rate, in contrast to the non-treated plates. Notably, the maximum amount of volume or bounding surface area accumulated by YFP–RABA2a throughout all the events was not statistically different between ES7 and controls (Supplementary Fig. S3), indicating that vesicle accumulation remains unaffected by the inhibition of callose. Taken together, the data suggest that inhibition of cytokinetic callose disrupts the phase transition from cytokinetic vesicle/volume accumulation to volume reduction and cell plate maturation.

### Expansion rate analysis identifies a critical point for callose deposition

Prior models have relied on radial expansion to stage cell plate maturation, using confocal microscopy data (Higaki *et al.*, 2008; van Oostende-Triplet *et al.*, 2017). To gain deeper insights into the morphological stages of cell plate development and how they are impacted by callose inhibition, we also adopted the cell plate diameter as a measure of expansion (Fig. 7; Supplementary Fig. S4). At each time point, we measured the diameter at the longest distance across the outermost opposing edges of detectable YFP–RABA2a at the cell plate’s rim, using the FM4-64 plasma membrane stain to determine the predicted final cross-wall width, and normalized the diameters, accounting for cell size variations (Chow *et al.*, 2008; van Oostende-

Triplet *et al.*, 2017). The diameter analysis (Fig. 7A; Supplementary Fig. S4A, B) displayed a logarithmic expansion pattern in control plants. In contrast, the ES7-treated plants exhibited unstable growth with a reduction trend observed after 10–12 min (Fig. 7A; Supplementary Fig. S4C, D). These findings provide valuable insights into the effect of callose inhibition on cell plate development and its impact on the expansion dynamics of the cell plates.

Interestingly, during the first 8–10 min that marked the bulk of vesicle volume accumulation, both ES7-treated and control cell plates reached the same expansion levels corresponding to ~60% of the predicted final diameter. While control cell plates continued growing exponentially, ES7-treated cell plates showed minimal expansion beyond the first 10 min (Fig. 7A). Based on these data, the intersection of the two growth curves indicates a critical point at which callose is essential for cell plate expansion. Notably, this time interval corresponds to the cell plate phase transition from phase I to phase II, during which volume growth changes from a positive to a negative rate and a significant volume loss occurs (Fig. 3B, C).

Our previously developed biophysical model highlights the importance of a spreading force, probably by the deposition of callose, for a cell plate to transition from a vesicular membrane network to a fenestrated sheet and finally to a mature cell plate (Jawaid *et al.*, 2022). Combined with the presented data, we hypothesize that cell plate formation is characterized by a distinct, callose-dependent transition that changes from membrane accumulation to membrane recycling within ~10 min. We suppose that some ES7-treated cell plates achieve a considerable level of expansion, probably due to the timing of the treatment. However, the majority tend to collapse or fragment, and fail to reach the parental cell wall.

There were significant technical difficulties in reliably measuring the thickness of the somewhat irregular cell plates, which led us to use the cell plate volume divided by the bounding cell plate surface to estimate plate thickness. The volume-to-surface area ratio in control cell plates shows a bell curve distribution (Fig. 7B), with an initial volume accumulation phase followed by flattening, thinning, and diametric expansion of the cell plate. However, when treated with callose-inhibiting ES7, the volume-to-bounding surface ratio followed a fluctuating flat line without a significant volume loss (Fig. 7B). This behavior might be indicative of a mechanism that critically inhibits ‘radial’ expansion and potential redistribution/recycling of membrane material. Polynomial fitted cell plate diameters were grouped into 20 intervals (bins) which were subjected to statistical analysis comparing control versus ES7-treated cell plates (Fig. 7C). All but one interval was statistically different (Fig. 7D; Supplementary Fig. S4E). Notably, this one interval identifies the intersection of the ES7 and control cell plate expansion curves and is a critical point in which callose’s presence is essential.

### Callose deposition appears in the late cytokinetic stages

Next, we examined the localization of callose in relation to YFP–RABA2a to test if its presence corresponds to the predicted critical point during cell plate expansion. Using the callose-specific stain aniline blue fluorochrome (Evans and Hoyne, 1982) and employing multichannel live cell imaging, we characterized the transient presence of callose in relation to the cytokinesis marker YFP–RABA2a. During the early stages of cell plate development, no callose signal was identified (Fig. 8A), while significant YFP–RABA2a accumulation was observed, marking an expanding cell plate. During later stages of cell plate development, callose was clearly identifiable and spatially distinct from YFP–RABA2a. The cytokinetic vesicle marker YFP–RABA2a showed a ring or partial ring pattern (Fig. 8C, D), while callose was observed in an expanded disk form (Fig.

8C–E). We observed callose deposition beginning at this critical morphological transition point corresponding to the ~8–10 min mark characterized by a change from a disk-shaped to a ring-shaped YFP–RABA2a pattern. We conclude that the polysaccharide is deposited during the transitional stages of YFP–RABA2a volume reduction and cell plate expansion. This pattern distinctly corresponds to phases II and III and covers the interval beyond the crossover point predicted by cell plate diameter expansion.

## Discussion

Mitosis, being the fundamental process of life that drives growth and development, necessitates a deeper understanding of its intricate details and complexity. Thus, the ability to image cytokinesis at a high spatiotemporal level is of immense value in advancing developmental biology. In plants, cytokinesis is unique as it involves the *de novo* formation of a cell plate that expands centrifugally, leading to the separation of two daughter cells. The dynamic nature of various cell plate development stages that occur simultaneously demands sensitive imaging techniques with minimal photobleaching to comprehensively capture the entire process. Although electron tomography studies have contributed significantly to our current knowledge of cytokinesis (Samuels *et al.*, 1995; Seguí-Simarro *et al.*, 2004), they lack the ability to provide consecutive time points in the same sample, limiting their capacity for robust statistical analysis. Moreover, conventional laser scanning confocal microscopy, despite its excellent lateral, axial, and temporal resolution, is too photo-damaging to conduct high-quality, extended time-lapse acquisitions.

The development of LLSM affords imaging at much faster rates, with less light exposure of the sample, minimizing photobleaching and phototoxic effects, which extends the observation time, while affording higher axial resolution and maintaining near confocal microscopy-type lateral resolutions (Chen *et al.*, 2014). In this context, LLSM allows the collection of previously

unobtainable datasets to dissect mitosis. Taking advantage of the resolution, speed, and gentle illumination, LLSM has been used to dissect mitosis and endomembrane dynamics in a variety of systems, including single cells in culture, *Caenorhabditis elegans*, zebrafish ([Chen et al., 2014](#); [Aguet et al., 2016](#)), and human cells ([Sen et al., 2021](#)), providing new insights into cell division and its regulatory processes. The plant research community is slowly embracing the benefits that light sheet microscopy and vertical imaging offer ([Vyplelová et al., 2017](#); [Glanc et al., 2018](#); [Ovecka et al., 2022](#)). In plants, apart from root hair studies ([Tichá et al., 2020](#); [Ovecka et al., 2022](#)), the potential of LLSM has not been explored to understand regulatory mechanisms in cytokinesis. A likely factor is the still limited availability of the instrumentation and the substantial effort needed in the post-processing and quantitative analysis.

Further, given that plant cell walls can introduce aberrations in super-resolution imaging methods ([Chatterjee et al., 2018](#); [Novák et al., 2018](#); [Ovecka et al., 2022](#)), performance of LLMS is understandably a potential concern when imaging plants. This study, however, illustrates the feasibility and power of LLSM for attaining hitherto unobtainable detailed spatiotemporal data in plants over time periods of 30–40 min on a whole organismal level and within a biologically relevant context. Volume imaging at ~25–30 s time intervals allowed a detailed view of cell plate transition stages with high enough quality to segment and quantify at a biologically relevant scale. High imaging frequency is particularly exciting and valuable when observing transient events that appear somewhat randomly and unpredictably, such as cell plate formation within the intact root tip. The ability to capture complete (temporally and spatially) sporadic events embedded within plant tissue with sufficient resolution and in statistically significant numbers represents a major step forward in methodology and an opportunity for experimentation.

**Cell plate volume behavior follows three distinct and consistent phases**

Our robust cytokinetic YFP–RABA2a vesicle volume analysis during the entire process of cytokinesis showed distinct behavioral patterns that allowed the identification of three phases based on volume growth patterns. We attempt to assign previously structurally described cell plate development stages (Samuels *et al.*, 1995) to the identified phases.

**(i)** Phase I is characterized by a positive volume accumulation rate that peaks at ~7–10 min before reaching an inflection point, representing the initial cell plate biogenesis stage. Our analysis showed a relative diameter increase of 50–60% of the parental cell width during phase I. The vesicle fusion, tubular vesicular network (FVS, TVN), and some tubular network (TN) transitions (Samuels *et al.*, 1995) are probably included in this phase that corresponds to the delivery and fusion of cytokinetic vesicles at the cell plate edge and membrane network formation at the core of the cell plate disk.

**(ii)** Phase II, transitioning through an easily identifiable inflection point, is characterized by a negative volume growth rate with rapid loss reaching a minimum within ~15 min. We reason that during this phase, representing a ring phragmoplast stage, the center of the cell plate has transitioned to a fenestrated sheet (PFS) (Samuels *et al.*, 1995), requiring massive membrane recycling (Seguí-Simarro *et al.*, 2004). The observed recycling is consistent with earlier predictions estimating a 75% membrane reduction during cell plate maturation in endosperm cellularization (Otegui *et al.*, 2001). The cell plate during this phase reaches almost 70–80% of the final cell plate diameter.

**(iii)** Phase III, marked by the remaining period of cell plate development, is characterized by a minimal but stable positive volume growth rate. The overall return to net positive growth probably represents PFS structures (Samuels *et al.*, 1995; Seguí-Simarro *et al.*, 2004) associated with a discontinuous phragmoplast with minimal cytokinetic vesicle delivery,

leading to the final expansion and maturation of the cell plate until it fuses with the parental cell wall.

Because cell plate development encompasses several stages that occur simultaneously in each phase, recycling of excess membrane material may already begin during phase I; however, based on the vast vesicle delivery, the net rate is positive, contrasting with phase II, dominated by membrane recycling and a net negative volume growth rate. Phase III requires minimal membrane addition but stabilization and maturation of the cell plate, thus reverting to a net positive volume growth rate. The minimal net positive increase could be due to the reorganization of the cell plate membrane at the edge, as it needs to combine with the parental plasma membrane carrying the targeted and necessary machinery and cargo for joining with the parental cell wall.

Earlier models based on cell plate diameter suggest a gradual decrease in cell plate expansion rates (Higaki *et al.*, 2008) or a biphasic pattern (van Oostende-Triplet *et al.*, 2017) as the cell plate expands towards the parental wall. The model of van Oostende-Triplet *et al.* identifies a primary centrifugal growth (PCG) phase in BY-2 cells with an average diameter growth rate of  $1.44 \pm 0.44 \mu\text{m min}^{-1}$  and a secondary centrifugal growth (SCG) phase with a rate of  $0.35 \pm 0.13 \mu\text{m min}^{-1}$ , along with similar estimates in Arabidopsis (PCG  $\sim 0.87 \pm 0.26 \mu\text{m min}^{-1}$ , SCG  $\sim 0.25 \pm 0.09 \mu\text{m min}^{-1}$ ) (van Oostende-Triplet *et al.*, 2017). Analysis of our diameter expansion data, as guided by the YPF-RABA2a marker, showed an initial high growth rate of  $4.09 \pm 0.26 \mu\text{m min}^{-1}$  followed by a gradual decrease, which can be grouped in two bins that average  $1.1 \pm 0.05 \mu\text{m min}^{-1}$  and  $0.59 \pm 0.04 \mu\text{m min}^{-1}$  ( $n=18$ ) (Supplementary Fig. S5A), consistent with the earlier calculated rates described above (van Oostende-Triplet *et al.*, 2017). The extremely rapid expansion rate within the first 2.5 min of cell plate development

([Supplementary Fig. S5B, C](#)) aligns with cell plate biogenesis during vesicle delivery. It corresponds to the initial plate assembly (IPA) stage postulated by [van Oostende-Triplet \*et al.\* \(2017\)](#), for which expansion rates were not detectable. Taken together, this is a clear example of LLSM enabling the recording of cell plate biogenesis and the calculation of the corresponding rates, as it can capture early events prior to well-defined cell plate appearance in the field of view.

It is apparent in comparing different models that understanding cell plate development based on volumetric growth provides more straightforward cut-off points for phase transitions and complements cell plate diameter analysis. Proof of this concept is demonstrated in this study with the volume accumulation rates of the easily trackable cytokinesis marker. This analysis allows the prediction of quantitative behaviors during cell plate development and their interrogation to understand the contribution of different components. For example, models of phragmoplast expansion ([Higaki \*et al.\*, 2008](#)) can be tested, similarly to what was done here, to evaluate the contributions of the array that helps build the cell plate. The easily identifiable inflection points between phases mark critical points during the transition of the membrane network and cell plate expansion that requires the onset of specific contributing factors. We propose that during the transition from phase I to II, clathrin-mediated recycling is enhanced, and that polysaccharide deposition and assembly are dominant during the transition from phase II to III. Future studies can leverage the method and explore the proposed model to interrogate different markers such as clathrin, dynamin, and SNARE proteins involved in different aspects of cell plate development. It is plausible that the volumetric-based transitions will vary based on the marker used, for example SNARE versus clathrin ([Bednarek and Backues, 2010](#); [El Kasmi \*et\*](#)

*al.*, 2013; *Jürgens et al.*, 2015; *Dahhan and Bednarek*, 2022; *Park et al.*, 2023), which will help to build more comprehensive models.

## Callose is necessary during cell plate expansion for the transition beyond phase I

An example of how the current analysis and proposed model can provide insights into cell plate development is the contribution of callose, a polysaccharide transiently deposited during cell plate development. The specific stage at which callose plays a critical role has long been debated, with views arguing on either the transition from a TN to PFS or the cell plate insertion in the parental cell wall (*Samuels et al.*, 1995; *Thiele et al.*, 2009). Different methods to dissect its role, direct detection of callose with antibodies against the polysaccharide with electron microscopy (*Samuels et al.*, 1995) versus confocal 2D staining and mutant characterization (*Thiele et al.*, 2009), might contribute to this difference. The developed approach and the derived model here, in combination with pharmacological treatment, allow the detailed dissection of each stage, providing insights into the biological role of the polymer. Upon inhibition of callose with ES7, phase I is prolonged. An irregular pattern is seen following the initial phase, with no distinguishable phase II and III. This clearly illustrates that polysaccharide is essential during the transition beyond phase I.

A modeling approach was previously implemented to understand better the cell plate stage transition from a vesicular network to a fenestrated sheet and mature cell plate. The model predicts that the onset of a 2D spreading/stabilizing force, coupled with a concurrent loss of spontaneous curvature, is necessary for cell plate expansion (*Jawaid et al.*, 2022). Biophysical modeling highlights the need for a spreading force during the transition of the membrane network (TN) to a fenestrated sheet (PSF) (*Jawaid et al.*, 2022), which overlaps with the phase

transition (phase I to phase II) in our study. Directly detecting callose via fluorescent staining corresponding to these phases validates the prediction of the biophysical model. Callose, due to its amorphous structure, can lead to alterations in the physical and mechanical properties at the deposition site (Piršelová and Matušíková, 2013; Zhang *et al.*, 2021; Ušák *et al.*, 2023). The polysaccharide has the ability to enhance rigidity while maintaining flexibility and to reduce permeability to various compounds across a range of functions (Yim and Bradford, 1998; Parre and Geitmann, 2005; Vatén *et al.*, 2011). Additionally, callose's unique composition compared with other polysaccharides enables controlled degradation when no longer necessary, underlining its significance as a compound that can operate both spatially and temporally (Samuels *et al.*, 1995; Ušák *et al.*, 2023).

## Lattice light sheet microscopy along with 4D volume-based phase transition analysis is robust for cytokinesis dissection

The quantitative prediction of phase transitions, with unbiased characterization, provides an advantage over descriptive interpretations of fragmented datasets. Further, it establishes a roadmap into which other components can be incorporated. Structural cell wall proteins, such as extensins (Cannon *et al.*, 2008), wall matrix polysaccharides (Moore and Staehelin, 1988), cellulose (Miart *et al.*, 2014), and other forms of linear glucose can be interrogated with the same analysis methodology. Cellulose, the load-bearing cell wall polysaccharide, is a prime candidate for this analytical approach, especially in combination with conditional genetic mutations or pharmacological inhibition of cellulose synthases (Chen *et al.*, 2018). Interestingly, a 5 d inhibition of cellulose synthase activity with isoxaben causes reduction of cell elongation but does not have a prominent effect on cell plate biogenesis or expansion (Jawaid *et al.*, 2022), which suggests a role for cellulose in the formed cell wall instead of cell plate expansion. A

quantitative analysis during cell plate phase transition can help dissect the contribution of cellulose or other linear  $\beta$ -1,4-glucans. Beyond cellulose synthase, cellulose synthase-like proteins (CSLs), such as CSLD3, produce linear glucan polymers (Yang *et al.*, 2020). CSLD5, a cytokinesis-specific protein (Gu *et al.*, 2016), produces a  $\beta$ -1,4-glucan polysaccharide, similar to that produced by CSLD3 (Yang *et al.*, 2020). Adaptation of our quantitative analysis in conditional mutations of these proteins might pin down the specific contributions to cell plate development and indicate associations with other polysaccharides or cell wall components. Such a study can address the potential interaction of CSLD5 products with callose in creating a scaffold (Abou-Saleh *et al.*, 2018) for the establishment of the spreading force necessary for cell plate maturation.

While our study was centered on callose, the described model of cytokinetic vesicle behavior can be interrogated for an array of contributions to cell plate development (Smertenko, 2018; Cheng and Bezanilla, 2021; Dahhan and Bednarek, 2022; Gu and Rasmussen, 2022; Sinclair *et al.*, 2022; Lebecq *et al.*, 2023; Nan *et al.*, 2023; Park *et al.*, 2023), for example pharmacological inhibition of secretory traffic, cytoskeleton dynamics at the phragmoplast, and its interaction with vesicle delivery. In a recent study, the application of the Small Molecular Inhibitor Formin Homology 2 (SMIFH2) revealed the function of formins in several aspects of cytokinesis, including cell plate membrane organization, microtubule polymerization, and nucleating F-actin at the cell plate (Zhang *et al.*, 2021). The application of LLSM and the methodology developed here can aid in further dissecting the role of formins in cell plate development and phragmoplast organization. The pharmacological inhibition of actin or microtubule polymerization has been extensively used to study phragmoplast expansion and was recently employed for cell plate development studies using a radial expansion model (van

Oostende-Triplet *et al.*, 2017). Extending these studies to a 4D analysis based on rates of volume accumulation can provide extra depth, allowing for direct correlations of the contributions of cytoskeleton dynamics, secretory traffic, and protein synthesis in cell plate biogenesis and expansion.

## Conclusion

The development of a comprehensive 4D image acquisition and processing pipeline using LLSM represents an important step forward in both utilizing cutting-edge microscopy tools and addressing long-standing questions about spatiotemporal dynamics in cytokinesis. Despite the advantages, today LLSM-based imaging of plant seedlings is still limited. The current approach requires genetically encoded fluorophores with high photostability, thus not all markers are ideally suited. Multiplex imaging of different fluorophores may be impacted by crosstalk and requires multichannel camera systems. Another major challenge is the substantial data size generated during the image analysis and archiving. For instance, the current study produced ~40 TB of data, which poses significant demands on Information technology (IT) infrastructures for processing and storage. However, it is important to highlight a distinctive feature of this experimental design—the ability to conduct prolonged imaging over a large field of view.

The developed 4D imaging pipeline using LLSM, along with the tools for processing the acquired images, are documented and are available through plugins in ImageJ and MATLAB. The segmentation pipeline employed in Imaris is also documented for easy adaptation ([Fig. 2](#)). The cell plate development model can be applied using different modalities beyond LLSM to dissect plate cytokinesis. We hope that this study inspires the community to adopt the methodology of exploring LLSM in plants, take advantage of the image analysis pipeline tools

developed, and refine the model of cell plate development and its factors contributing to each phase.

More importantly, our study was able to showcase first-of-its-kind data of the complete process of cell plate development with minimal photobleaching, higher axial resolution, and faster imaging rates compared with traditional laser scanning confocal microscopy. The study revealed three distinct developmental phases of cell plate growth, from rapid vesicle accumulation to subsequent volume reduction and cell plate expansion, and the critical role of callose in the phase transition. The use of the chemical inhibitor ES7 in combination with LLSM provided quantitative insights into the timing and role of callose in stabilizing the cell plate during expansion and maturation. Inhibition of callose deposition led to impaired cell plate expansion, resulting in fragmented and aberrant membrane accumulation patterns. The findings of this study have significant implications for understanding the spatiotemporal dynamics of cell plate development and the role of callose along with other components in this process.

We see this pioneering effort in quantitative dissection of cell plate development helping to understand the array of factors controlling plant cytokinesis. Taken together, this research contributes to the broader understanding of plant cell biology and suggests new avenues for further investigations into the molecular mechanisms underlying cell plate assembly and expansion.

## Supplementary data

The following supplementary data are available at *JXB* online.

Fig. S1. Quantitative YFP–RABA2a dynamics and FM4-64-stained membrane accumulation at the cell plate

Fig. S2. Representative morphologies of ES7-induced arrested development of cell plate growth.

Fig. S3. Maximum accumulation of volume and surface area across treatments.

Fig. S4. Expansion rates of individual cell plates based on their radial growth across treatments.

Fig. S5. Binning of cell plate's radial growth rate by time, based on growth rate values.

Fig. S6. Overlay of polynomial fit to YFP-RABA2a segmented volume over time.

Table S1. Quantitative data used for cell plate analysis.

Table S2. Quantitative data used for ES7 pulse-treated cell plate analysis.

Table S3. Quantitative data used to generate [Supplementary Fig. S1](#).

Video S1. 4D rendering of YFP-RABA2a cell plate accumulation with surface segmentation.

Images were acquired with LLSM. Scale bar=20  $\mu\text{m}$ .

Video S2. 4D rendering of YFP-RABA2a cell plate accumulation with surface segmentation

under 2 h treatment with 50  $\mu\text{M}$  ES7 displaying relatively no expansion. Images were acquired

with LLSM. Scale bar=20  $\mu\text{m}$ .

Video S3. 4D rendering of YFP-RABA2a cell plate accumulation with surface segmentation

under 2 h treatment with 50  $\mu\text{M}$  ES7 displaying minimal relative expansion. Images were

acquired with LLSM. Scale bar=20  $\mu\text{m}$ .

## **Acknowledgements**

This manuscript is dedicated in memory of Professor Andrew Staehelin whose work and contribution to the field inspired us in this study. We want to thank all the members of AIC and the Drakakaki lab for their input, and Dr Destiny J. Davis for her critical reading of the manuscript.

## **Author contributions**

TW and GD: conceptualization and supervision; RMS, MW, MZJ, TW, and GD: methodology;

RMS, TW, MZJ, DC, and JH: formal analysis; GD, RMS, TW, MW, and TL: investigation;

KMD, TW, and GD: resources; RMS, TW, and GD: data curation; RMS, TW, and GD: writing—original draft; RMS, TW, MW, MZJ, DC, and GD: writing—review & editing; RMS, TW, and MZI: validation; RMS, JA, KMD, JH, TW, and GD: visualization; MZJ, BR, EW, KMD, and JH: software; GD: project administration; DC and GD: funding acquisition.

## Conflict of interest

The authors declare no competing interests.

## Funding

This work was supported by NSF Grant MCB 1818219 to GD and DC. GD was additionally partially supported by the Department of Agriculture Hatch (CA-D-PLS-2132-H). RS acknowledges the Department of Plant Sciences, UC Davis for the award of a GSR scholarship funded by endowments, particularly the James Monroe McDonald Endowment, administered by UCANR and the DEB fellowship. We acknowledge the NIH award 1S10OD026702-01 that was used to purchase the Zeiss 980 laser scanning confocal microscope.

## Data availability

Representative datasets used in the study are available on Zenodo at [10.5281/zenodo.10515765](https://zenodo.org/doi/10.5281/zenodo.10515765)

## References

- ☑ **Abou-Saleh RH, Hernandez-Gomez MC, Amsbury S, *et al.*** 2018. Interactions between callose and cellulose revealed through the analysis of biopolymer mixtures. *Nature Communications* **9**, 4538.
- ☑ **Aguet F, Upadhyayula S, Gaudin R, *et al.*** 2016. Membrane dynamics of dividing cells imaged by lattice light-sheet microscopy. *Molecular Biology of the Cell* **27**, 3418–3435.

- ☑ **Bednarek SY, Backues SK.** 2010. Plant dynamin-related protein families DRP1 and DRP2 in plant development. *Biochemical Society Transactions* **38**, 797–806.
- ☒ **Berson T, von Wangenheim D, Takáč T, Šamajová O, Rosero A, Ovečka M, Komis G, Stelzer EHK, Šamaj J.** 2014. Trans-Golgi network localized small GTPase RabA1d is involved in cell plate formation and oscillatory root hair growth. *BMC Plant Biology* **14**, 252.
- ☑ **Cannon MC, Terneus K, Hall Q, Tan L, Wang Y, Wegenhart BL, Chen L, Lampert DTA, Chen Y, Kieliszewski MJ.** 2008. Self-assembly of the plant cell wall requires an extensin scaffold. *Proceedings of the National Academy of Sciences, USA* **105**, 2226–2231.
- ☑ **Chatterjee K, Pratiwi FW, Wu FCM, Chen P, Chen BC.** 2018. Recent progress in light sheet microscopy for biological applications. *Applied Spectroscopy* **72**, 1137–1169.
- ☑ **Chen BC, Legant WR, Wang K, et al.** 2014. Lattice light-sheet microscopy: imaging molecules to embryos at high spatiotemporal resolution. *Science* **346**, 1257998.
- ☑ **Chen HW, Persson S, Grebe M, McFarlane HE.** 2018. Cellulose synthesis during cell plate assembly. *Physiologia Plantarum* **164**, 17–26.
- ☒ **Chen XY, Liu L, Lee EK, Han X, Rim Y, Chu H, Kim SW, Sack F, Kim JY.** 2009. The *Arabidopsis* callose synthase gene *GSL8* is required for cytokinesis and cell patterning. *Plant Physiology* **150**, 105–113.
- ☑ **Cheng X, Bezanilla M.** 2021. SABRE populates ER domains essential for cell plate maturation and cell expansion influencing cell and tissue patterning. *eLife* **10**, e65166.

- ☑ **Chow CM, Neto H, Foucart C, Moore I.** 2008. Rab-A2 and Rab-A3 GTPases define a trans-Golgi endosomal membrane domain in *Arabidopsis* that contributes substantially to the cell plate. *The Plant Cell* **20**, 101–123.
- ☑ **Dahhan DA, Bednarek SY.** 2022. Advances in structural, spatial, and temporal mechanics of plant endocytosis. *FEBS Letters* **596**, 2269–2287.
- ☑ **Desprez T, Juraniec M, Crowell EF, Jouy H, Pochylova Z, Parcy F, Höfte H, Gonneau M, Vernhettes S.** 2007. Organization of cellulose synthase complexes involved in primary cell wall synthesis in *Arabidopsis thaliana*. *Proceedings of the National Academy of Sciences, USA* **104**, 15572–15577.
- ☑ **Drakakaki G.** 2015. Polysaccharide deposition during cytokinesis: challenges and future perspectives. *Plant Science* **236**, 177–184.
- ☑ **Drakakaki G, Robert S, Szatmari AM, et al.** 2011. Clusters of bioactive compounds target dynamic endomembrane networks in vivo. *Proceedings of the National Academy of Sciences, USA* **108**, 17850–17855.
- ☑ **El Kasmi F, Krause C, Hiller U, Stierhof YD, Mayer U, Conner L, Kong L, Reichardt I, Sanderfoot AA, Jürgens G.** 2013. SNARE complexes of different composition jointly mediate membrane fusion in *Arabidopsis* cytokinesis. *Molecular Biology of the Cell* **24**, 1593–1601.
- ☑ **Evans NA, Hoyne PA.** 1982. A fluorochrome from aniline blue: structure, synthesis and fluorescence properties. *Australian Journal of Chemistry* **35**, 2571–2575.

- ☑ **Geitmann A.** 2023. Seeing clearly—plant anatomy through Katherine Esau’s microscopy lens. *Journal of Microscopy* **291**, 92–104.
- ☑ **Geldner N, Déneraud-Tendon V, Hyman DL, Mayer U, Stierhof YD, Chory J.** 2009. Rapid, combinatorial analysis of membrane compartments in intact plants with a multicolor marker set. *The Plant Journal* **59**, 169–178.
- ☑ **Glanc M, Fendrych M, Friml J.** 2018. Mechanistic framework for cell-intrinsic re-establishment of PIN2 polarity after cell division. *Nature Plants* **4**, 1082–1088.
- ☑ **Gu F, Bringmann M, Combs JR, Yang J, Bergmann DC, Nielsen E.** 2016. *Arabidopsis* CSLD5 functions in cell plate formation in a cell cycle-dependent manner. *The Plant Cell* **28**, 1722–1737.
- ☑ **Gu Y, Rasmussen CG.** 2022. Cell biology of primary cell wall synthesis in plants. *The Plant Cell* **34**, 103–128.
- ☑ **Higaki T, Kutsuna N, Sano T, Hasezawa S.** 2008. Quantitative analysis of changes in actin microfilament contribution to cell plate development in plant cytokinesis. *BMC Plant Biology* **8**, 80.
- ☑ **Jawaid MZ, Sinclair R, Bulone V, Cox DL, Drakakaki G.** 2022. A biophysical model for plant cell plate maturation based on the contribution of a spreading force. *Plant Physiology* **188**, 795–806.
- ☑ **Jürgens G.** 2005. Cytokinesis in higher plants. *Annual Review of Plant Biology* **56**, 281–299.

☒ **Jürgens G, Park M, Richter S, Touihri S, Krause C, Kasmi FE, Mayer U.** 2015. Plant cytokinesis: a tale of membrane traffic and fusion. *Biochemical Society Transactions* **43**, 73–78.

☒ **Lebecq A, Goldy C, Fangain A, Gascon E, Belcram K, Pastuglia M, Bouchez D, Caillaud MC.** 2023. The phosphoinositide signature guides the final step of plant cytokinesis. *Science Advances* **9**, eadf7532.

Lee YR, Liu B. The rise and fall of the phragmoplast microtubule array. 2013 *Curr Opin Plant Biol.* 2013 Dec;16(6):757-63. doi: 10.1016/j.pbi.2013.10.008. Epub 2013 Oct 27.

Lukowitz W, Mayer U, Jürgens G. Cytokinesis in the Arabidopsis embryo involves the syntaxin-related KNOLLE gene product. *Cell.* 1996 Jan 12;84(1):61-71. doi: 10.1016/s0092-8674(00)80993-9. PMID: 8548827.

☒ **Mayers JR, Hu T, Wang C, Cárdenas JJ, Tan Y, Pan J, Bednarek SY.** 2017. SCD1 and SCD2 form a complex that functions with the exocyst and RabE1 in exocytosis and cytokinesis. *The Plant Cell* **29**, 2610–2625.

☒ **McDonald KL.** 2014. Out with the old and in with the new: rapid specimen preparation procedures for electron microscopy of sectioned biological material. *Protoplasma* **251**, 429–448.

☒ **McDonald KL, Webb RI.** 2011. Freeze substitution in 3 hours or less. *Journal of Microscopy* **243**, 227–233.

- ☑ **Miart F, Desprez T, Biot E, Morin H, Belcram K, Höfte H, Gonneau M, Vernhettes S.** 2014. Spatio-temporal analysis of cellulose synthesis during cell plate formation in *Arabidopsis*. *The Plant Journal* **77**, 71–84.
- ☑ **Moore PJ, Staehelin LA.** 1988. Immunogold localization of the cell-wall-matrix polysaccharides rhamnogalacturonan I and xyloglucan during cell expansion and cytokinesis in *Trifolium pratense* L.; implication for secretory pathways. *Planta* **174**, 433–445.
- ☑ **Nan Q, Liang H, Mendoza J, Liu L, Fulzele A, Wright A, Bennett EJ, Rasmussen CG, Facette MR.** 2023. The OPAQUE1/DISCORDIA2 myosin XI is required for phragmoplast guidance during asymmetric cell division in maize. *The Plant Cell* **35**, 2678–2693.
- ☑ **Novák D, Vadovič P, Ovečka M, Šamajová O, Komis G, Colcombet J, Šamaj J.** 2018. Gene expression pattern and protein localization of *Arabidopsis* phospholipase D alpha 1 revealed by advanced light-sheet and super-resolution microscopy. *Frontiers in Plant Science* **9**, 371.
- ☑ **Otegui MS.** 2020. Electron tomography and immunogold labeling as tools to analyze de novo assembly of plant cell walls. *Methods in Molecular Biology* **2149**, 365–382.
- ☑ **Otegui MS, Mastrorarde DN, Kang BH, Bednarek SY, Staehelin LA.** 2001. Three-dimensional analysis of syncytial-type cell plates during endosperm cellularization visualized by high resolution electron tomography. *The Plant Cell* **13**, 2033–2051.

- ☑ **Ovecka M, Sojka J, Tichá M, Komis G, Basheer J, Marchetti C, Samajová O, Kubenová L, Samaj J.** 2022. Imaging plant cells and organs with light-sheet and super-resolution microscopy. *Plant Physiology* **188**, 683–702.
- ☑ **Park E, Díaz-Moreno SM, Davis DJ, Wilkop TE, Bulone V, Drakakaki G.** 2014. Endosidin 7 specifically arrests late cytokinesis and inhibits callose biosynthesis, revealing distinct trafficking events during cell plate maturation. *Plant Physiology* **165**, 1019–1034.
- ☑ **Park M, Mayer U, Richter S, Jürgens G.** 2023. NSF/ $\alpha$ SNAP2-mediated cis-SNARE complex disassembly precedes vesicle fusion in *Arabidopsis* cytokinesis. *Nature Plants* **9**, 889–897.
- ☑ **Parre E, Geitmann A.** 2005. More than a leak sealant. The mechanical properties of callose in pollen tubes. *Plant Physiology* **137**, 274–286.
- ☑ **Piršelová B, Matušíková I.** 2013. Callose: the plant cell wall polysaccharide with multiple biological functions. *Acta Physiologiae Plantarum* **35**, 635–644.
- ☑ **Qi X, Kaneda M, Chen J, Geitmann A, Zheng H.** 2011. A specific role for *Arabidopsis* TRAPP<sub>II</sub> in post-Golgi trafficking that is crucial for cytokinesis and cell polarity. *The Plant Journal* **68**, 234–248.
- ☑ **Qi X, Zheng H.** 2013. Rab-A1c GTPase defines a population of the trans-Golgi network that is sensitive to endosidin1 during cytokinesis in *Arabidopsis*. *Molecular Plant* **6**, 847–859.

- ☑ **Samuels AL, Giddings TH, Staehelin LA.** 1995. Cytokinesis in tobacco BY-2 and root tip cells: a new model of cell plate formation in higher plants. *Journal of Cell Biology* **130**, 1345–1357.
- ☑ **Seguí-Simarro JM, Austin JR, White EA, Staehelin LA.** 2004. Electron tomographic analysis of somatic cell plate formation in meristematic cells of *Arabidopsis* preserved by high-pressure freezing. *The Plant Cell* **16**, 836–856.
- ☑ **Sen O, Harrison JU, Burroughs NJ, McAinsh AD.** 2021. Kinetochore life histories reveal an Aurora-B-dependent error correction mechanism in anaphase. *Developmental Cell* **56**, 3405.
- ☑ **Shi Y, Luo C, Xiang Y, Qian D.** 2023. Rab GTPases, tethers, and SNAREs work together to regulate *Arabidopsis* cell plate formation. *Frontiers in Plant Science* **14**, 1120841.
- ☑ **Sinclair R, Hsu G, Davis D, Chang M, Rosquete M, Iwasa JH, Drakakaki G.** 2022. Plant cytokinesis and the construction of new cell wall. *FEBS Letters* **596**, 2243–2255.
- ☑ **Smertenko A.** 2018. Phragmoplast expansion: the four-stroke engine that powers plant cytokinesis. *Current Opinion in Plant Biology* **46**, 130–137.
- ☑ **Smertenko A, Assaad F, Baluška F, et al.** 2017. Plant cytokinesis: terminology for structures and processes. *Trends in Cell Biology* **27**, 885–894.
- ☑ **Staehelin LA, Hepler PK.** 1996. Cytokinesis in higher plants. *Cell* **84**, 821–824.
- ☑ **Thiele K, Wanner G, Kindzierski V, Jürgens G, Mayer U, Pahl F, Assaad FF.** 2009. The timely deposition of callose is essential for cytokinesis in *Arabidopsis*. *The Plant Journal* **58**, 13–26.

- ☑ **Tichá M, Richter H, Ovečka M, Maghelli N, Hrbáčková M, Dvořák P, Šamaj J, Šamajová O.** 2020. Advanced microscopy reveals complex developmental and subcellular localization patterns of ANNEXIN 1 in *Arabidopsis*. *Frontiers in Plant Science* **11**, 1153.
- ☑ **Ueda K, Sakaguchi S, Kumagai F, Hasezawa S, Quader H, Kristen U.** 2003. Development and disintegration of phragmoplasts in living cultured cells of a GFP::*TUA6* transgenic *Arabidopsis thaliana* plant. *Protoplasma* **220**, 111–118.
- ☑ **Ušák D, Haluška S, Pleskot R.** 2023. Callose synthesis at the center point of plant development—an evolutionary insight. *Plant Physiology* **193**, 54–69.
- ☑ **van Oostende-Triplet C, Guillet D, Triplet T, Pandzic E, Wiseman PW, Geitmann A.** 2017. Vesicle dynamics during plant cell cytokinesis reveals distinct developmental phases. *Plant Physiology* **174**, 1544–1558.
- ☑ **Vatén A, Dettmer J, Wu S, et al.** 2011. Callose biosynthesis regulates symplastic trafficking during root development. *Developmental Cell* **21**, 1144–1155.
- ☑ **Vyplelová P, Ovečka M, Šamaj J.** 2017. Alfalfa root growth rate correlates with progression of microtubules during mitosis and cytokinesis as revealed by environmental light-sheet microscopy. *Frontiers in Plant Science* **8**, 1870.
- ☑ **Yang J, Bak G, Burgin T, Barnes WJ, Mayes HB, Peña MJ, Urbanowicz BR, Nielsen E.** 2020. Biochemical and genetic analysis identify CSLD3 as a beta-1,4-glucan synthase that functions during plant cell wall synthesis. *The Plant Cell* **32**, 1749–1767.

☑ **Yim KO, Bradford KJ.** 1998. Callose deposition is responsible for apoplastic semipermeability of the endosperm envelope of muskmelon seeds. *Plant Physiology* **118**, 83–90.

☑ **Zhang L, Smertenko T, Fahy D, et al.** 2021. Analysis of formin functions during cytokinesis using specific inhibitor SMIFH2. *Plant Physiology* **186**, 945–963.

Fig. 1. YFP–RABA2a dynamics at the cell plate. YFP–RABA2a (green) vesicle accumulation and FM4-64- (purple) stained plasma membrane show the transition from vesicle accumulation to mature membrane throughout cell plate development in untreated plants. The accumulation of YFP–RABA2a at the cell plate periphery during maturation with a concurrent increase in the membrane content in the center shows centrifugal growth and maturation. The arrow indicates RABA2a at the cell plate. Data were collected on a Leica SP8 microscope. Scale bar=4  $\mu\text{m}$ .  $\Delta t=1$  min.

Fig. 2. Schematic representation of the lattice light sheet data processing pipeline. Schematic representation of the processing workflow for collecting plant cytokinesis events under lattice light sheet microscopy (LLSM). The workflow is separated into four overarching steps: (A) image collection and data organization; (B) data alignment with drift correction and ROI selection; (C) concatenation of each time point to create a 4D stack and bleach correction follow-up processing; (D) image segmentation and quantification. Scale bar=20  $\mu\text{m}$ .

Fig. 3. Quantitative YFP–RABA2a dynamics at the cell plate. (A) Representative snapshots of a time series showing the transition of YFP–RABA2a (green) in segmented cell plates (purple) during their expansion and maturation. Scale bar=5  $\mu\text{m}$ . (B and C) Volumes of segmented cell plates and their growth rates. (D and E) Bounding surface areas of segmented cell plates and their rates of change. Each line indicates an individually segmented cell plate. Note the cell plate

shown in (A) is highlighted in bold in all graphs. Normalized volumes and bounding surfaces , respectively, of developing cell plates were fitted to a polynomial (B and D). Additionally, the polynomials (B and D) were used to derive the rates of change of the volume and bounding surface area (C and E).  $n=24$ .

Fig. 4. YFP–RABA2a cell plate dynamics under Endosidin 7 (ES7) treatment. YFP–RABA2a (green) vesicle accumulation and FM4-64- (purple) stained plasma membrane show cell plate development under ES7 treatment. Note the abnormal pattern and the fragmentation of the cell plate as it transitions during different time points. The pattern of YFP–RABA2a at the cell plate periphery does not expand radially, as seen in the untreated plants. Further, the cell plate cannot follow normal maturation into membranes detectable with FM4-64. Data were collected on a Leica SP8. Scale bar=10  $\mu\text{m}$ .  $\Delta t=1.5$  min.

Fig. 5. Quantitative YFP–RABA2a dynamics at the cell plate under ES7 treatment. (A) Representative snapshots of a time series showing the YFP–RABA2a segmented cell plate transition under ES7 treatment. The segmented cell plate is shown in purple from its first emergence, not able to expand radially and flatten. (B–E) Volumes and bounding surfaces of segmented cell plates and their rates of change. Each line indicates an individually segmented cell plate. Note that the cell plate shown in (A) is highlighted in bold in all graphs. Normalized volumes and bounding surface areas of developing cell plates were fitted to a polynomial distribution (B and D). First-degree derivatives present the corresponding rates of change of the polynomial fits for the volume and the bounding surface area, respectively (C and E). Scale bar=10  $\mu\text{m}$ .  $n=18$ .

Fig. 6. Statistical comparison of volume accumulation. YFP–RABA2a normalized volume growth rates, averaged within pre-defined groups and shown with 95% confidence intervals. (A–

C) Bins 1–3 represent the rates corresponding to normalized volumes increasing from 0 to 0.33  $\mu\text{m}^3$ , 0.33  $\mu\text{m}^3$  to 0.66  $\mu\text{m}^3$ , and 0.66  $\mu\text{m}^3$  to 1  $\mu\text{m}^3$ , respectively. All bins correspond to the first derivative rates of volume growth. \*Indicates  $P < 0.005$ . (D and E) Bins 4 and 5 represent the rates corresponding to volumes decreasing from 1  $\mu\text{m}^3$  to 0.66  $\mu\text{m}^3$  and from 0.66  $\mu\text{m}^3$  to 0.33  $\mu\text{m}^3$ , respectively; bin 6 data are not shown due to the bin spanning over the region in which the end of collection has limited control over noise. All bins correspond to the first derivative rates of volume growth. \*Indicates  $P < 0.005$ . (F) Schematic representation of volume growth grouped in bins for further processing as shown in (A–E).

Fig. 7. Cell plate diameter expansion under control and Endosidin 7 (ES7) treatment. Cell plate transition based on cell plate diameter expansion under control and ES7 treatment. (A) Control cell plates show a logarithmic expansion pattern, while ES7 treatment causes a more level pattern. Cell plate diameters are normalized to the expected cross-wall length. Note the intersection between control and ES7 treatment, indicating a critical point for cell plate maturation. (B) Volume-to-bounding surface area ratio in control and ES7-treated cell plates. The average of the ratio for cell plates analyzed in [Figs 3 and 5](#) are shown. Control  $n=23$ , ES7  $n=12$ . (C) Polynomial fit was applied to cell plate diameters that have been normalized to the corresponding cross-wall. (D) Results of pairwise  $t$ -test comparisons along moving averages shown in (C). Analysis shows that all except one time point are statistically different on cell plate expansion when comparing control with the absence of callose via ES7 treatment. Non-treated  $n=24$ , treated  $n=18$ .

Fig. 8. Progression of the cell plate in the presence of callose. (A–E) Cell plate development in the presence of callose. (A) An early-stage cell plate before the accumulation of callose. At this stage, only vesicle accumulation by YFP–RABA2a (green) makes up the cell plate. (B–D) Later

stage cell plates where callose accumulation stained with aniline blue fluorochrome (magenta) is detectable. Note the transient accumulation of callose in later stages, leading to the maturation of the cell plate during normal cytokinesis. (B) Initial callose deposition overlapping with YFP-RABA2a. (C) As the cell plate maturation continues and the YFP-RABA2a accumulation takes a 'doughnut shape' pattern, callose deposition appears in the middle of the cell plate with minimal overlap with YFP-RABA2a at the leading edge. (D) Callose is present throughout the cell plate, while minimal YFP-RABA2a is shown at the discontinuous ring (E). Mature cell plate predominately labeled by callose. Scale bar=5  $\mu$ m.

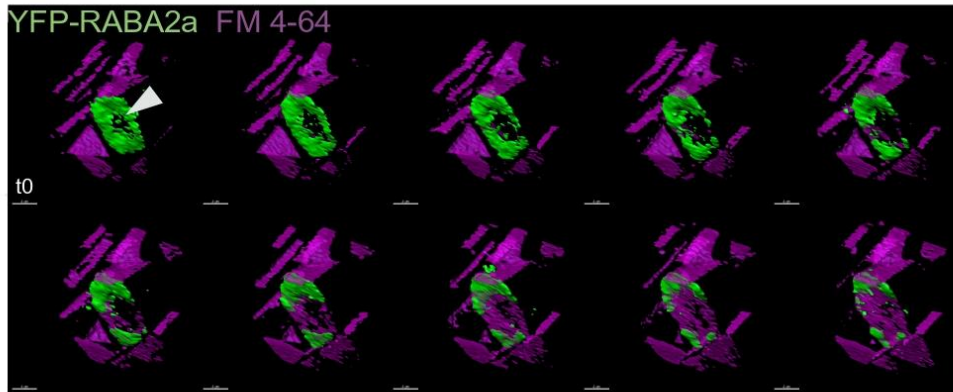


**Fig. 1.** YFP-RABA2a dynamics at the cell plate.

YFP-RABA2a (green) vesicle accumulation and FM 4-64 (purple) stained plasma membrane show the transition from vesicle accumulation to mature membrane throughout cell plate development in untreated plants. The accumulation of YFP-RABA2a at the cell plate periphery during the maturation with a concurrent increase in the membrane content in the center shows centrifugal growth and maturation. Arrow indicates RABA2a at the cell plate. Data was collected on a Leica SP8 microscope. Scale bar = 10  $\mu\text{m}$ .  $\Delta t = 1$  min.

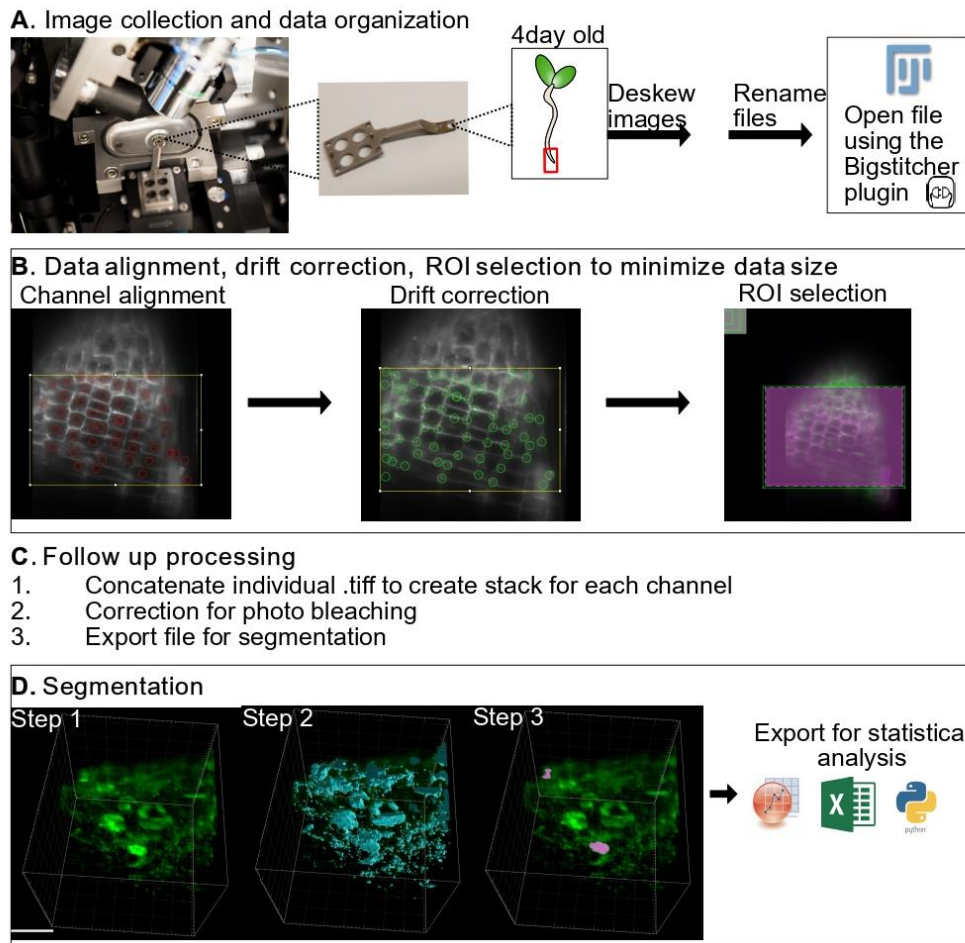


**Fig. 2.** Schematic representation of lattice light sheet data processing pipeline.

Schematic representation of the processing workflow for collecting plant cytokinesis events under lattice light sheet microscopy (LLSM). The workflow is separated into four overarching steps: **(A)** image collection and data organization, **(B)** data alignment with drift correction and ROI selection, **(C)** concatenation of each time point to create a Z stack and bleach correction follow-up processing, **(D)** image collection and data organization. Scale bar = 20  $\mu\text{m}$ .

**A** YFP-RABA2a cell plate dynamics

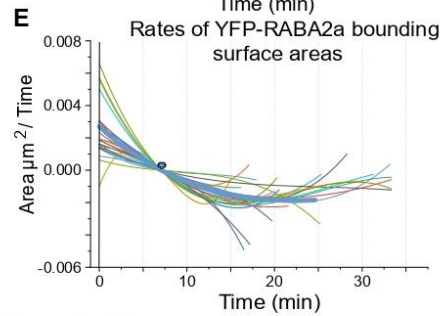
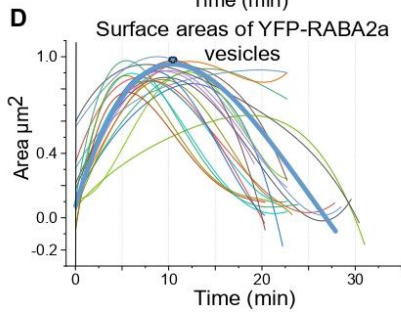
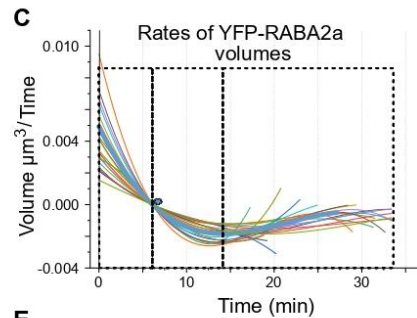
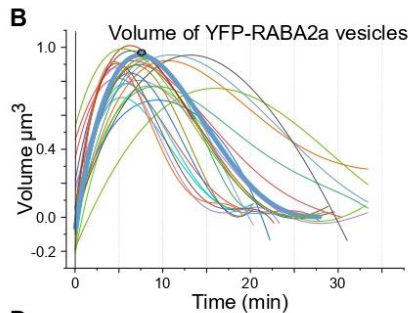
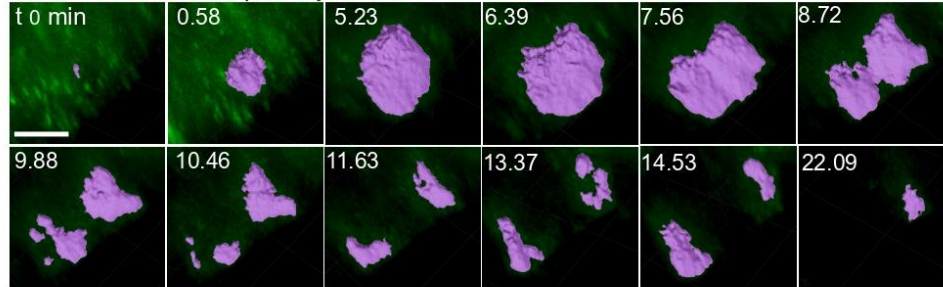


**Fig. 3.** Quantitative YFP-RABA2a dynamics at the cell plate

**A)** Representative snapshots of a time series showing the transition of YFP-RABA2a (green) in segmented cell plates (purple) during their expansion and maturation. Scale bar = 5  $\mu\text{m}$ . **B-C)** Volumes of segmented cell plates and their growth rates. **D-E)** Surface areas of segmented cell plates and their rates of change. Each line indicates an individually segmented cell plate. Note the cell plate shown in **(A)** is bolded in all graphs. Normalized volumes and areas, respectively, of developing cell plates were fitted to a polynomial **(B&D)**. Additionally, the polynomials **(B&D)** were used to derive the rates of change of the volume and bounding surface area **(C&E)**.  $n=24$

YFP-RABA2a cell plate dynamics under ES7

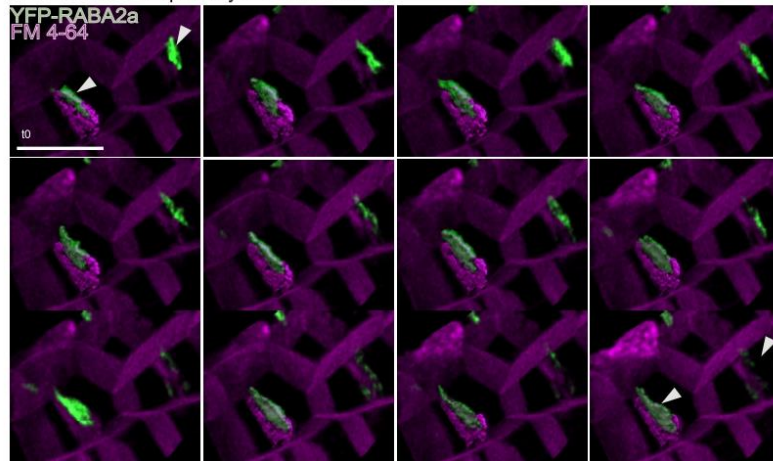


**Fig. 4.** YFP-RABA2a cell plate dynamics under Endosidin 7 treatment

YFP-RABA2a (green) vesicle accumulation and FM4-64 (purple) stained plasma membrane show cell plate development under Endosidin 7 (ES7) treatment. Note the abnormal pattern and the fragmentation of the cell plate as it transitions during different time points. The pattern of YFP-RABA2a at the cell plate periphery does not expand radially, as seen in the untreated plants. Further, the cell plate cannot follow normal maturation into membranes detectable with FM4-64. Data was collected on a Leica SP8. Scale bar = 10  $\mu\text{m}$ .  $\Delta t = 1.5$  min.

**A** YFP-RABA2a cell plate dynamics under ES7

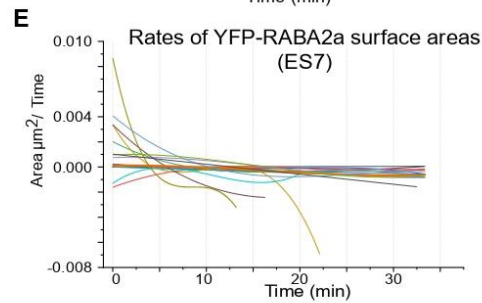
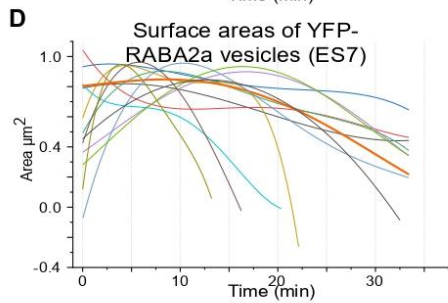
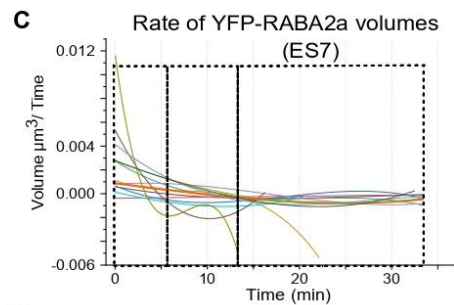
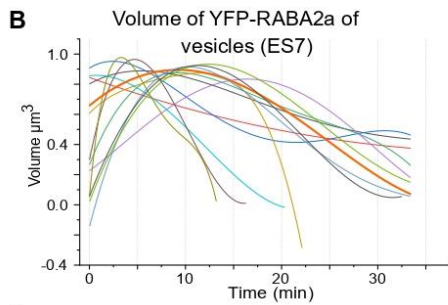
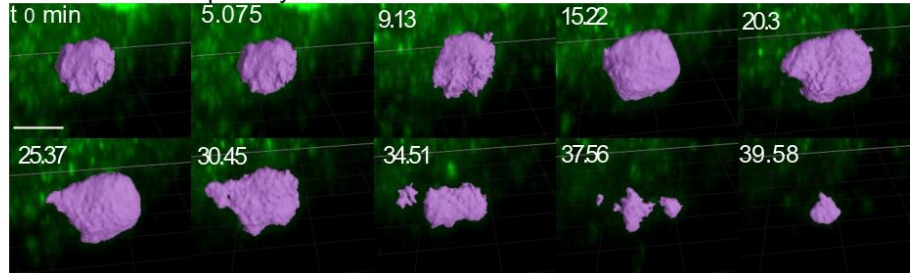


**Fig 5.** Quantitative YFP-RABA2a dynamics at the cell plate under ES7 treatment.

**A).** Representative snapshots of a time series showing the YFP- RABA2a segmented cell plate transition under ES7 treatment. The segmented cell plate is shown in purple from its first emergence, not able to expand radially and flatten.

**(B-E)** Volumes and bounding surfaces of segmented cell plates and their rates of change. Each line indicates an individually segmented cell plate. Note that the cell plate shown in **(A)** is bold in all graphs. Normalized volumes and bounding surface areas of developing cell plates were fitted to a polynomial distribution **(B&D)**. First-degree derivatives present the corresponding rates of change of the polynomial fits for the volume and the bounding surface area, respectively **(C&E)**. Scale bar = 10  $\mu\text{m}$ . n=18

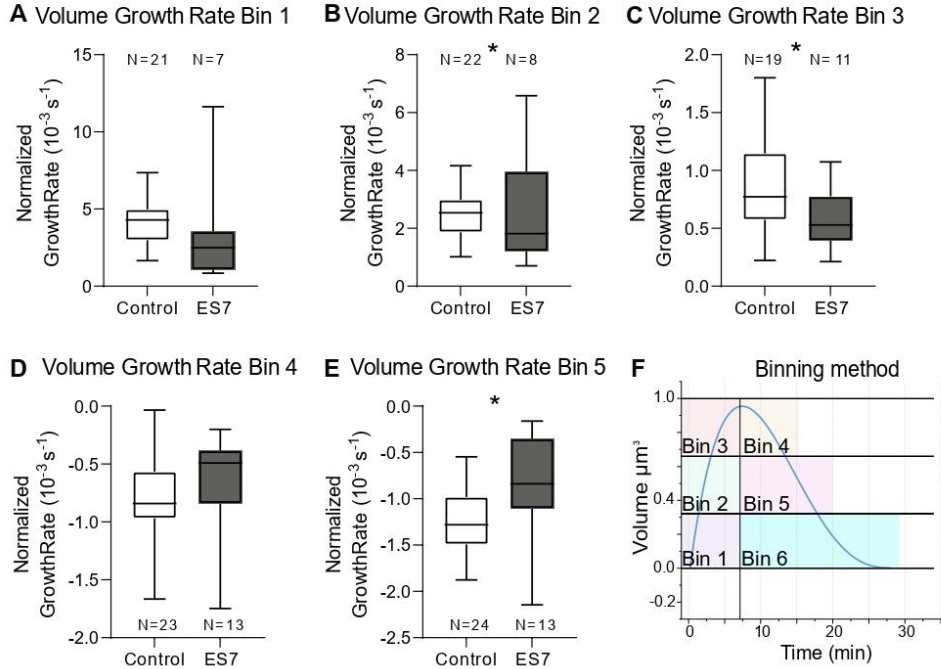


**Fig. 6.** Statistical comparison of volume accumulation.

YFP-RABA2a normalized volume growth rates, averaged within predefined groups and shown with 95% confidence intervals.

**(A-C)** Bins 1-3 represent the rates corresponding to normalized volumes increasing from  $0-0.33 \mu\text{m}^3$ ,  $0.33-0.66 \mu\text{m}^3$ , and  $0.66-1 \mu\text{m}^3$ , respectively. All bins correspond to the first derivative rates of volume growth. \* Indicates  $P < 0.005$ .

**(D-E)** Bins 4,5 represent the rates corresponding to volumes decreasing from  $1-0.66 \mu\text{m}^3$  and  $0.66-0.33 \mu\text{m}^3$ , respectively; bin 6 data are not shown due to the bin spanning over the region in which the end of collection has limited control over noise. All bins correspond to the first derivative rates of volume growth. \* Indicates  $P < 0.005$ .

**F)** Schematic representation of volume growth grouped in bins for further processing as shown in **A-E**.

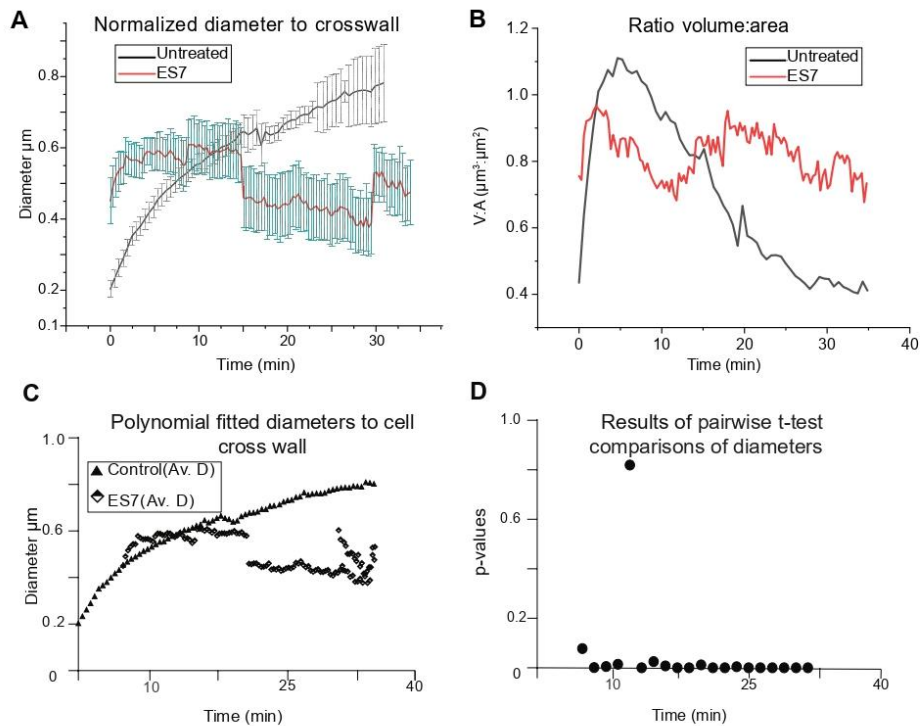


**Fig. 7.** Cell plate diameter expansion under control and Endosidin 7 treatment.

Cell plate transition based on cell plate diameter expansion under control and ES7 treatment.

**A)** Control cell plates show a logarithmic expansion pattern, while ES7 treatment causes a more level pattern. Cell plate diameters are normalized to the expected cross-wall length. Note the intersection between control and ES7 treatment, indicating a critical point for cell plate maturation.

**B)** Volume-to- bounding surface area ratio in control and ES7 treated cell plates. The average of the ratio for cell plates analyzed in **Figs. 3** and **5** are shown. Control n=23. ES7 n=12.

**C)** Polynomial fit was applied to cell plate diameters that have been normalized to the corresponding cross wall.

**D)** Results of pairwise t-test comparisons along moving averages shown in **C**). Analysis shows all but one time points are statistically different on cell plate expansion when comparing control with the absence of callose via ES7 treatment. Non treated n=24. Treated n=18.

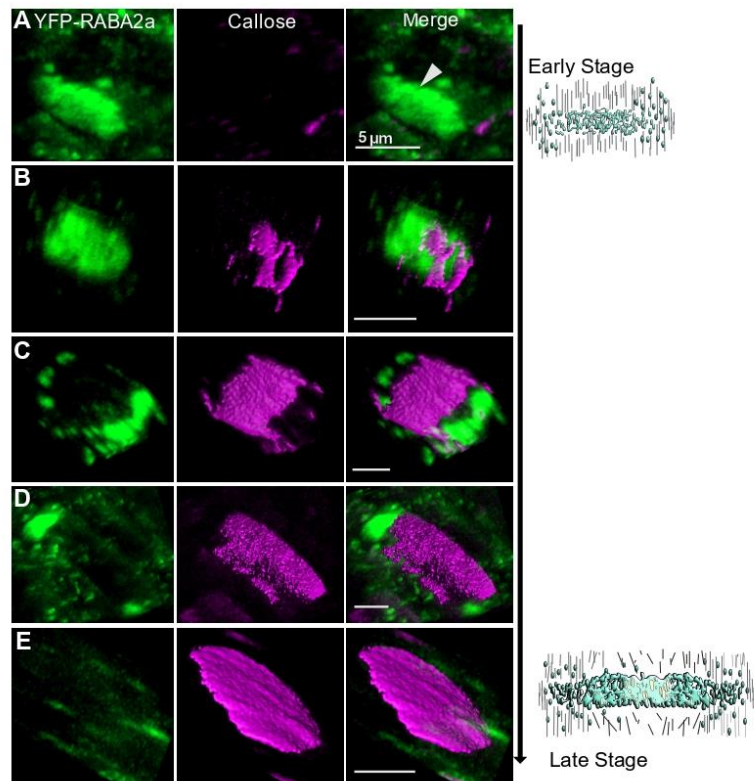


**Fig. 8.** Progression of the cell plate development in the presence of callose.

**(A-E)** Cell plate development in the presence of callose. **(A)** shows an early-stage cell plate before the accumulation of callose. At this stage, only vesicle accumulation by YFP-RABA2a (green) makes up the cell plate.

**(B-D)** Later-stage cell plates where callose accumulation stained with aniline blue fluorochrome (magenta) is detectable. Note the transient accumulation of callose in later stages, leading to the maturation of the cell plate during normal cytokinesis. **(B)** Initial callose deposition overlapping with YFP-RABA2a. **(C)** As the cell plate maturation continues and the YFP-RABA2a accumulation takes a "doughnut shape" pattern, callose deposition appears in the middle of the cell plate with minimal overlap with YFP-RABA2a at the leading edge. **(D)** Callose is present throughout the cell plate, while minimal YFP-RABA2a is shown at the discontinuous ring **(E)**. Mature cell plate predominately labeled by callose. Scale bar = 5 $\mu$ m.

## Conclusion and Future perspectives

A significant emphasis has been placed on understanding the role of callose in plant cytokinesis and its pivotal role as a potential spreading force in driving membrane transitions. This has not only deepened our understanding of plant cell division, but has also highlighted the challenges and future directions of this field.

The biophysical model laid the groundwork for further biological investigations of potential cell plate components contributing to the spreading force. The phenotypes caused by callose inhibition suggest that callose is the likely candidate for a spreading force as predicted by the model. In Chapter 3, I utilized four-dimensional imaging and developed quantitative imaging pipelines that allowed robust dissection of cell plate transitions based on cell plate vesicle volume dynamics.

Through these studies, I have leveraged multidisciplinary approaches, incorporating advanced imaging techniques and collaborating across disciplines, including animating science, to advance our understanding of plant cytokinesis and the role of transiently deposited callose in cell plate expansion. As I look to the future, the trajectory of the research I leave unfinished is poised to unravel further complexities, address lingering questions, and promise new discoveries.

Future work following Chapters 2 and 3 would involve investigating the enzyme responsible for synthesizing callose at the cell plate. The callose synthase/Glucan Synthase Like (GSL) family comprises twelve members in higher plants, with GSL8 presumably being the best candidate acting at the cell plate. I had the opportunity to characterize a fluorescent-tagged line of GSL8. Using this tool, we can detect the protein localization and its temporal relationship with other cell wall biosynthetic enzymes and their products at the cell plate. The combination of biological material with the tools created in Chapter 3 will allow further investigation of the dynamics and regulation of different cell wall biosynthetic enzymes and their products in cell plate assembly during cytokinesis. Additionally, the evolutionary conserved role of callose in cytokinesis was previously demonstrated with a study on *Penium margaritaceum* (Davis et al., 2020). I investigated the role of callose during *Chlamydomonas reinhardtii* (*C. reinhardtii*) cell division, establishing the presence of the polysaccharide and its significance when inhibited by ES7. Further work, with the use of

subcellular markers and cell wall biosynthetic mutants in *C. reinhardtii*, can aid in dissecting the evolutionary conserved mechanisms of cytokinesis between algae and land plants.

Looking ahead, the trajectory of questioning in plant cytokinesis research is poised for continued growth and innovation. With emerging technologies and collaborative efforts driving exploration, I anticipate uncovering further intricacies of this dynamic black box and unlocking new avenues for potential biotechnological applications.

## Appendix

Here I wish to present the other manuscripts I have been a part of during my time as a researcher at UC Davis that also culminates into all of the presented work. However, due to space limitations the citations are provided below:

1. R. Sinclair, “The Invitation of Sensory Equitable Botanical Art”. Plant science bulletin special issue By Botanical Society of America. Accepted- accepted
2. R. Sincalir, M. Rosquete, G. Drakakaki. “Post-Golgi Trafficking and Transport of Cell Wall Components” Frontier, December 2018 <https://doi.org/10.3389/fpls.2018.01784>
3. Allsman LA, Bellinger MA, Huang V, et al. Subcellular positioning during cell division and cell plate formation in maize. *Frontiers in Plant Science*. 2023 ;14:1204889. DOI: 10.3389/fpls.2023.1204889. PMID: 37484472; PMCID: PMC10360171.
4. Michel Ruiz Rosquete, Natasha Worden, Guangxi Ren, Rosalie M. Sinclair, Sina Pflieger, Michelle Salemi, Brett S. Phinney, David Domozych, Thomas Wilkop, Georgia Drakakaki, AtTRAPPC11/ROG2: A Role for TRAPPs in Maintenance of the Plant Trans-Golgi Network/Early Endosome Organization and Function, *The Plant Cell*, Volume 31, Issue 8, August 2019, Pages 1879–1898, <https://doi.org/10.1105/tpc.19.00110>